AD-A033 879

MICROWAVE SCANNING AND ASW HOLOGRAPHIC TECHNIQUES FOR N.D.T.

UNIVERSITY COLLEGE
LONDON, ENGLAND

JUNE 1976

005080

AD

MICROWAVE SCANNING AND ASW HOLOGRAPHIC

TECHNIQUES FOR N.D.T.

Final Technical Report

By

Eric A. Ash and Anis Husain

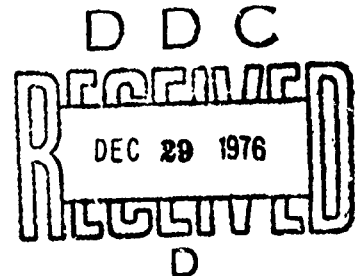June 1976

ADA033879

D D C

RECEIVED

DEC 29 1976

D

Department of Electronic and Electrical Engineering

University College London, U.K.

Approved for public release ; distribution unlimited

REPORT DOCUMENTATION PAGE		READ INSTRUCTIONS BEFORE COMPLETING FORM
1. REPORT NUMBER	2. GOVT ACCESSION NO.	3. RECIPIENT'S CATALOG NUMBER
4. TITLE (and Subtitle) MICROWAVE SCANNING AND ASW HOLOGRAPHIC TECHNIQUES FOR N.D.T.		5. TYPE OF REPORT & PERIOD COVERED FINAL TECHNICAL REPORT September 75 - February 76
		6. PERFORMING ORG. REPORT NUMBER
7. AUTHOR(s) ERIC A. ASH ANIS HUSAIN		8. CONTRACT OR GRANT NUMBER(s) DAERO-591-74-G0019
9. PERFORMING ORGANIZATION NAME AND ADDRESS DEPT. OF ELECTRONIC & ELECTRICAL ENGINEERING UNIVERSITY COLLEGE LONDON, U.K.		10. PROGRAM ELEMENT, PROJECT, TASK AREA & WORK UNIT NUMBERS 61102A-D0161102B35E-00-445
11. CONTROLLING OFFICE NAME AND ADDRESS USARSG (EUR) BOX 65 FPO NEW YORK 09510		12. REPORT DATE JUNE 76
		13. NUMBER OF PAGES 117
14. MONITORING AGENCY NAME & ADDRESS(if different from Controlling Office)		15. SECURITY CLASS. (of this report) UNCLASSIFIED
		15a. DECLASSIFICATION/DOWNGRADING SCHEDULE

16. DISTRIBUTION STATEMENT (of this Report)

APPROVED FOR PUBLIC RELEASE, DISTRIBUTION UNLIMITED

17. DISTRIBUTION STATEMENT (of the abstract entered in Block 20, if different from Report)

18. SUPPLEMENTARY NOTES

19. KEY WORDS (Continue on reverse side if necessary and identify by block number)

NON-DESTRUCTIVE TESTING: HOLOGRAPHY:
MICROWAVE SCANNING:

20. ABSTRACT (Continue on reverse side if necessary and identify by block number)

We have explored the feasibility of using two new techniques for non-destructive testing applications, one based on the use of microwaves, the other on acoustic surface waves.

The microwaves scanning microscope technique differs from other microwaves n.d.t. systems in that it aims not only to determine the existence of a defect, but also to locate it. The location is effected with an accuracy

which is more than two orders of magnitude better that the wavelength of the microwaves used.

The theory of the method has been developed and the dominant features are now well understood. We have constructed an instrument, working at 10 GHz, which has performed essentially in accordance with predictions. Using this instrument we have been able to detect microcracks in fatigue metal samples, with a width of the order of one micron. We were able to locate such cracks with an accuracy of better than 100 microns. The instrument has also proved capable of detecting very small changes in the electrical properties of the surface of a sample. In particular, it is able to detect changes in dielectric constant which are substantially less than 1%. As another example, it can measure the ferrimagnetic line width of a ferrite sample - over an area with dimensions of the order of 100 microns. The instrument is already capable of performing testing functions which cannot be duplicated by other means. In our view, it could be further developed for routine testing in a wide class of applications.

The accoustic surface wave technique differs from those previously employed in that we have adopted a holographic technique, whereby it is possible to record the accoustic field along a single line, and from this recover the complete field. It is therefore able to detect defects in the surface of a sample by reconstruction based on a single record. Our method is based on the use of a phase sensitive laser probe, followed by subsequent computer reonstruction. Using this technique we have been able to detect very small defects on a quartz surface. It is possible that the technique can be used effectively for determining surface flaws in highly polished surfaces.

ACCESSION for

NTIS   White Section
DDC   Buff Section
UNANNOUNCED
JUSTIFICATION.....................

....

DISTRIBUTION/AVAILABILITY CODES

DIST.	AVAIL. and/or SPECIAL	
A		

D D C

DEC 29 1976

D

ABSTRACT

We have explored the feasibility of using two new techniques for non-destructive testing applications, one based on the use of microwaves, the other on acoustic surface waves.

The microwaves scanning microscope technique differs from other microwaves n.d.t. systems in that it aims not only to determine the existence of a defect, but also to locate it. The location is effected with an accuracy which is more than two orders of magnitude better than the wavelength of the microwaves used.

The theory of the method has been developed and the dominant features are now well understood. We have constructed an instrument, working at 10 GHz, which has performed essentially in accordance with predictions. Using this instrument we have been able to detect microcracks in fatigue metal samples, with a width of the order of one micron. We were able to locate such cracks with an accuracy of better than 100 microns. The instrument has also proved capable of detecting very small changes in the electrical properties of the surface of a sample. In particular, it is able to detect changes in dielectric constant which are substantially less than 1%. As another example, it can measure the ferrimagnetic line width of a ferrite sample - over an area with dimensions of the order of 100 microns. The instrument is already capable of performing testing functions which cannot be duplicated by other means. In our view, it could be further developed for routine testing in a wide class of applications.

The acoustic surface wave technique differs from those previously employed in that we have adopted a holographic technique, whereby it is possible to record the acoustic field along a single line, and from this recover the complete field. It is therefore able to detect defects in the surface of a sample by reconstruction based on a single record. Our method is based on the use of

a phase sensitive laser probe, followed by subsequent computer reconstruction. Using this technique we have been able to detect very small defects on a quartz surface. It is possible that the technique can be used effectively for determining surface flaws in highly polished surfaces.

TABLE OF CONTENTS

Page

SECTION A.   MICROWAVE SCANNING TECHNIQUE

1.   INTRODUCTION

This is the Final Report covering the progress in the last quarter from
1 October to 31 December, as well as the work done throughout the project.   The
work on the microwave scanning technique is discussed in section A, whilst that
on acoustic surface wave holography is presented in section B.

We believe that both of the techniques have been shown capable of performing
certain non-destructive testing functions which go beyond the capabilities of
existing methods. A brief overall assessment of the program and plans for future
work are presented in section C.

Experiments have been carried out to assess the
potential use of the microscope in non-destructive testing
applications.   These demonstrate that the microscope is
capable of resolving object details separated by distances
more than two orders of magnitude smaller than the illuminat-
ing wavelength.   The sensitivity of the instrument to changes
in surface topography of metals has been exploited to detect
micron wide fatigue cracks in metals;   the microscope is also
very sensitive for the detection of breaks in thin metallic
films on substrates, this makes it useful in the testing for
cracks in thin film circuitry.

A technique whereby we can selectively image small
changes in electric and magnetic properties of the object is
described.   The limited depth of field of the microscope
enables us to characterise the properties of both dielectric
and ferrite thin films.   It would be extraordinarily difficult
to visualise these changes, non-destructively, in any other
way.

2. BASIC PRINCIPLE OF METHOD

The basic principle of the method depends on the use of an aperture in a metallic plate which is small compared with the illuminating wavelength, Fig.1.1. We view the object through the aperture. If the object is transparent, one can detect the transmitted wave through the hole; if it is reflecting, one can detect the scattered wave through the aperture. By scanning the sample under the pupil and recording the signal we can eventually scan the whole sample with a resolution which is somewhat less than that of the aperture dimension but more than two order of magnitude less than the wavelength.

The "objective" of our microscope consists of an aperature in one of the side walls of a resonant cavity, which in our case is a microstrip resonator (Fig. 1.2). The object beneath the hole perturbs the frequency of the resonator. By operating on the linear portion of the resonator Q curve, we can translate this frequency shift into a corresponding amplitude change, which is demodulated in the receiver and displayed on a X-Y plotter. The object

is illuminated by the evanescent fields associated with the small aperature. We must therefore detect a signal which is very small compared with the illumination power in order to obtain a significant improvement over the classical resolution. Moreover, this signal is superimposed on a much larger background radiation so that the contrast will be poor. This deficiency can be overcome by vibrating the object at an acoustic frequency. The required signal is then "tagged" by this modulation frequency, and is readily separated in the receiver system.
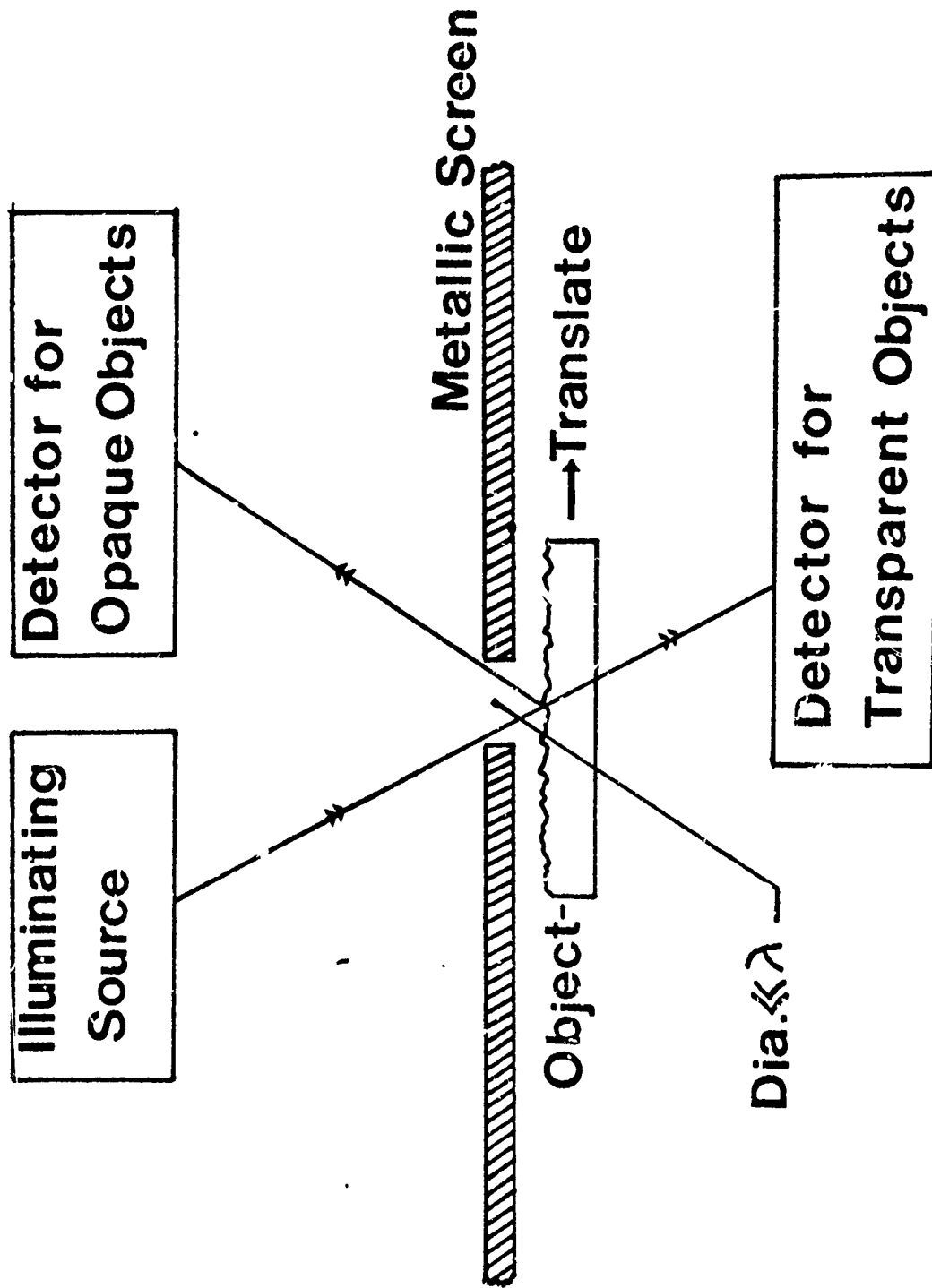
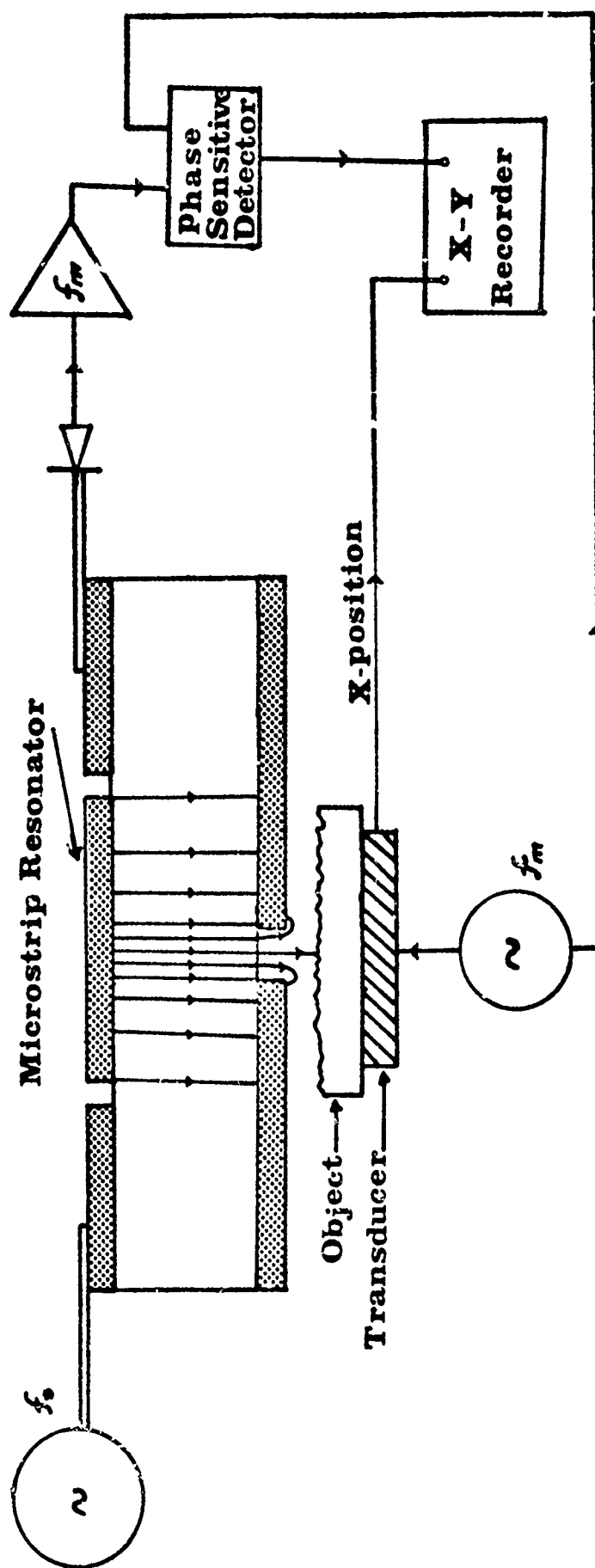Figure 1.1   Basic Principle of Super-Resolution Microscope

Figure 1.2   Basic Experimental Configuration

In the case of some materials it is possible to apply the modulation in an electrical rather than a mechanical form. For example, in the case of a ferrite object it is possible to modulate the magnetic field, by modulating a current in a suitable auxiliary coil.

3. THEORY OF MICROSCOPE

In aperture microscopy, just as in ordinary microscopy, we are interested in assessing the resolution and sensitivity of the instrument to various materials and material defects. In this section, we shall present approximate theories to explain the response of the instrument to both simple variations in the surface topography as well as changes in the electric and magnetic permittivity of the sample.

In order to predict the performance of the system, we have used an approximate theory to assess the signal strength as a function of position of a metallic plane below the aperture. However, in practice, we are far more interested in how small deviations in the flat plane affect the signal. We have therefore developed a first order theory to assess the perturbation in signal from a defect, simulated as a slot in a metal object.

In the use of apertures which are small as compared with one wavelength, it is meaningful to distinguish between electric and magnetic contrast; this is used to explain the ability of the microscope to image small perturbations in the relative dielectric constant as well as variations in the permeability of the object.

3.1 Aperture Superresolution

The imaging properties of the microscope are determined by the evanescent fields produced by the cavity aperture. Our ability to obtain high resolution is based on the fact that this evanescent field contains spatial frequencies which are much higher than the inverse wavelength. We have looked at this issue quantitatively by, computing the Fourier transforms of approximate versions of the aperture field distribution.

Using the magnetic dipole approximation to the aperture field, we computed the transverse spectral density function in the X direction. (due to the symmetry of the fields this is the same as the spectral density in the Y direction), the result is shown in Fig. 2.5a. The calculation was performed for an aperture diameter we have been using in experiments of $\lambda/100$, and for a typical operating distance of $Z = \lambda/1000$ away from the diaphragm. The shaded region in the figure shows that the spatial frequencies which are more than two orders of magnitude higher than the inverse wavelength are transferred by the aperture. It is precisely this part of the spectrum on which we rely to obtain super-resolution imaging of the object.

It was of interest to evaluate the spectral power density in the Z direction. This was computed from Bethe's approximation to the d_z component and is shown in Fig. 2.5b. The figure indicates that we in fact have super-resolution in depth as well as in the transverse direction. It also
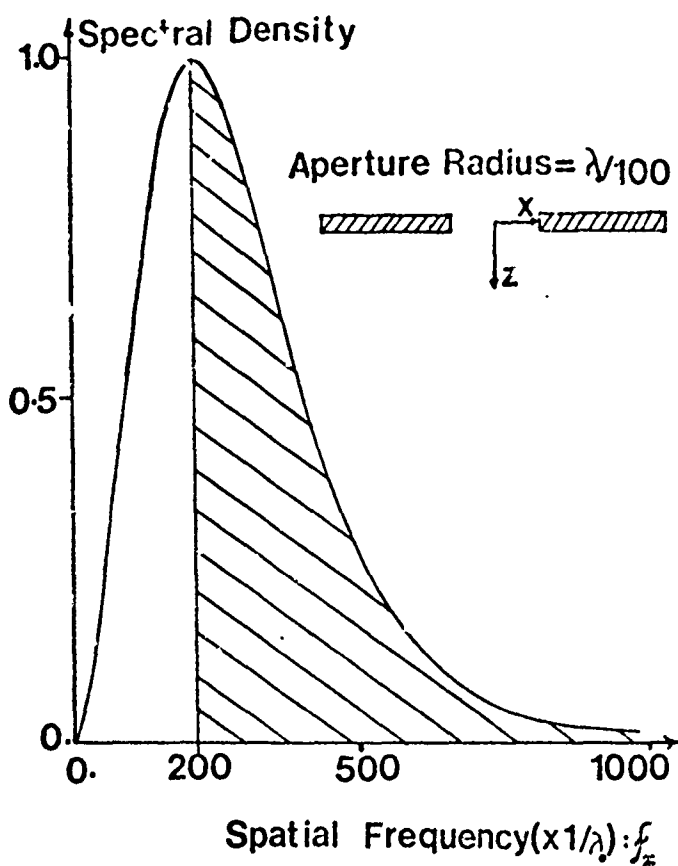
Figure 2.5(a)   Spectral Density of Aperture Fields
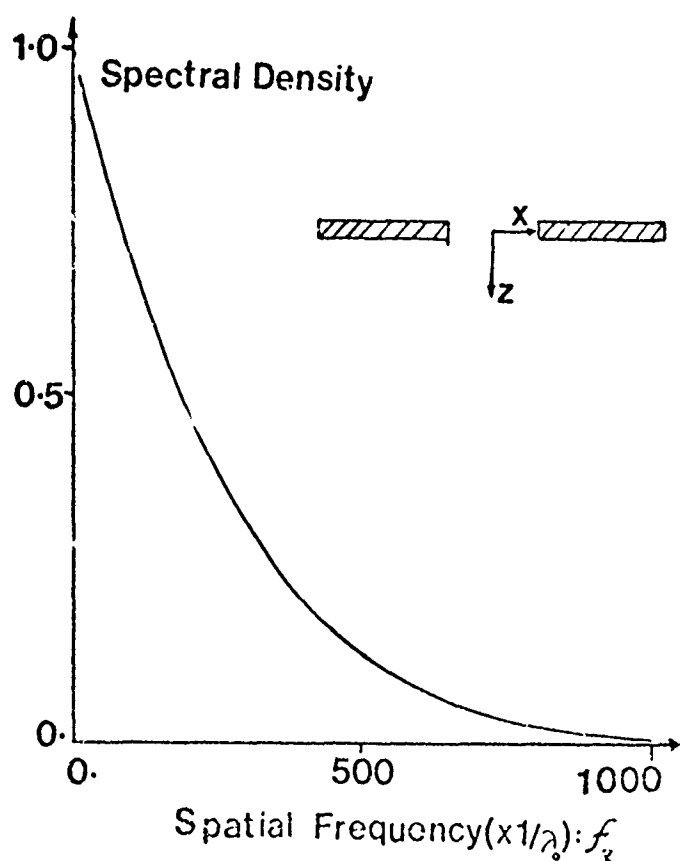in the X-Direction (Bethe's Theory)

Figure 2.5(b)   Spectral Density of Aperture Fields

shows that the resolution decreases very rapidly as we move away from the aperture in the Z direction. This result has two important implications. First, as any practical instrument will have a limited dynamic range, we must operate as close to the aperture as possible if we are to detect these high spatial frequencies to obtain the high resolutions predicted. Secondly, the fact that the depth of field of the microscope is itself less than an aperture diameter, suggests that we might see surface changes which would be extraordinarily difficult to detect in any other way. In Section 7.3 we shall present the results obtained on the imaging of variations in the properties of thin films which confirms this important property.

The spectral density functions considered are useful to illustrate the principle of aperture super-resolution; the results indicate that the aperture facilitates the transfer of very high spatial frequencies, so that one might expect to achieve resolutions much less than an aperture diameter. In practice, the resolution we can achieve depends on the interaction of the aperture fields with the particular object under investigation as well as the overall dynamic range of the microscope. The determination of the object/aperture field interaction requires a detailed field calculation for each particular type of object; consequently, we have not attempted to solve these very complex problems. However, we can say that for most objects, the attainable resolution will be of the order of the aperture diameter ($\lambda/100$ in our case).

3.2   Principle of Operation

The basic concept of the microscope is shown in Fig. 1.2. We illuminate a thin metallic screen with an aperature of diameter, a, which is very much smaller than the illuminating wavelength, λ. This small aperature gives rise to a distribution of electromagnetic waves which are evanescent in a direction normal to the diaphragm. We must therefore detect a signal which is very small as compared to the illuminating power. Moreover, this signal is super-imposed on a much larger background radiation, so that the 'contrast' will be very poor. The loss of signal may always be recovered by the use of sufficiently long integration times. The more serious problem of the loss of contrast can be over-come by vibrating the object at an audio frequency, and subsequently searching for this modulated component in the receiver.

Bethe has shown, that fields on the object side of the diaphragm (Z>0) can be approximated by a pair of magnetic and electric dipoles. If the screen is illuminated so as to produce a predominantly magnetic dipole orientated in the plane of the screen, then the object/aperature field interaction gives rise to a dipole field in the region Z<0 above the diaphragm. The strength and orientation of this field will contain the desired information of the object. For the case when the electric dipole predominates and is orientated in a plane normal to the aperture, only the strength of the dipole fields in a region Z < 0 will provide information on the properties of the object.

An alternative way of looking at the theory of operation is to consider a technique which applies more closely to the theory which will be developed in the following sections.   In our case, the dipole radiates into a microstrip resonator.   The object under the aperture will perturb the resonant frequency of the resonator as well changing the unperturbed Q of the resonator.   It will be shown in Section 3.2 that we are primarily interested in changes in the resonant frequency.   By operating on the linear portion of the resonator Q curve, we can translate this frequency shift to a corresponding amplitude change, which is then demodulated in the receiver system and displayed

The sources of object contrast are found in the distribution of electric and magnetic permittivities and in the distribution of conductivity which alter the energy stored in the vicinity of the aperture.   If there are sufficient gradients of these quantities within the dipole field, there will also be a contribution to the signal arising from the distortion of the dipole field.

3.3   Effect of Metallic Plane

In order to obtain some estimate of the signal strength, we have calculated the frequency perturbation caused by a metal object which is vibrated so as to close the aperture at one part of the cycle, and which is removed, effectively outside the range of the dipole near-field, half a cycle later.

Using simple perturbation theory, assuming that the change in resonant frequency δf is given by

$$\frac{|\delta f|}{f_0} = \frac{|U_E - U_H|}{2 U_{RES}}$$ 3.1

where U_E & U_H are the electric and magnetic energies stored in the near field of the aperture, and U_{RES} is the total energy stored in the resonator. For the case of an open resonator[10], the signal power, modulated at the frequency fm was calculated at the optimum frequency (displaced from the resonent frequency by a fraction $3^{\frac{1}{2}}/Q$, took the form

$$S \simeq 0.28 \times 10^{-2} \frac{(k_0 a)^3 P_{IN}}{\alpha (k w_0)^2}$$ 3.2

$k_0 = 2\pi/\lambda$ is the wave number. Typically $\alpha = 10^{-2}$ and the aperture diameter $a = \lambda/100$, wo being the minimum spot diameter; the signal power is approximately 52dB below the input power.

We have evaluated the signal amplitude which we obtain when a metallic object is removed from contact with the aperture to a position outside the range of the dipole field. However, we need finer grained information - how the signal varies with the amplitude of vibration and with mean position of the object. Essentially we are concerned with a quasi-static field theory. If we can regard the object as being a good conductor, its effect can be taken into account using image theory. The image of the aperture is itself imaged in the aperture plane and this too can be

incorporated in the theory (Fig. 3.3), the process can be continued in the "hall of mirrors", the effect of each successive image to the total field being increasingly less important. As long as the distance between the object and the image plane is large as compared with the aperture diameter, we have a formulation which is very nearly rigorous. In practice we must deal with object/aperture separations which are comparable to the aperture diameter. In this regime, our theory becomes progressively less reliable. Nevertheless, it should grasp the most important features of the situation and provide a useful guide to design.

The calculation of the signal strength involves evaluating the self energy of the dipole and its M images, as well as the cross or mutual energy terms associated with the dipole and each of its M images.

The basic technique we have adopted begins by approximating the aperture fields. The object is assumed to be a perfect conductor and its effect may then be taken into account using image theory. The resultant fields in the vicinity of the aperture are then represented as a set of plane waves. The change in energy stored as the screen is displaced is then computed in the frequency domain rather than in the configuration domain. In the first part of the analysis we deal with the one dimensional problem - the case of the infinite slot aperature (Fig 3.4); this is then extended to include the two dimensional problem of a square aperture.

First, we assume that the function $g(x,0)$ is a good approximation of the aperture field distribution in the
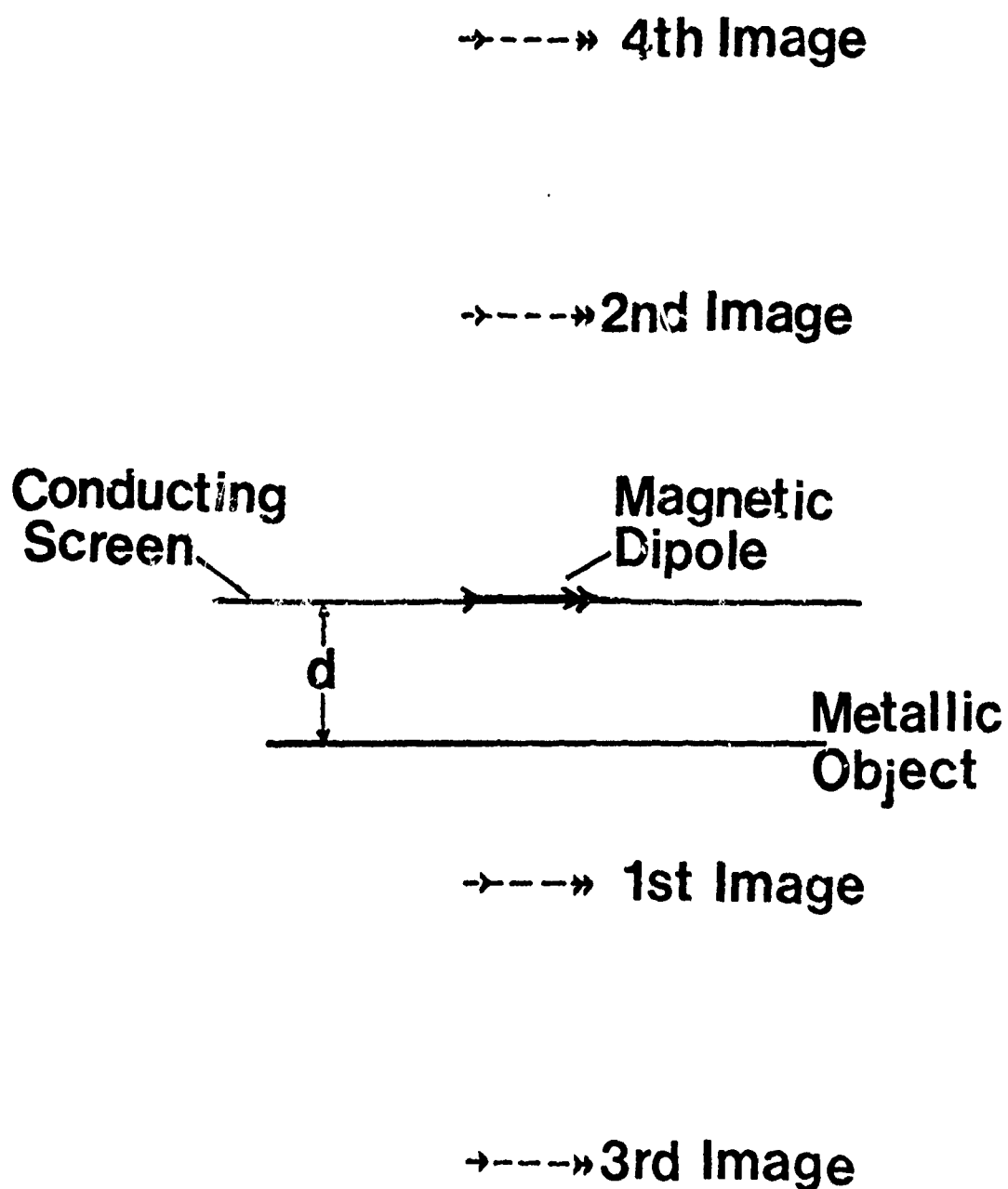
Figure 3.3   Imaging of Dipole in Metallic
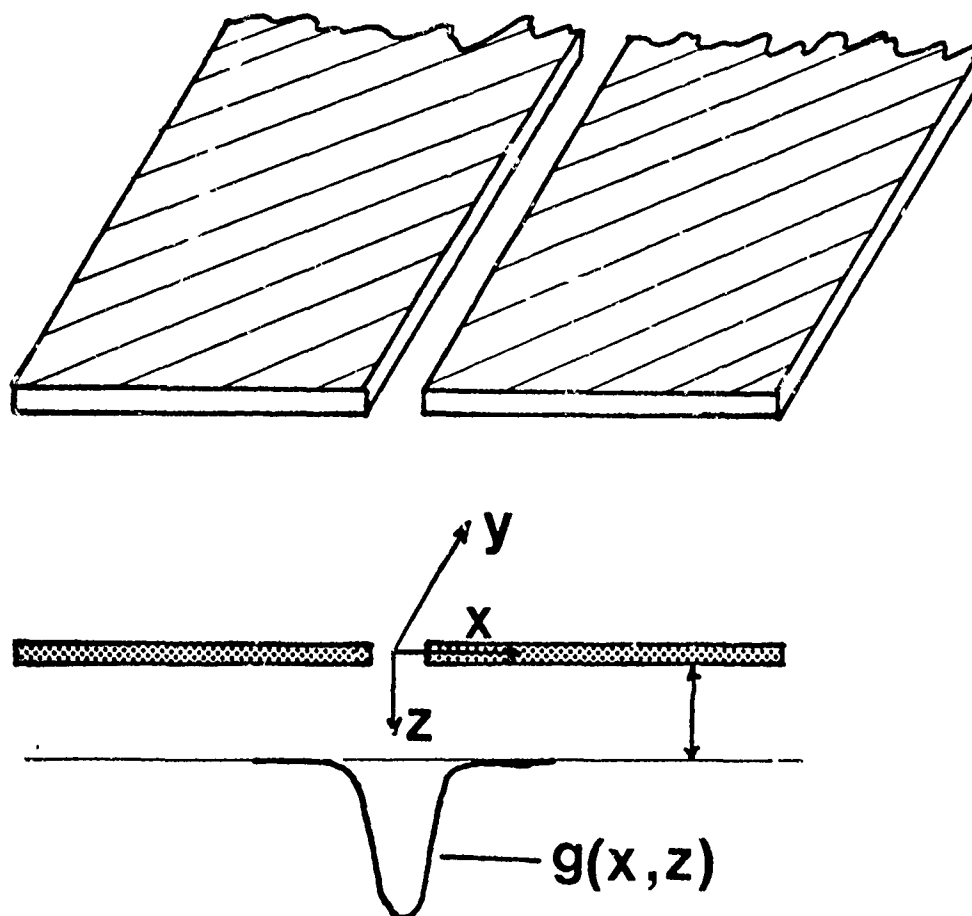Object and in Conducting Screen

Figure 3.4   Infinite Slot Aperture and
Assumed Aperture Distribution

The field in the vicinity of the hole may be represented by a set of plane waves:

$$g(x,0) = \int_{-\infty}^{\infty} G(f_x) e^{-jk_x x} d(f_x) \qquad ..(3.3)$$

where $G(f_x)$ is the fourier transform of $g(x,0)$. Each term of equation 3.18 is a plane wave, and we may express the field distribution at a position Z away from the aperture as:

$$g(x,z) = \int_{-\infty}^{\infty} G(f_x) e^{-jk_x x - jk_z z} d(f_x) \qquad ..(3.4)$$

From the wave equation, k_z is given by:

$$k_z^2 = k_o^2 - k_x^2 \qquad ..(3.5)$$

We are operating in the very near field of the aperture, i.e. in the induction zone, and consequently for the most important field components the approximation $k_x^2 >> k_o^2$ will be valid; and 3.20 may be rewritten as:

$$|k_z| \simeq j|k_x| \qquad ..(3.6)$$

From 3.4 and 3.6 we obtain:

$$g(x,z) \simeq \int_{-\infty}^{\infty} G(f_x) e^{-jk_x x - |k_x| z} d(f_x) \qquad ..(3.7)$$

The energy stored per unit length as the screen is displaced from $Z = 0$ to $Z = d$, for the source can be shown to be:

$$W = \frac{1}{2} \varepsilon_0 \int_{f_x = -\infty}^{\infty} |G(f_x)|^2 d(f_x) \int_{z=0}^{d} e^{-2k_x z} dz \qquad ..(3.8)$$

A method using Discrete Fourier Transforms is particularly useful in evaluating this equation as the technique readily lends itself to computer numerical methods.

From equation 3. 8, the energy per unit length of the slot is:

$$W = \varepsilon_0 L \sum_{n=0}^{N} |G(f_n)|^2 (\Delta f)^2 \int_{z=0}^{d} e^{-2k_n z} dz \qquad ..(3.9)$$

As $k_n = 2\pi f_n$ and $f_n = n/L$ we may rewrite equation 3.9 as:

$$W = \frac{\varepsilon_0 L}{4\pi} \Delta f^2 \sum_{n=0}^{N} \frac{G(n/L)}{(n/L)} \left\{ 1 - e^{-\frac{4\pi n d}{L}} \right\} \qquad ..(3.10)$$

Let us assume that the aperture field distribution $g(x,0)$, is a gaussian given by:

$$g(x,0) = e^{-\left(\frac{x}{x_0}\right)^2} \qquad ..(3.11)$$

x_0 being the gaussian decay constant.

If the effect of the conducting plane is taken into account using image theory and using equation 3.10 and 3.11 a typical component for the M'th image is:

$$g(x,z) = 2\Delta f \sum_{n=0}^{N} G(\xi_n) e^{-jk_n x - k_n(z + d(m))} \qquad ..(3.12)$$

where: $d(0)$ refers to the case of the source alone

$d(m) = md;$ if m is even

and $d(m) = (m + 1)$; if m is odd

The self energy terms for the source and its M images becomes:

$$W_{SELF} = \frac{\varepsilon_0 x_0^2}{4} \sum_{m=0}^{M} \sum_{n=0}^{N} \left\{ \frac{e^{-\frac{n^2 x_0^2}{2L^2}}}{n} \left\{ e^{-\frac{4\pi d(m)n}{L}} - e^{-\frac{4\pi}{L}(d(m)+d)} \right\} \right\} \qquad ..(3.13)$$

while the cross or mutual energy terms are given by:

$$W_{CROSS} = \frac{\varepsilon_0 x_0}{4} \sum_{m=0}^{M_1} \sum_{S=M+1}^{M} \sum_{n=0}^{N} \left(\frac{e^{-\frac{n^2 x_0^2}{2L^2}}}{n}\right) \left\{ e^{-\frac{2\pi n}{L}(d(m)+d(s))} - e^{-\frac{2\pi n}{L}(2d+d(m)+d(s))} \right\} \quad ..(3.14)$$

where, in this case: $d(m) = (1 + m/2)d$ if m is even,

and $d(m) = (1 + m)d/2$ if m is odd

These results may be extended to the two dimensional case of the square aperture if the following assumptions are made: (a) we assume that the aperture field distribution g(x,y,0) is separable, this allows the complicated two dimensional manipulations to be reduced to the more simple one dimensional manipulations; (b) we further assume that the separable functions are both symmetric. We may then write equation 3.12 for the two dimensional case as:

$$g(x,y,z) = 4(\Delta f)^2 \sum_{n=0}^{N} \sum_{p=0}^{N} \left\{ G(f_n) \cdot G(f_p) \, e^{-j(k_n x + k_p y) - (k_n^2 + k_p^2)^{\frac{1}{2}}} \right\} \quad ..(3.15)$$

In the above, we have assumed that g(x) is a gaussian as before and $g(x) \equiv g(y)$, we may therefore put $G(f_n) \equiv G(f_p)$; the subscript "p" referring to the summation performed in the Y plane.

It may be shown that the self energy for the square aperture is:

$$W_{SELF} = \frac{\varepsilon_0 \pi x_0^4}{4L} \sum_{m=0}^{M} \sum_{n=0}^{N} \sum_{p=0}^{N} \left\{ \frac{e^{-(p^2+n^2)\frac{x_0^2}{2L^2}}}{(n^2+p^2)^{1/2}} \left\{ e^{-4\pi \frac{(n^2+p^2)^{\frac{1}{2}}d(m)}{L}} - e^{-4\pi(n^2+p^2)^{\frac{1}{2}}(d(m)+d)} \right\} \right\} \quad ..(3.16)$$

and the mutual energy terms:

$$W_{CROSS} = \frac{\varepsilon_0 \pi x_0^4}{4L} \sum_{m=0}^{M} \sum_{s=m+1}^{M} \sum_{n=0}^{N} \sum_{p=0}^{N} \left\{ \frac{e^{-(p^2+n^2)\frac{x_0^2}{2L^2}}}{(n^2+p^2)^{\frac{1}{2}}} \left\{ e^{-\frac{2\pi}{L}(d(m)+d(s))(n^2+p^2)^{\frac{1}{2}}} - e^{-\frac{2\pi}{L}(d(m)+d(s)+2d)(n^2+p^2)^{\frac{1}{2}}} \right\} \right\} ..(3.17)$$

The total energy stored in the quasi-static aperture fir'.d
is simply:

$$W_{total} = W_{cross} + W_{self} \qquad ..(3.18)$$

The relative decay of the signal as the screen is displaced
is simply the differential of the total energy stored with
respect to the movement, d, from the aperture in the Z
direction:

$$S\Big|_{z=d} = \frac{\partial(W_{total})}{\partial z} \qquad ..(3.19)$$

A computer programme was developed to calculate the signal
as a function of screen movement for the source and its
multiple images.   The results are shown in Fig. 3.5, where
it must be remembered that by the time the object has
approached to within one aperture diameter, the theory becomes
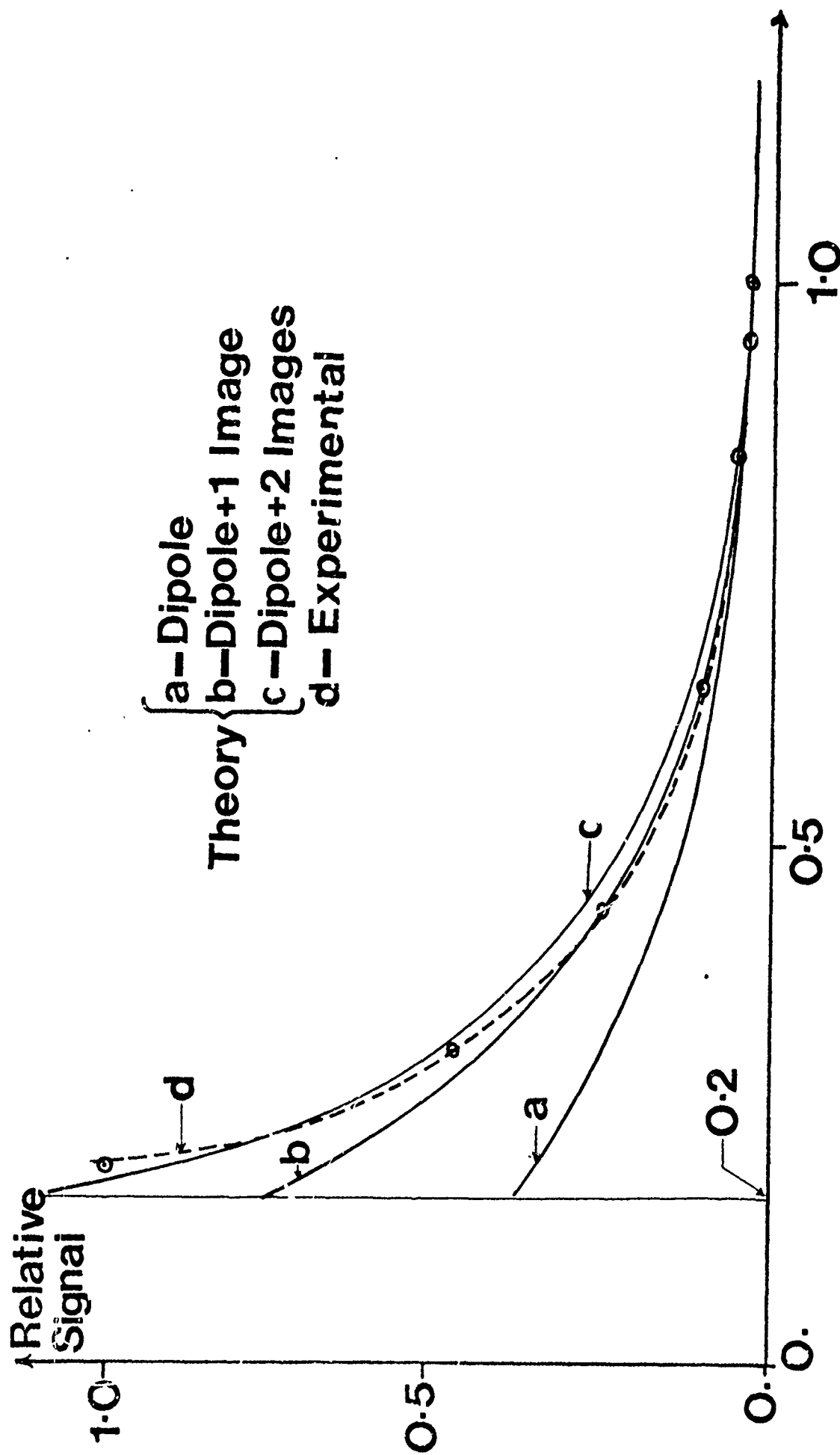
Distance in Apertures

Figure 3.5   Signal Strength as a Function of the
Displacement of a Metallic Object

progressively more suspect.   Nevertheless, we find encouraging agreement between
theory and experiment.

3.4   Perturbation Due to Slot in Metal Object

In practice, we are concerned with how small deviations in the surface topography and material changes affect the signal.   Even for the simplest

defect geometry, such as a slot in a metal object, an electro-static field solution would be very complex indeed.   We have therefore made no attempt to solve the problem rigorously. Instead, we have developed an approximate theory which provides a first order guide in assessing the perturbation in signal arising from a defect, simulated as a slot in the metal object surface.

We wish to evaluate the change in energy stored in the vicinity of the aperture by the presence of a slot of of width, W, depth, D, and length, L, located symmetrically below a square aperture in a metallic object (Fig. 3.6). The slot is represented as a waveguide and the field components in the slot are calculated.   The energy stored in the slot can then be determined.   There will also be a contribution to the energy stored by the slot as a result of the perturba-tion of the fields above the slot.   This contribution has been neglected as we only require an order of magnitude estimate of the perturbation due to the slot.   We have also

neglected second order effects, such as the interaction of the edge of the slot with the side of the aperture.

Let us consider the case when the aperture fields may be regarded as due to those of magnetic dipole.   This corresponds to exciting the slot with a magnetic field com-ponent H_x, the electric field component E_z being zero.
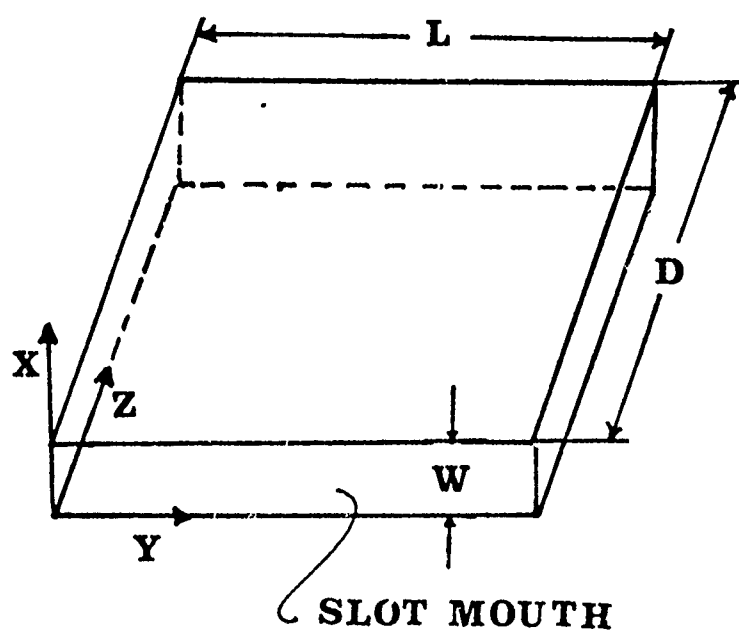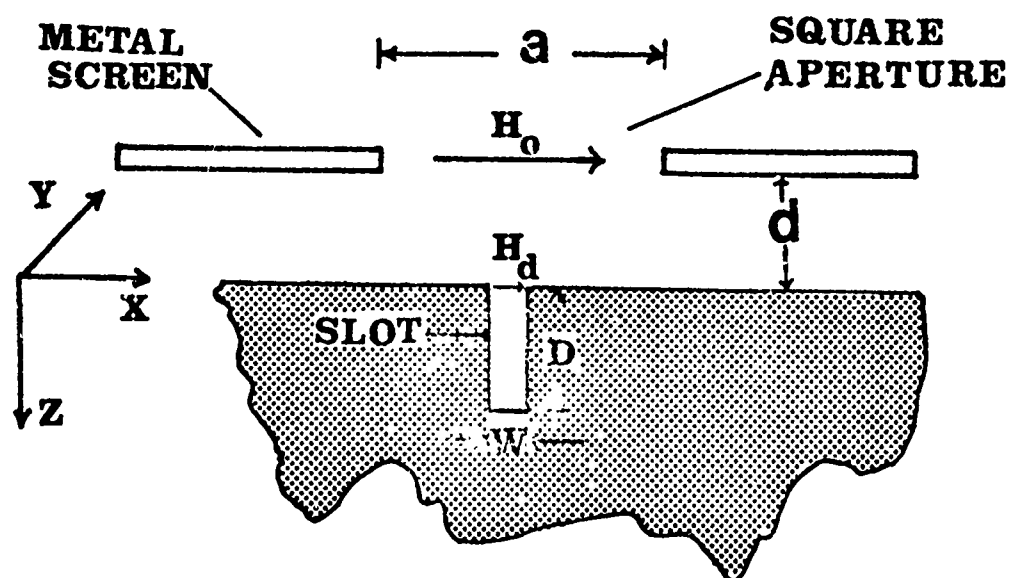
Figure 3.6   Geometry of Slot in Metal Object
Used for Analysis

The field components in the slot were evaluated and used to

calculate the energy stored in the slot:

$$U_{SLOT} = \mu \frac{H_D{}^2 W^2 L}{8}\left\{1 - e^{-2D/W}\right\} \quad ..(3.28)$$

Equation 3.20 indicates that for thin deep slots ($W \ll D$),
the signal related to the slot depth will saturate.
Experimental results which verify the theory will be
presented in Chapter 6. The equation also predicts that
the signal should be proportional to the square of the width
of the slot. Experimental results indicate that the
dependence of signal on width is in fact more nearly linear.

The theory accurately predicts the decay of signal
with the depth of the slot, but not the variation of signal
with the width of the slot. This apparent anomaly can be
explained if we consider how each quantity arises in the
final expression. The decay of the signal is related

primarily to the attenuation constant in the slot and this
parameter can be calculated accurately. However, the change
in signal with width of slot is determined by the precise

field configuration inside and outside the slot. We have
not determined these fields with any great accuracy, thus
the discrepancy in the theoretical and experimental results.

For slots which have $W \ll D$, the energy stored in the
slot may be approximated to:

$$U_{SLOT} \simeq \frac{\mu}{8} H_D^2 W^2 L$$

..(3 21)

In order to evaluate the perturbation in signal
due to the slot in a metallic object positioned at a distance,
d, away from the aperture, we must first calculate the energy
stored due to the aperture and plane in the absence of the
slot. The energy stored in the near field of a square
aperture in the presence of a metallic plane was calculated
in Chapter 3.2. The energy stored for the dipole and its
first image was:

$$U_{PLANE} \simeq 0.393 \mu H_D^2 \left\{ e^{5d/a} \right\} a^3$$

..(3 22)

Let us consider a slot which has $W \ll D$ - this
corresponds to the type of fatigue cracks we have been
detecting. From equations 3.44 and 3.45 the perturbation
in energy, ΔU due to the slot in a metallic object positioned,
d, away from the aperture plane is:

$$\Delta U = \frac{U_{SLOT}}{U_{PLANE}} = 0.32 \left\{ e^{-\frac{5d}{a}} \right\} \frac{W^2 L}{a^3} \; ; \left(W < D \right) \qquad ..(3.23.)$$

If a unity signal to noise ratio is used as the criterion, the minimum detectable perturbation of the system is ΔU_{min}, where:

$$\Delta U_{min} = 1/(S/N) \qquad ..(3.24)$$

For a typical height of $d = a/10$ of the metallic plane below the aperture, of diameter $a = 300 \, \mu$, and length of slot $L = 300 \, \mu$, the predicted minimum slot width which can be detected for a system S/N ratio of 45 dB is about $4 \, \mu$. Experimental results (Chapter 6) indicate that equation 3.47 does predict the order of magnitude of the detection sensitivity.

3.5   Dielectric and Ferrite Imaging

We have mentioned that the microscope is sensitive to changes in the distribution of the electric and magnetic permittivity of the object. In this section, we consider a scheme which will enable us to utilise the microscope selectively to image variations in the relative dielectric constant and variations in the permeability of the object.

The imaging properties of the microscope may be explained by studying the changes in the energy stored in the vicinity of the aperture by the object. To a first

approximation, the aperture fields can be represented by either a magnetic or an electric dipole depending on the form of illumination. Let us consider the energy stored in the induction field of the aperture for both the electric and the magnetic dipole case. It can be shown that for the magnetic dipole, the principle energy storage mechanism is magnetic and

$$U_{MAG} \simeq 0.043 \mu H_0 a^3 \qquad \qquad \text{.. (3.25)}$$

While for the electric dipole it is the electric energy stored which is of consequence:

$$U_{ELEC} \simeq 0.011 a^3 \varepsilon E_0 \qquad \qquad \text{.. (3.26)}$$

The above equations only apply when the material in the half space below the aperture is filled with a material of dielectric constant, ε, in the electric dipole case, and a material of permeability, μ, in the magnetic dipole case If the perturbation in either, ε, or, μ, is small,

$$U_{MAG} \propto \mu \qquad \qquad \text{.. (3.27)}$$

$$U_{ELEC} \propto \varepsilon \qquad \qquad \text{.. (3.28)}$$

However, if there are significant gradients in the electric or magnetic permittivity of the object, there will also be a contribution to the signal due to the distortion of the aperture fields, and the signal will no longer be proportional

to these quantities i.e. first order perturbation theory
fails.

Two important points emerge from this very approx-
imate theory. If we suitably illuminate the aperture to
obtain a predominantly electric dipole, the microscope will
be very much more sensitive to changes in the relative
dielectric constant than to changes in the permeability
of the object. Similarly, for an essentially magnetic
dipole aperture field, the instrument will be more sensitive
to variations in the permeability of the sample. Experiments
to corroborate these findings are presented in Chapter 7.3.

4.   RESONATOR AND APERTURE DESIGN

The "heart" of a microscope is the objective;
in our case, this consists of a resonator with an aperture
in one of the side walls.   In this chapter we shall deal
with the design and optimisation of the microscope "objective".

The main design criterion is to maximise the
object/aperture field interaction.   It was shown in Section
3.   that the signal was proportional to the energy stored
in the fields outside the aperture, W_0, and inversely
proportional to the energy stored in the resonator, W_r.
We therefore need to increase the ratio W_0/W_r.   The increase
in W_0 may be effected by confining the fields illuminating
the aperture into the smallest possible area so as to have
a maximum field intensity at the aperture.

The choice of the type of microwave resonator other than optimising
the signal to power ratio, depends on factors such as the size, ease of fabrication,
and stability of the resonator.   These considerations indicated that a micro-
strip resonator would have significant advantages over the open resonator as the
microstrip objective.

4.1   The Microstrip Resonator

Several forms of microstrip resonators were invest-
igated, both experimentally and theoretically with the aim of
optimising the detection signal.   They are shown in Fig. 4.1.

The investigation revealed that the linear resonator was able to confine the
substrate fields to a much smaller area than the disc resonator [1], or

(a) Linear
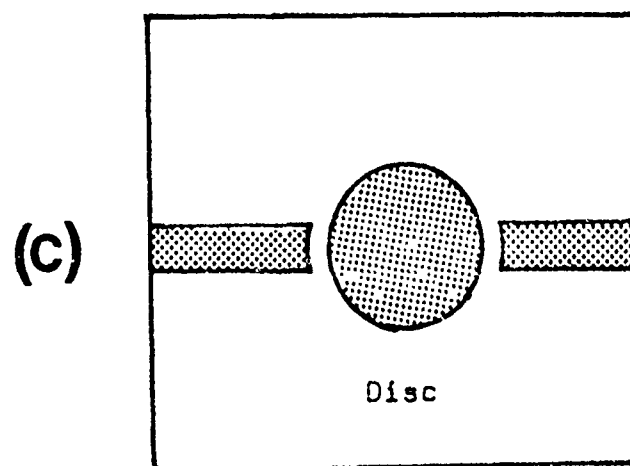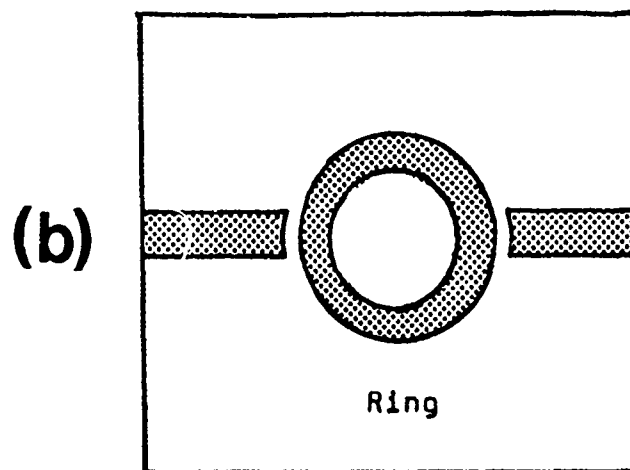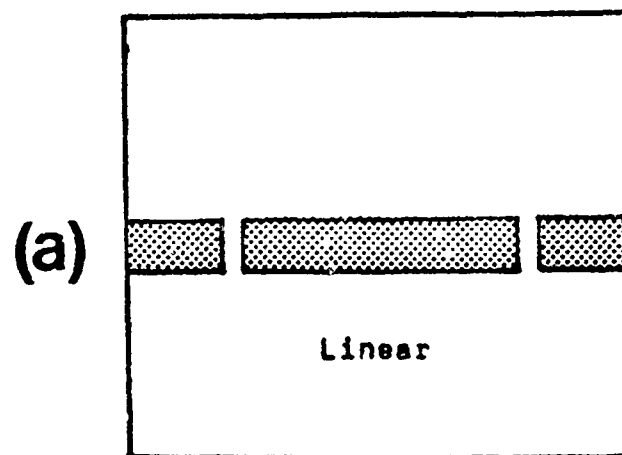
(b) Ring

(c) Disc

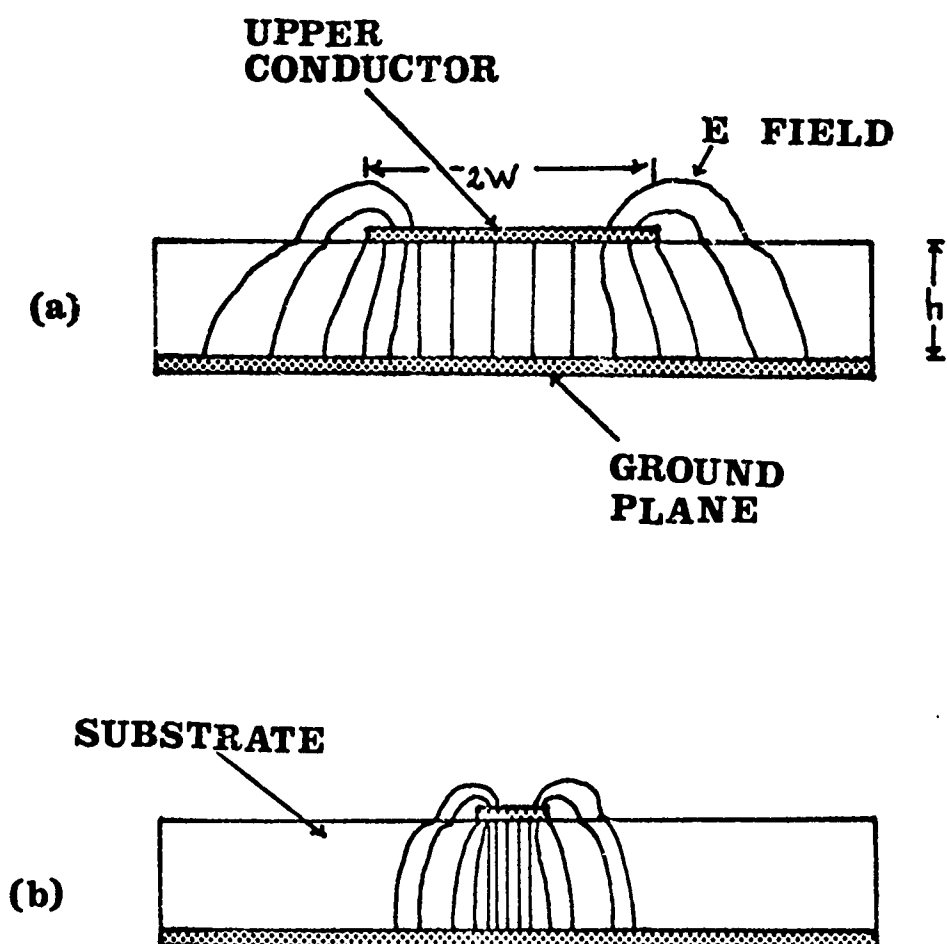Figure 4.1   Microstrip Resonators

Figure 4.2   Linear Microstrip Resonator

Having chosen the linear resonator, we pro-
ceeded   to select the optimum design parameters.   In the
following analysis we shall consider a linear λ_s open circuit
resonator for convenience;   the choice of a λ_s rather than
the optimum $\lambda_s/2$ resonator is explained in the next section.

The linear resonator we are analysing is shown in
Fig. 4.3.   It consists essentially of two discontinuities
in the microstrip line, of length λ_s.   We shall assume that
the gaps in the line have been adjusted for optimum coupling,
and that the aperture is positioned in the ground plane so
that we have a maximum electric field at the aperture.   In
this case, the aperture fields are essentially those produced
by an equivalent electric dipole.   Fig. 4.2 shows the field
configuration for the case of a strip conductor above a
conducting plane separated by a dielectric sheet.   We shall
also assume that the propogating microstrip mode can be
approximated closely by a TEM mode[3].

It can be shown   that the signal to
input power is related by:

$$\frac{S}{P} = 0.163 \frac{W_o}{W_r} Q \qquad \qquad ..(4.1)$$

While the energy stored outside the aperture for an electric
dipole,

Using this analysis* we have calculated the S/P ratio to be:-

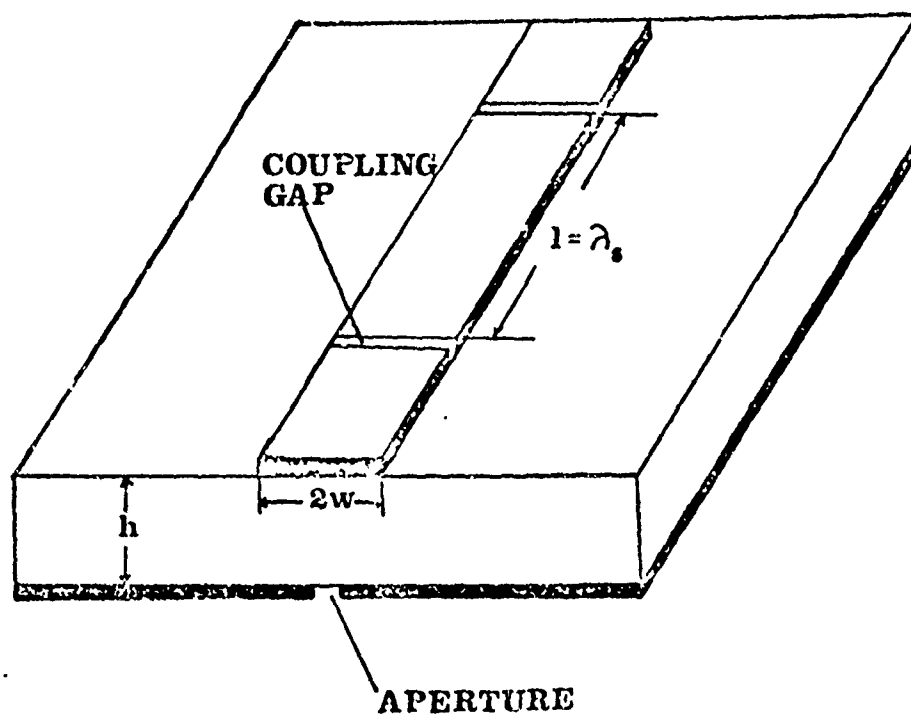* (The detailed analysis may be found in A.Husain's PhD Thesis).

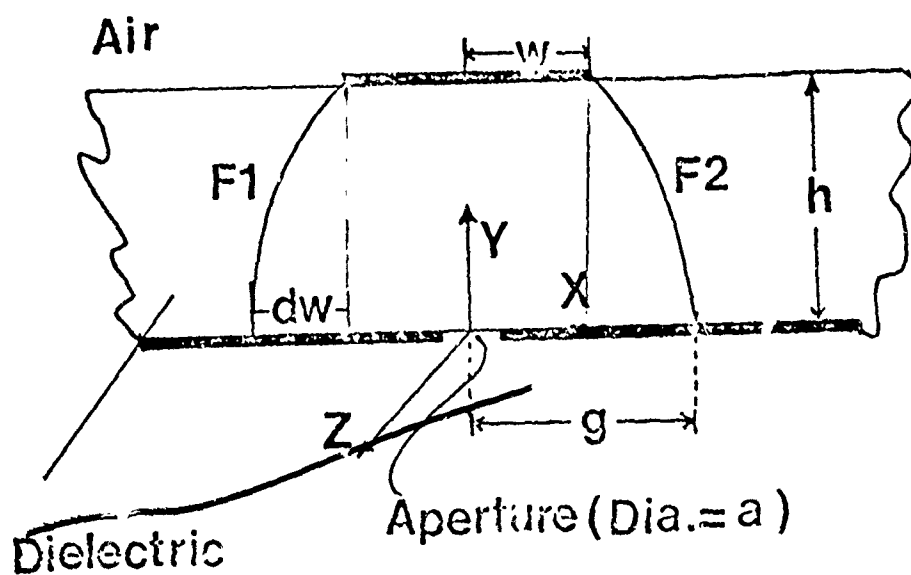Figure 4.3   Geometry of Microstrip Resonator

Figure 4.4   Geometry of Strip and Variables
Used in Text

$$W_o = \frac{7}{648\pi} \, a^3 \varepsilon_o \, E'^2 \qquad \qquad ..(4.2)$$

where E' is the electric field normal to the plane of the aperture. It now remains to evaluate the energy stored in the resonator and determine the field incident on the aperture in the ground plane.

A detailed theory to evaluate E' and W_r would be very complicated. As we only required an approximate guide to the optimum resonator design parameters, we have developed a first order theory based on Wheeler's analysis[3].

Thus for a particular aperture size and frequency of operation, we must select the parameters: h, w/h, ε_r and Q in order to optimise the S/P ratio. Equation 4.14 suggests that for large S/P we need to increase Q and w/h, while decreasing ε_r and h. However, these four quantities are not simply related. For a given h, a decrease in ε_r increases the characteristic impedance Z_o and hence changes the Q. The radiation that occurs from an open circuit microstrip resonator also varies with ε_r, Z_o, h, and operating frequency. Troughton[2] has shown that if these factors are taken into account and allowance made for the resistive losses, then the Q (for a given h) is a maximum at a particular impedance.

In the numerical optimisation procedure, the value of Z_o for a particular, w/h, was obtained from the work of Yamashita and Mittra[4], and the corresponding Q from the theoretical work of Troughton[5]. The effective dielectric constant was calculated from equation 4.6. Using equation 4.14, it can be shown that for h = 0.25 mm, the signal to

h = 0.625 mm or 1.25 mm; consequently, h, was set to the minimum value (0.25 mm) for which experimental results were available.

Fig. 4.5 shows that the S/P varies with the parameter w/h for different values of k. The S/P ratio was calculated for an operating frequency of 10 GHz, and an aperture diameter of 300 μ. It is clear from the figure that, subject to assumptions made earlier, the optimum parameters of the linear resonator are:

$$h \quad = \quad 0.25 \text{ mm}$$
$$2w/h \quad = \quad 1.25 \pm 0.25$$
$$k \quad = \quad 9 \pm 1$$
$$Z_o \quad = \quad 45 \pm 4 \text{ ohms}$$

The variation in the various resonator parameters shown above were calculated for a 5% reduction in the signal to power ratio. The S/P ratio for the above parameters were calculated to be 0.5×10^{-4}.

This effect was taken into consideration in the calculation of the optimum resonator parameters using Wheelers theory. The result of the correction is shown in Fig. 4.7 where we have plotted the optimum S/P vs. w/h curve (for k = 8.9), as well as the uncorrected version for comparision. The effect of this correction is to alter the optimum value of w/h slightly from w/h = 1.25 to w/h = 1.4.
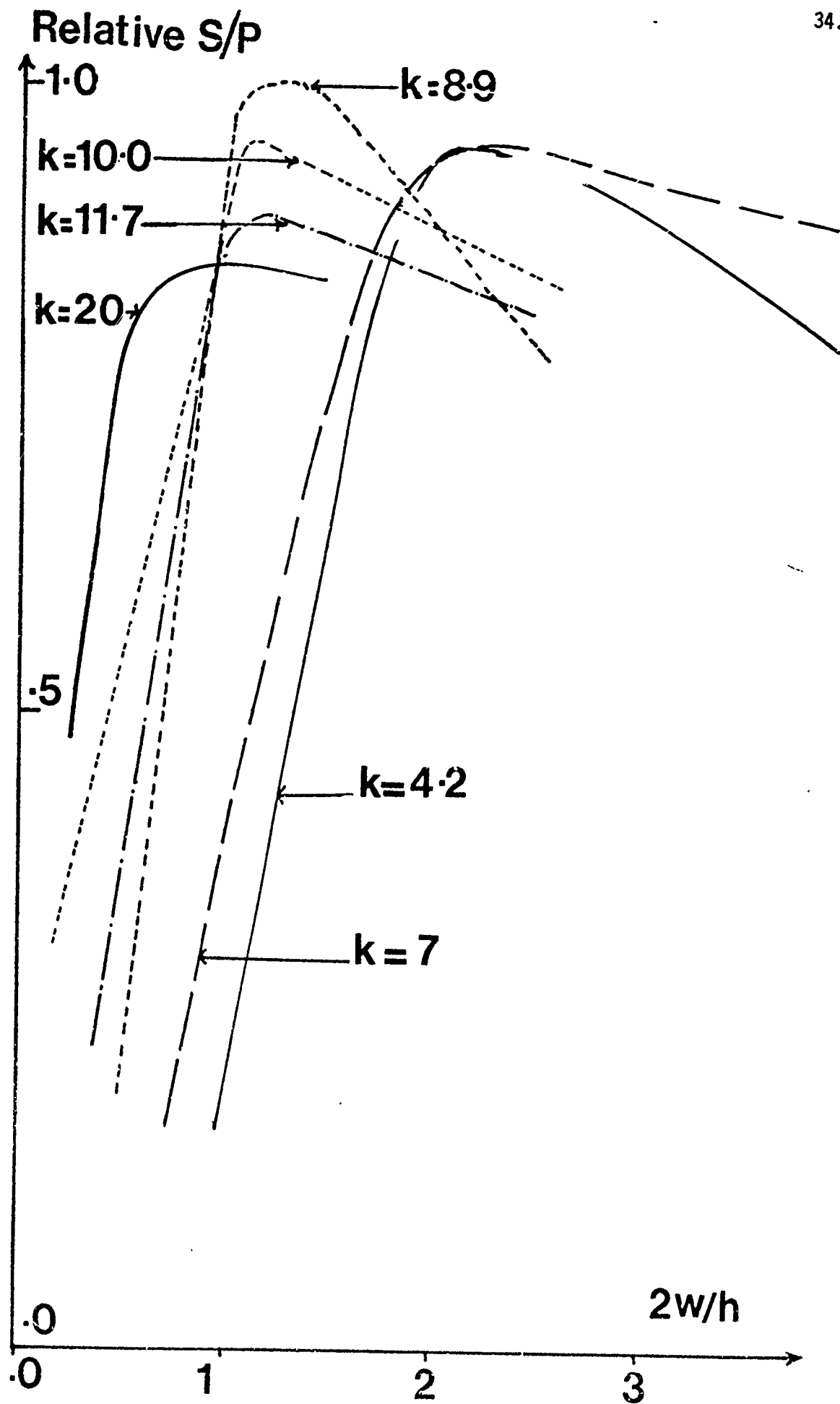
Figure 4.5   Optimisation of Signal to Input Power
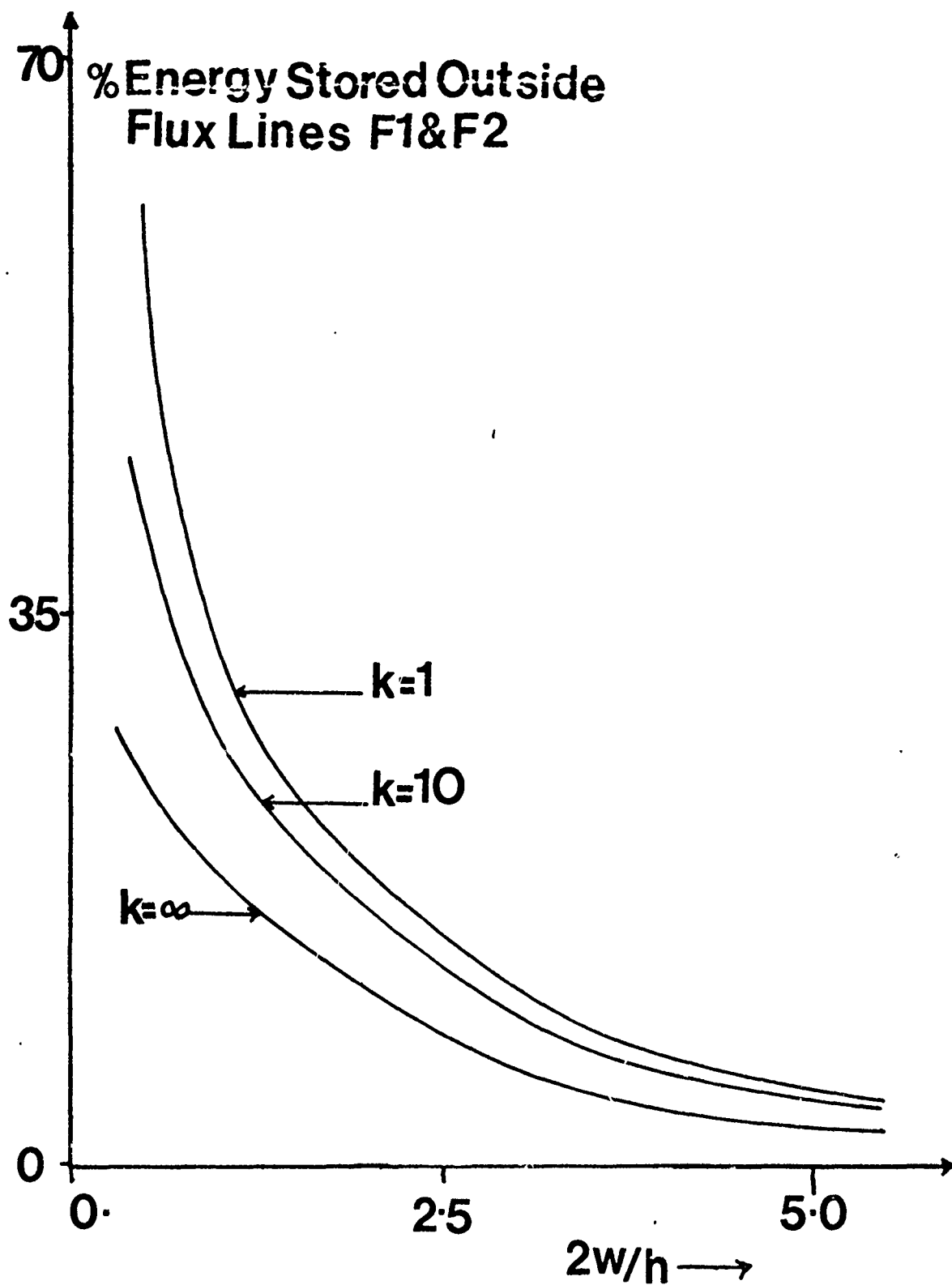by varying w/h and k

Figure 4.6   Ratio of Energy Stored Outside
             Flux Lines F1 and F2 to the
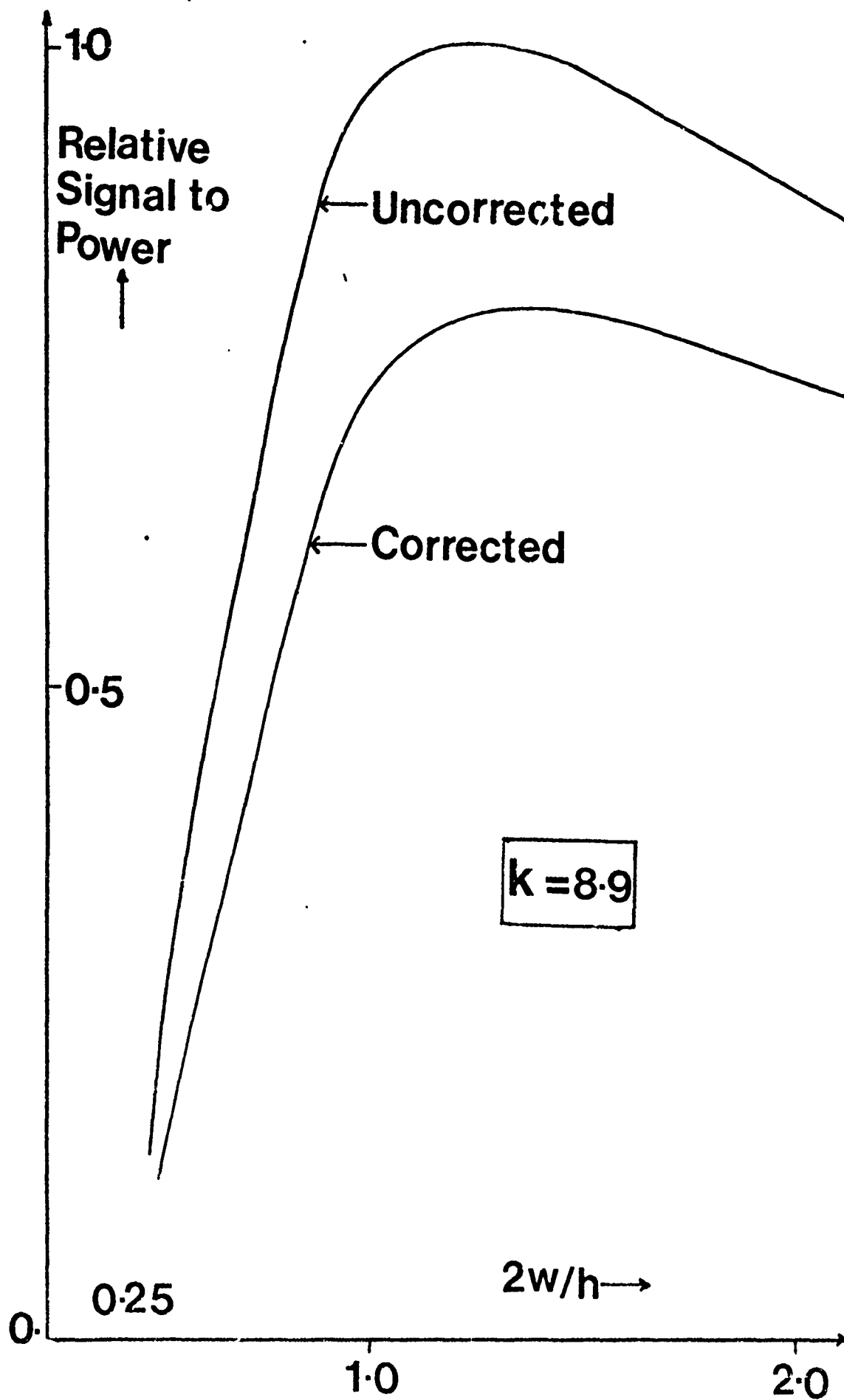   Total Energy Stored for Varying
             w/h and k

Figure 4.7   Optimum Resonator Parameter Curve Corrected for
Energy Stored Outside Flux Lines F1 and F2

Having calculated the optimum design parameters, we
can now discuss some of the technological aspects of resonator
construction.   The microstrip resonator was fabricated on a
copper coated alumina substrate using conventional photolith-
ographic techniques.   The substrates used had a surface finish

•   In practice, we found that the optimum 0.25 mm
thick substrates were very fragile, and had a tendency to
crack easily under slight pressure (such as an accidental
collision with the vibrating object).   We therefore resorted
to use a thicker substrate of h = 0.5 mm, even though this
meant we had to sacrifice a loss in signal of about 3dB.

In our experiments, the microstrip circuit was
mounted on a jig.   This was constructed to allow us freedom
to scan large specimens beneath the aperture plane;   which
required the probes to be arranged to couple to the microstrip
at an angle (Fig. 4.8);   resulting in some radiation from the
bends in the probes.   There was also radiation from the edge
of the microstrip circuit.   One consequence of this was that
a spurious signal was generated;   this arose from the modulation
of the energy leaking from the substrate by objects (vibrating
at the same acoustic signal frequency) outside the resonator.
We found that this effect could be virtually eliminated by
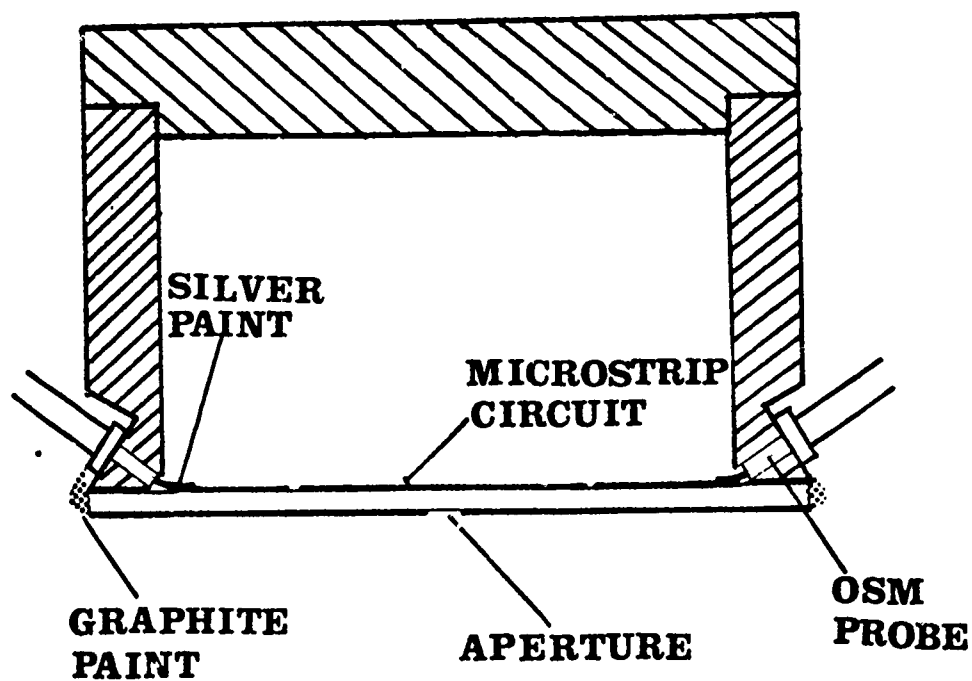applying graphite paint around the edges of the substrate.

Figure 4.8   Experimental Details of
Microstrip Circuit and
Jig Assembly

The microstrip configuration described presents considerable advantages over the open resonator which was used in our initial experiments. The main advantages are outlined below:

1. For similar conditions of operation, the signal we obtained is approximately 10dB's higher in the microstrip case. The physical significance of this fact is that: though the microstrip resonator has a much smaller Q (about 100 times smaller), the microstrip resonator is very much better at confining the substrate fields to a smaller area than the open resonator.

2. In our initial experiments with the open resonator, drift in the transmitter frequency as well as variations in the cavity resonator frequency was the major source of signal instability. This effect was largely overcome by the incorporation of a frequency tracking system which compensated for fluctuations in either the cavity resonant frequency or the variations in the transmitter output frequency. Owing to the fact that the microstrip resonator is an inherently low Q device as compared to the open resonator, this

places a much less stringent requirement on
the tolerable frequency drift due to the
transmitter or the cavity; consequently
the frequency tracking system was not required
for the microstrip case.

3. The microstrip resonator is not only substan-
tially easier to fabricate but it is far
simpler to alter its design e.g. the coupling
gaps may be optimised by etching off the
unwanted copper. In addition, the micro-
strip version is considerably lighter and more
compact than the open resonator. Microstrip
technology may be used to integrate many of
the components used in our system onto one
single substrate (Fig. 4.10): this is not
only convenient as a space saving operation,
but has the added advantage that the resulting
system would be significantly less sensitive
to both thermal and microphonic effects.

4. In the case of the open resonator, air coupling
between the vibrating object and the lower
resonator plate resulted in the generation
of a slowly varying spurious signal as the
object was translated beneath the plat.
The effect of a fluctuating spurious signal
is to reduce the overall system dynamic range.
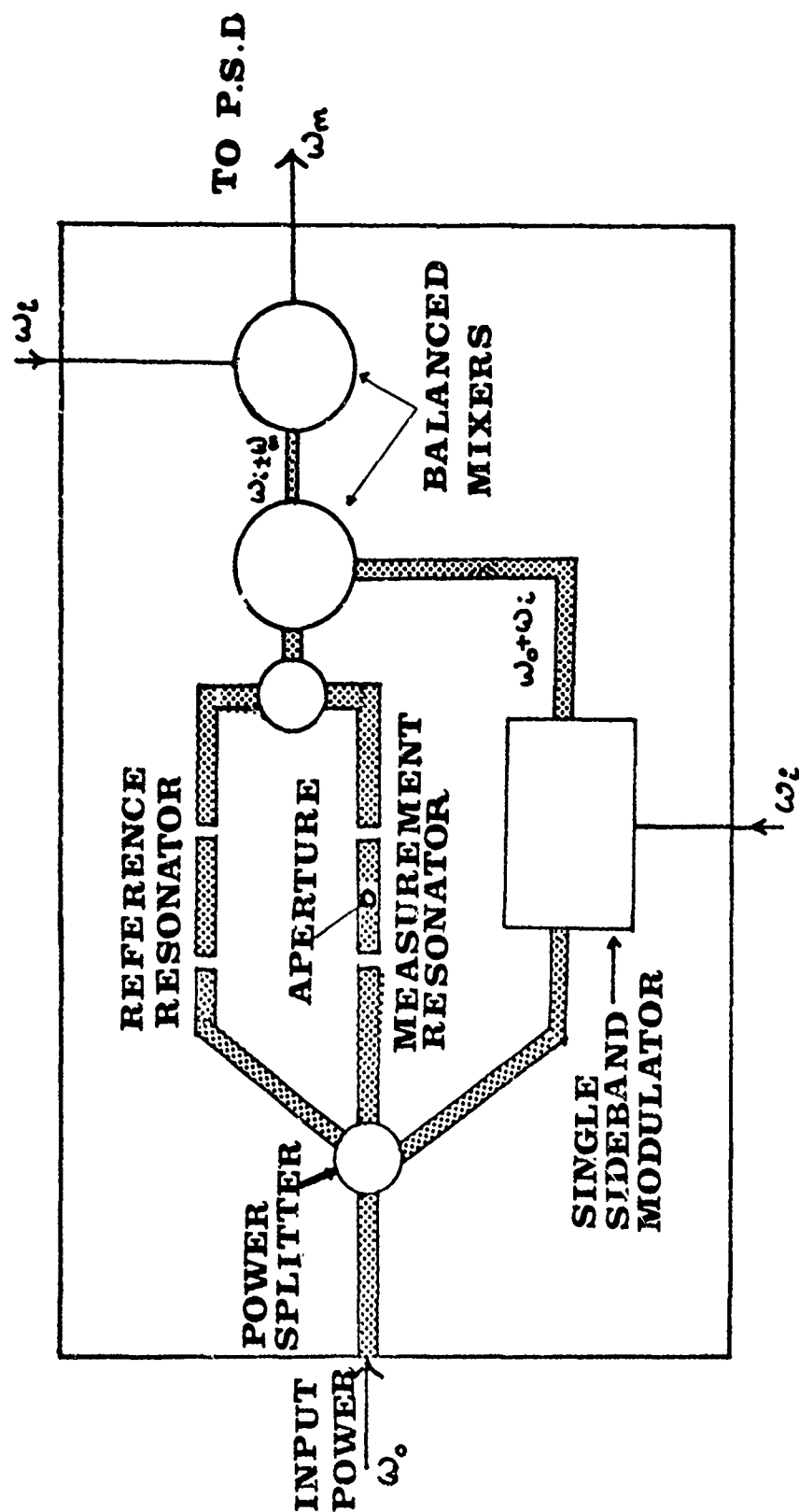Though this effect could be eliminated by

Figure 4.10   Components which may be integrated into
One Microstrip Circuit

suitable signal processing we would loose some of our main signal. This problem does not occur in the microstrip case.

5. In its present form, the microscope is limited to the inspection of flat surfaces. However, the adoption of a microstrip resonator opens up the possibility of inspecting curved surfaces, by resorting to flexible substrates.

6. One significant advantage of the microstrip resonator is that by suitably positioning the aperture in the ground plane we can produce either an electric or a magnetic dipole; it would be very much harder to implement this sort of change in the open resonator.

4.2 Aperture Design

The aperture is perhaps the single most important component of our system. We have already demonstrated that the shape and size of the aperture determines the signal strength, depth of field and the resolution we can achieve. In Section 2.3 we established that the ability of the microscope to image changes in the properties of an object depended on the form of illumination and the use of apertures which were small as compared to the wavelength.

The significance of the aperture dimension on the resolution has already been established. In our experiments we have used circular apertures down to $\lambda/200$ in diameter and have demonstrated a two dimensional resolution capability of better than $\lambda/375$. However, if we wished to improve the resolution by a factor of say 10 by decreasing the aperture diameter, the signal would be reduced by a factor of 30dB. A more promising approach for certain NDT applications, such as detecting cracks, which usually have large length to width aspect ratios, is the use of a rectangular aperture. To a first approximation the energy stored by an aperture is proportional to its area (provided the significant dimension is very much less than the wavelength). If we keep the areas of the circular and the rectangle equal, we can obtain roughly the same signal. By appropriate choice of the length of the rectangle, we can maintain the signal level as compared to the circular aperture and improve the resolution by decreasing the width. In addition, the time required to effect a scan would be reduced by the factor L/a, where, L, is the length of the rectangle and, a, is the aperture diameter. The penalty for improved resolution in the X direction (Fig 4.11) is a corresponding decrease in resolution in the Y direction. Inspite of the loss of resolution in one direction, this technique seems eminently suitable for detecting the presence of cracks in metals.
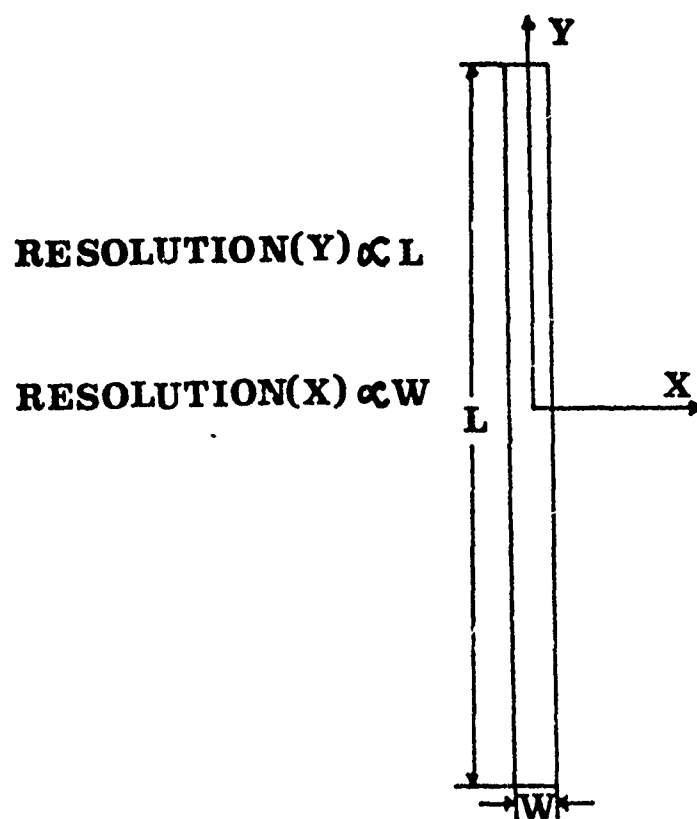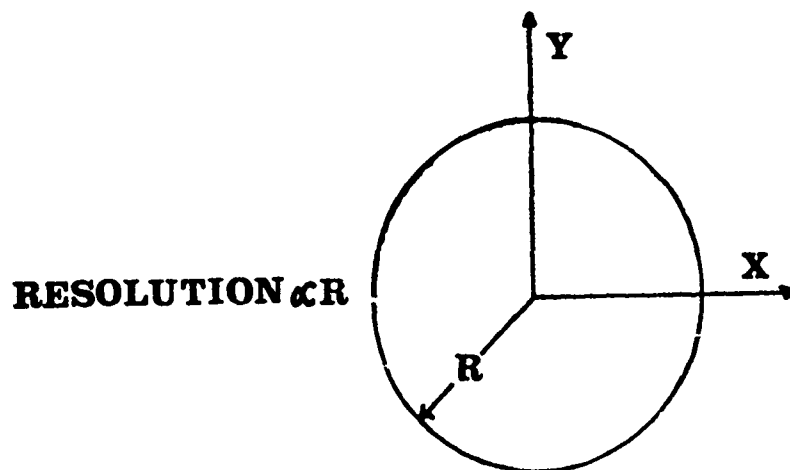
RESOLUTION $\propto$ R

RESOLUTION(Y) $\propto$ L

RESOLUTION(X) $\propto$ W

Figure 4.11   Circular and Rectangular
                 Aperture

5.   THE EXPERIMENTAL SYSTEM

In our system we are using the reflected wave from the object and consequently, the detected signal consists of the large primary reflection from the resonator ground plate and the very much smaller signal from the object. By only detecting the signal of interest, we can substantially increase the input power. An effective technique to discriminate between these two signals is to make the resonator part of a bridge circuit. The components in the other arm being adjusted so as to suppress the large incident reflection. The "contrast" can be further enhanced by vibrating the object at an acoustic frequency and subsequently searching for this component in the receiver system.

These considerations led us to adopt a suppressed-carrier-single-sideband arrangement; the main elements of the system which are shown in Fig. 5.1. The power from a 10 GHz impatt oscillator is amplified to 1 watt by a TWT amplifier which feeds the microstrip resonator; the attenuator and phase shifter in the bridge circuit are adjusted to suppress the carrier so as not to overload the first mixer. The single sideband modulator (SSBM) generates a local oscillator signal which is locked to the source, and which after mixing yields an i.f. of 30 MHz. This is then demodulated using a homodyne technique and the signal at ω_m is finally compared in a phase sensitive detector supplied with a reference from the acoustic modulator source. The output of the phase sensitive detector can then be displayed.
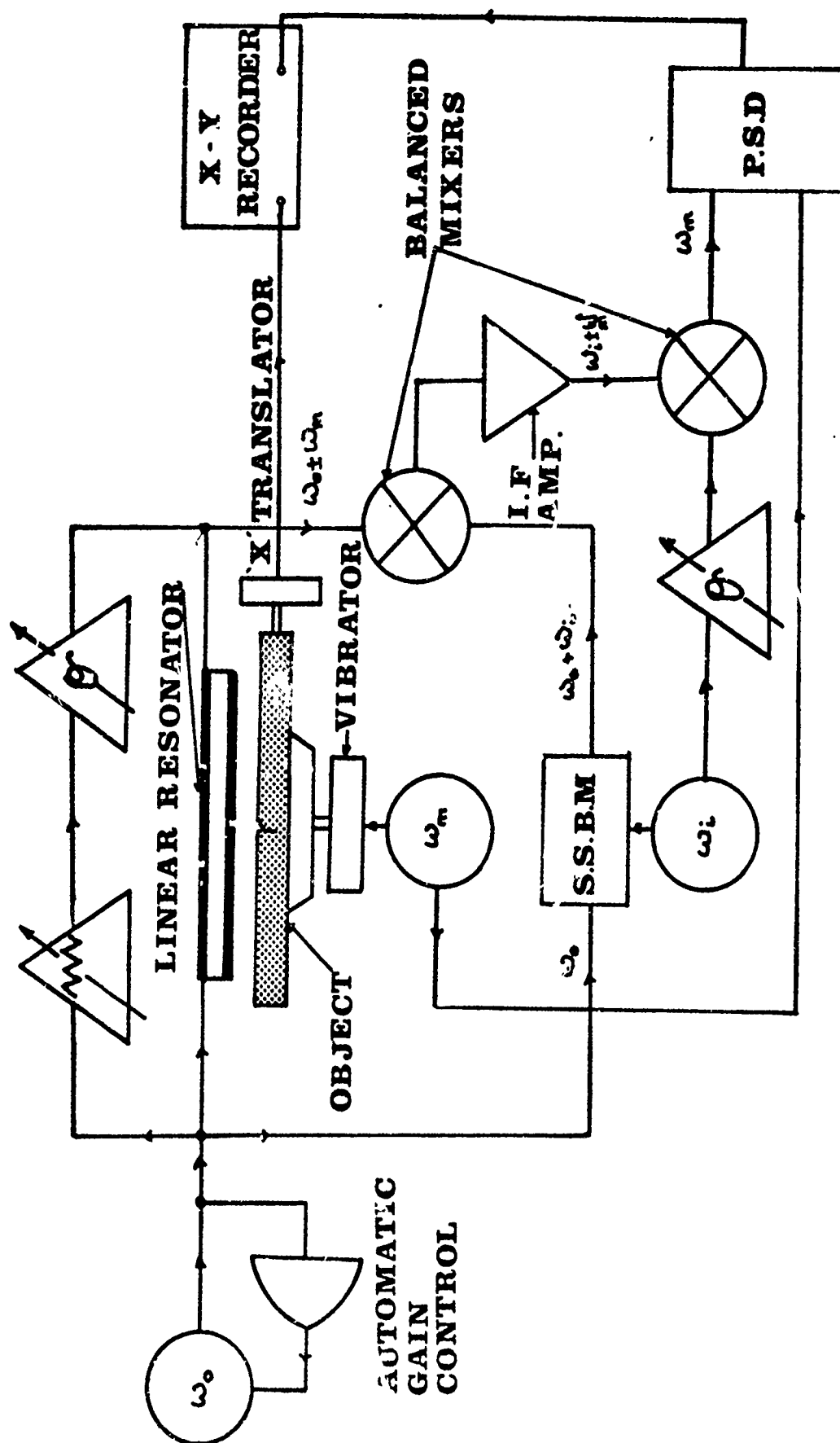
Figure 5.1   Experimental Configuration of Microscope

A theoretical analysis which examined the noise processes associated with transmitter and the various received components was carried out in order to determine the major sources of system noise.

The nalysis indicated that only when the input power exceeded 100 watts would one be dominated by a multiplicative noise process.

Let us consider the "noise" processes associated with the transmitter. We have established that the effects of transmitter multiplicative noise may be neglected in estimating the signal to noise ratio. We have verified this experimentally by plotting the overall system signal to noise ratio as a function of input power. The result is shown in Fig. 5.4, which clearly indicates that there is no evidence of transmitter multiplicative noise for powers up to about 10 watts.

We have found, that the usable dynamic range was substantially lowered on account of slow variations of the source output power which could not be distinguished from the wanted signal. These long term fluctuations (occurring at intervals greater than 1 second in our case) are primarily due to thermal effects in the source and variations in the current supplied to the impatt oscillator. This problem was largely overcome by the inclusion of an automatic gain control system (AGC) based on a PIN modulator;

Using this technique, we have reduced fluctuations in the output power from $1: 5 \times 10^{-3}$ of the signal to about $1: 10^{-5}$; this was achieved for variations occurring up to about 20 Hz. Fig. 5.5 shows a trace of the output signal from the system with and without the AGC operating. These results indicate that even with the use of the AGC system, we are limited by slow variations in the transmitter power. The actual usable dynamic range is therefore only 50dB's as co...ed to the short term S/N

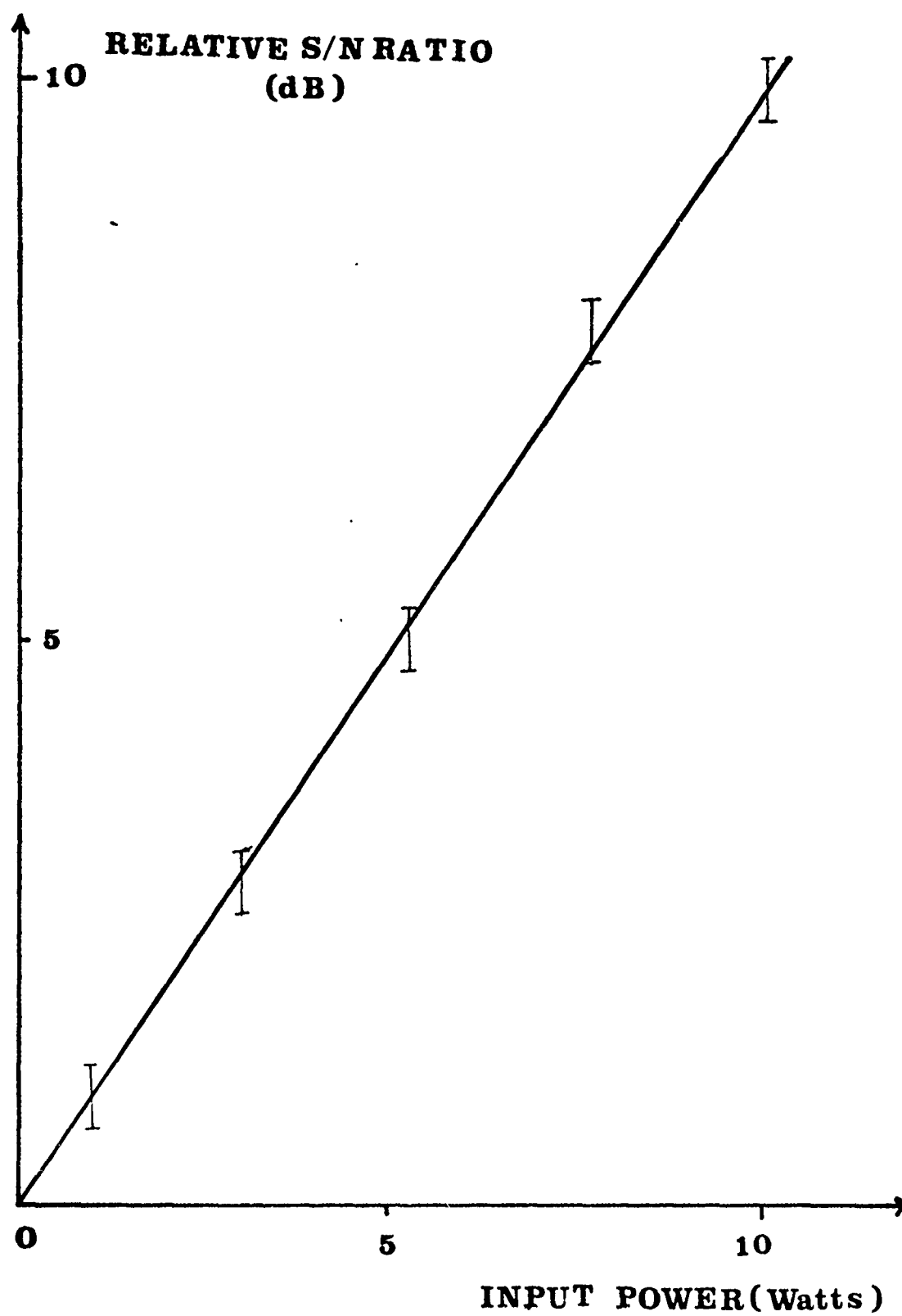**RELATIVE S/N RATIO (dB)**

INPUT POWER (Watts)

Figure 5.4   Relative S/N Ratio vs Input Power

Variations of the object/aperture spacing while translating the object results in the generation of a spurious signal undistinguishable from the wanted signal; secondly, any deviation from parallelism between the object surface and the aperture plane results in a variation of the output signal which limits the maximum sensitivity that can be achieved.

The object and vibrator were scanned below the aperture by a X-Y translation stage (obtained from a travelling microscope). Even slight unevenness in the slide mechanism results in a spurious signal; for example, a deviation in the mean separation of only $\pm 1\,\mu$ would cause a fluctuation in the output signal of about $\pm 0.1\%$. It is therefore meaningful to distinguish between the "static" and the "dynamic" signal to noise ratio. The static measurement being made with the object only vibrating under the aperture, and the dynamic measurement being taken while the object is scanned while vibrating beneath the aperture. The dynamic signal to noise ratio was measured for various positions along the translation stage while the specimen was being scanned; the final usable signal to noise was $45 \pm 2dB$.

Let us consider the noise added by the receiver. It was found that the first mixer was the major source of receiver noise. The other sources of noise in decreasing importance were the second mixer, and the i.f. amplifier.

Fig. 5.6 shows the relative noise added by each receiver component.
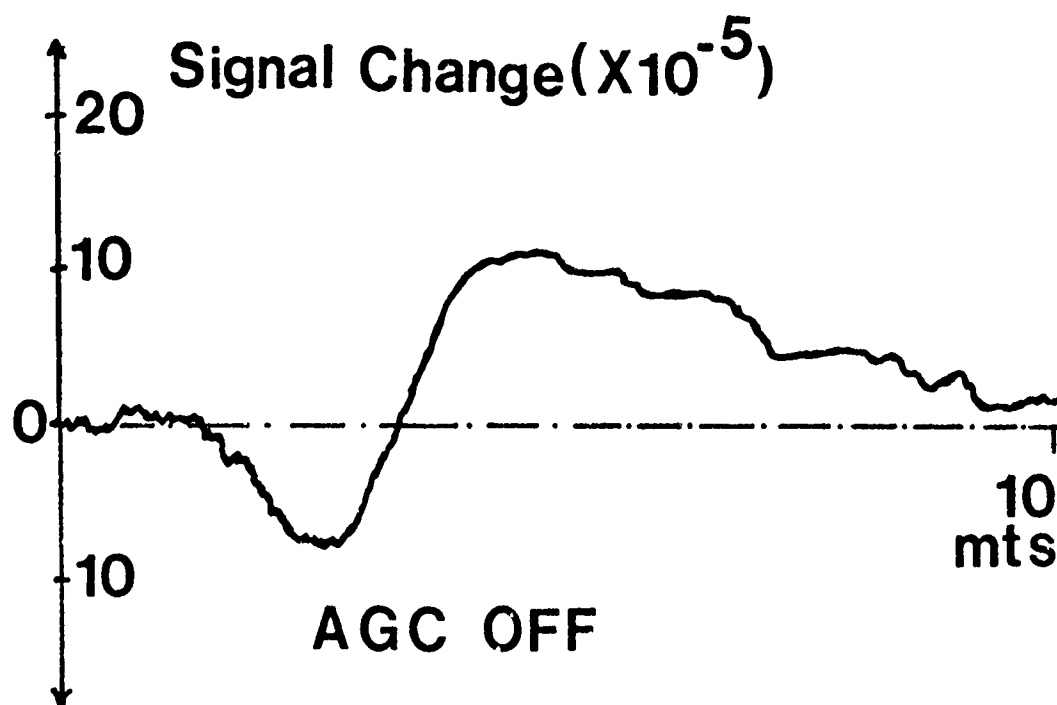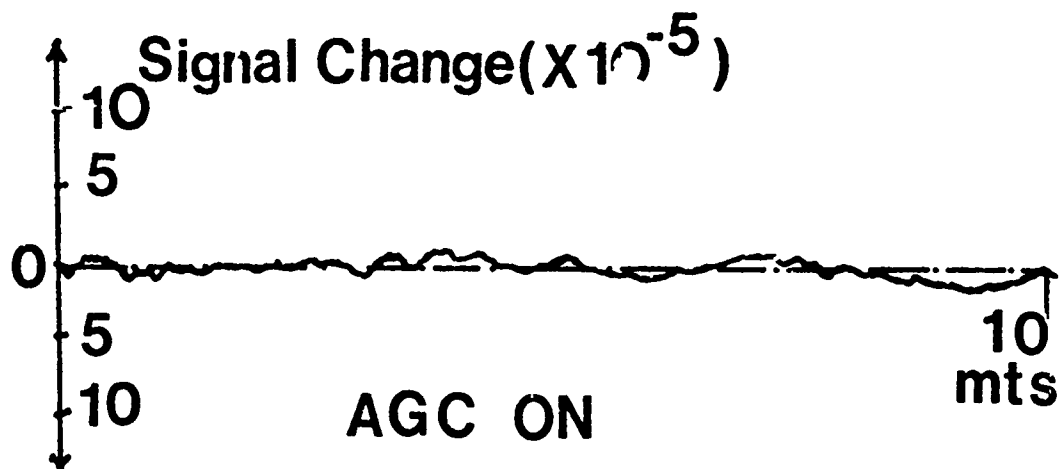
Figure 5.5   Evaluating Performance of AGC –
Signal Output with and without
AGC in Operation

We have now established the factors which are limiting the usable dynamic range of the microscope. These are in decreasing importance: variations in the object/aperture separation, fluctuations in the source power (even with the AGC in operation), receiver additive noise, and finally transmitter multiplicative noise.

The signal to noise is dependent on the nature of the specimen, the aperture dimension and the final system bandwidth. The resolution and detectability is also dependent on these three parameters. The overall system performance is thus necessarily a compromise between the sensitivity, resolution and the time required to effect a scan. The following example illustrates this point.

The effects of fluctuations in the transmitter and variations in the object/aperture distance can be reduced by using more sophisticates signal processing techniques on the records obtained. Consider the case when we are seeking to detect a specific type of defect such as a crack. We possess a priori knowledge that the cracks are small and hopefully rare. This information can be used selectively to filter out very high fourier components that are physically not possible, as well as filtering out the lower frequencies which do not correspond to the typical crack signature; the deconvolution procedure described in Chapter 3 could be used after this preliminary filtering to further enhance the final signal to noise ratio.
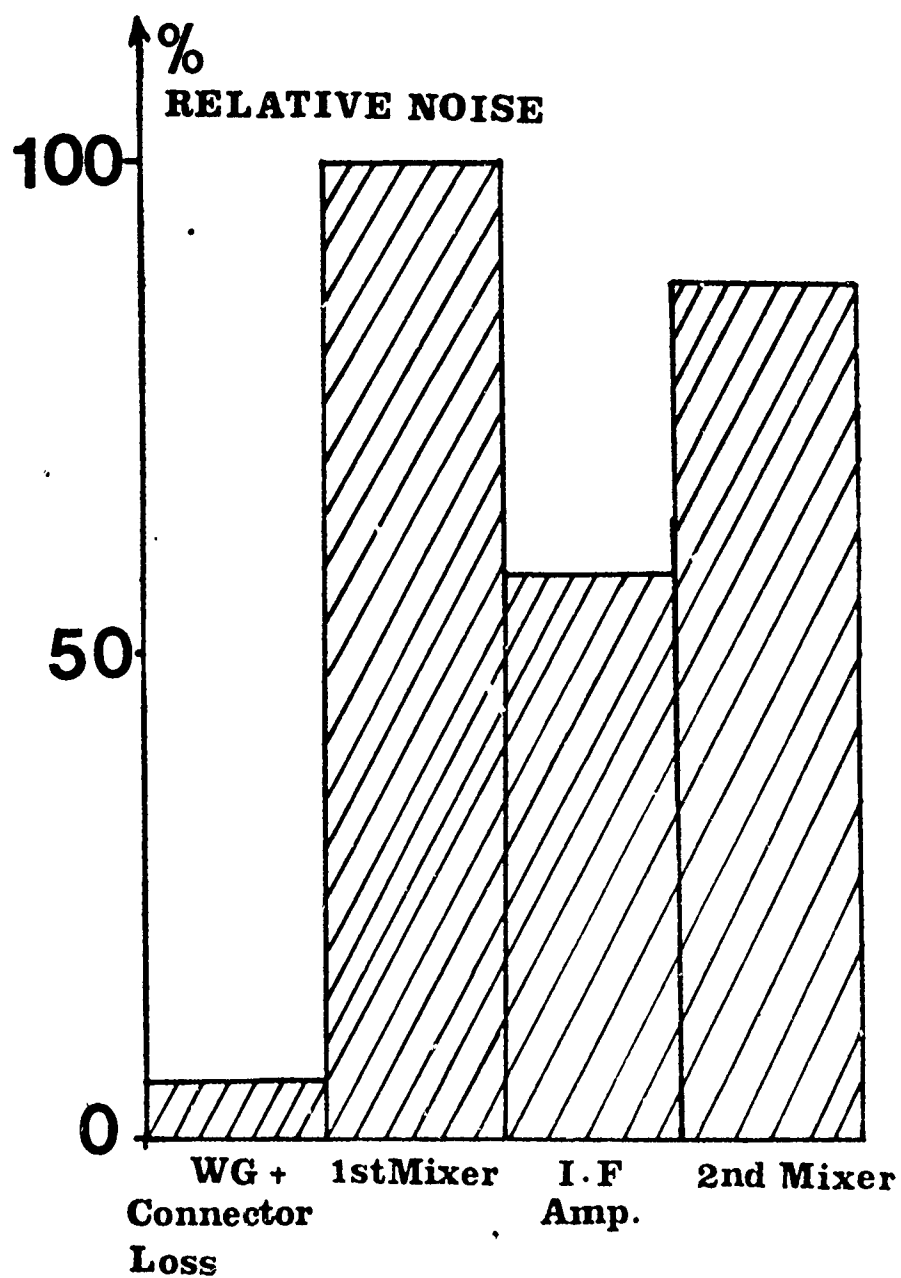
Figure 5.6   Calculated Relative Noise ... ...
by Receiver Components

6. CHARACTERISING THE PERFORMANCE OF THE MICROSCOPE

In this chapter the results obtained from a series of experiments designed to assess the performance of the microscope and correlate these results with the theory developed ea. ie are presented.

6.1. Experimental Operating Conditions

The operating conditions under which the measurements were made are as follows: 1 watt, 10 GHz source was used to illuminate the 300 u aperture in the microstrip resonator- the samples were positioned at a mean position of about 50 μ away from the microstrip ground plane, and were vibrated (at 300 Hz) at an amplitude of approximately $\pm$ 30 μ. The samples were translated beneath the aperture at a constant speed of about 2.5 mm per minute. In all the experiments the AGC system was in operation. For tests on metal objects, the aperture was illuminated so as to produce a magnetic dipole. This was because the signal due to a magnetic dipole is roughly 6 dB's higher than the corresponding signal obtained with an electric dipole for metal objects.

6.2 Signal vs. Distance of Plane

We have developed an approximate theory of the instrument to be able to predict how the signal varies as we move a conducting plane away from the aperture. As pointed out earlier, this theory becomes progressively more suspect as the object approaches within one aperture diameter. Nevertheless, we find some encouraging agreement between the theory and experiment as shown in Fig. 6.1. The best fit here is obtained using two images in the range 0.25 to 1.0 aperture diameters away from the diaphragm. It should be noted that the theory was derived for a square aperture whereas in practice we are using a circular one; and that the
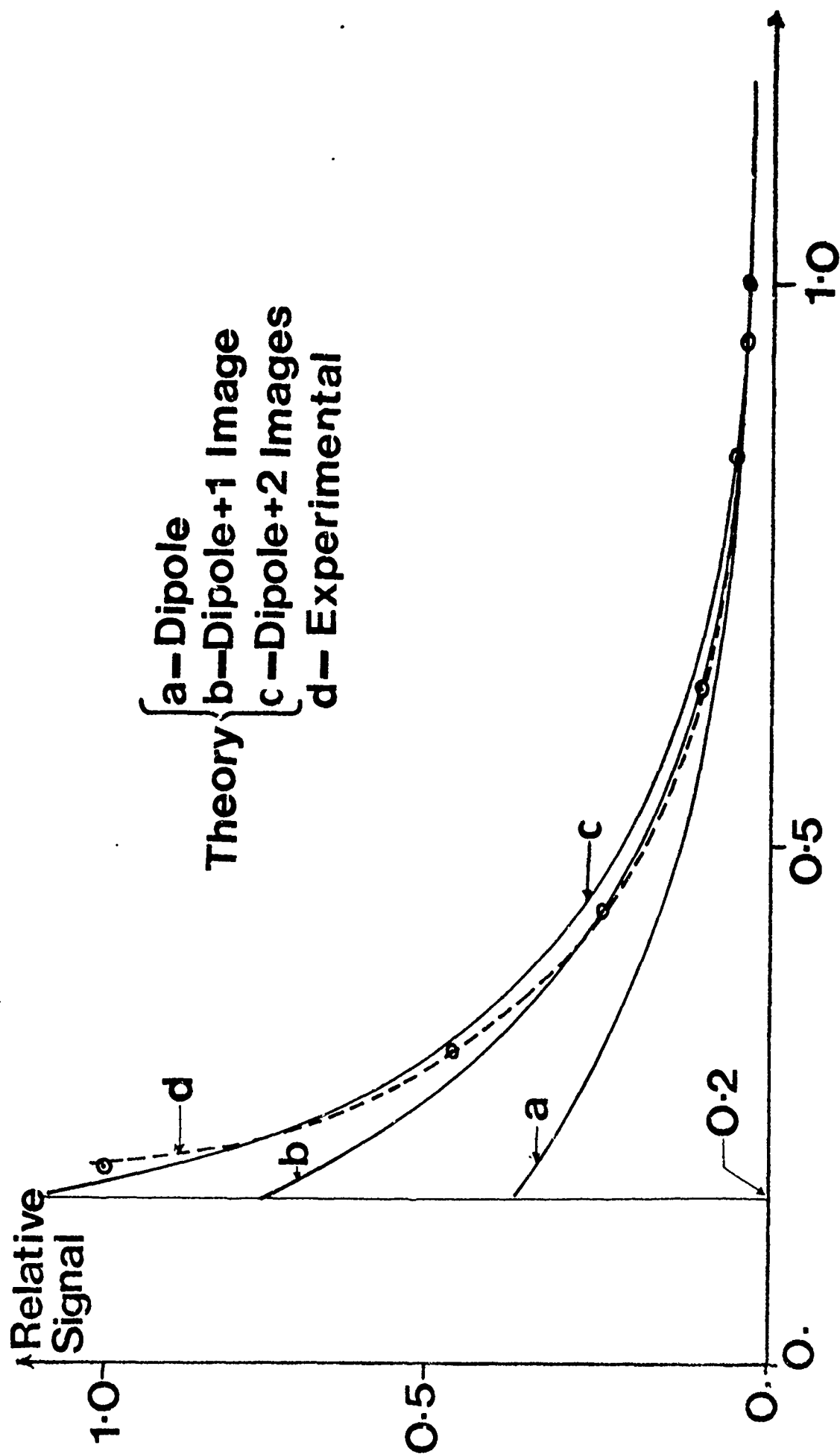
Figure 6.1   Signal Strength as a Function of the
              Displacement of a Metallic Object

theoretical and experimental results were matched at a
distance of one aperture.

6.3   Signal vs. Aperture Diameter

In Chapter 3 we established that the signal was pro-
portional to the cube of the aperture diameter.   Experiments
were performed to test the validity of this theory.   Apertures
of 350, 300, 250 and 200 microns were fabricated in the ground
plane of the microstrip resonator and the signal obtained as
a metallic object was vibrated at a constant amplitude under
each aperture was recorded.

The test object was vibrated at a fixed amplitude
of about $\pm$ 30 μ, with a mean separation of approximately 50 μ
away from the aperture plane.   In order to compare the signal
obtained from each aperture, we must normalise these results.

The
normalised signal to noise ratio for these four apertures
is plotted in Fig. 6.2.   The theoretical and practical
results agree within the limitations of the experiments, and
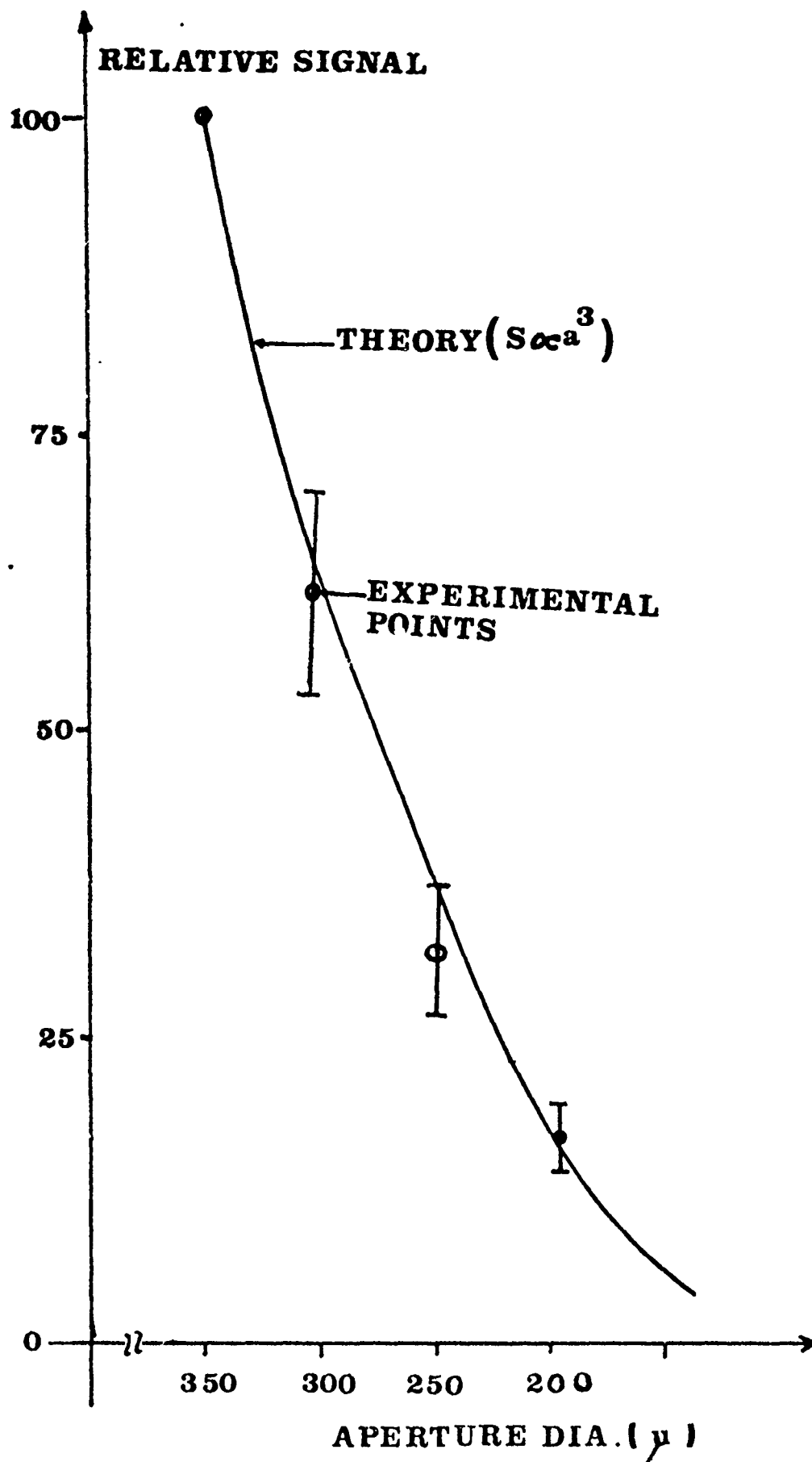the calculated correcting factors.

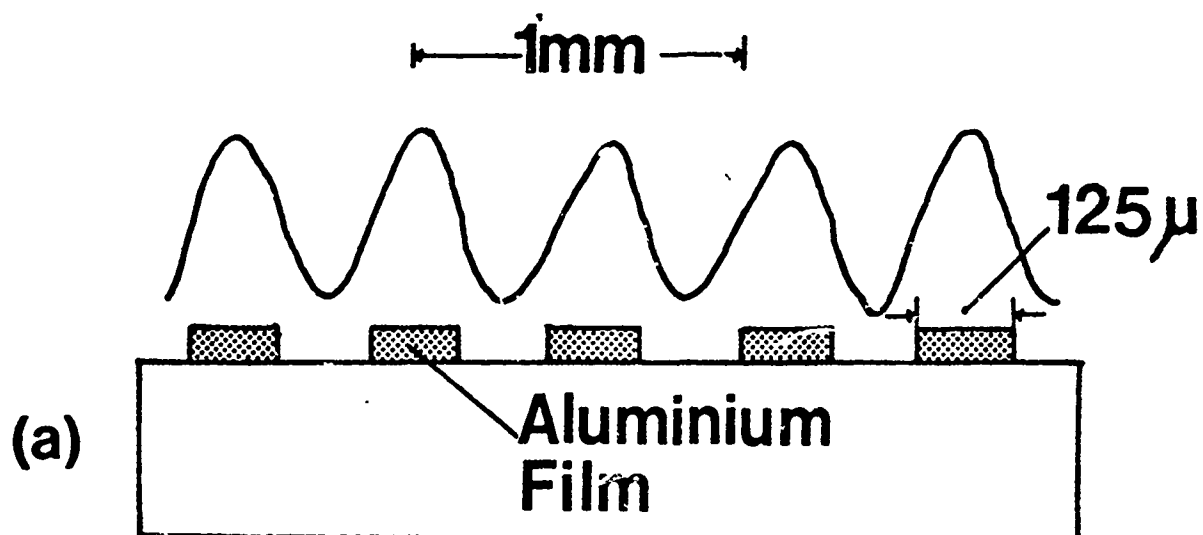Figure 6.2   Signal as a function of Aperture
Diameter

6.4   Resolution Tests

The attainable resolution is limited by the aperture
dimension, the dynamic range of the detection system, and the
properties of the sample we are investigating.   We have carried
out tests on metallic gratings consisting of a 0.2 μ aluminium
film on glass substrates to assess the resolutions we can
achieve for such an "ideal" object.   Fig. 6.3(a) shows a
scan across a grating of line-width 125 μ using an aperture
diameter of 300 μ.   Fig. 6.3(b) shows a similar scan obtained
with an aperture diameter of 200 μ, for a grating having a
line-width of only 80 μ;   this result demonstrates a resolution
capability of better than $\lambda/375$ with the present instrument.
Experiments on polished glass substrates are admittedly at least
one step away from realistic n.d.t. applications;   however,
there are some problems which do involve the detection of
microcracks on smooth metallic surfaces;   and the results
obtained provide a useful guide to assess system performance.

6.5   Results on Slots in Metal Objects

We have developed an approximate theory to be able
to predict how the signal varies as a function of the depth
and width of a slot located symmetrically below a square
aperture.   Quantitive experiments were performed using a
circular aperture to test the validity of this theory.

Variable depth spark machined slots in brass of the
same width were investigated.   The results are shown in
Fig. 6.4(a), where we have plotted the maximum signal from

(a)

├─1mm─┤

Aluminium Film

125μ

Aperture Dia.=300 μ

Resolution = λ/240

(b)

├─1mm─┤

80μ

Glass Substrate

0.2μ
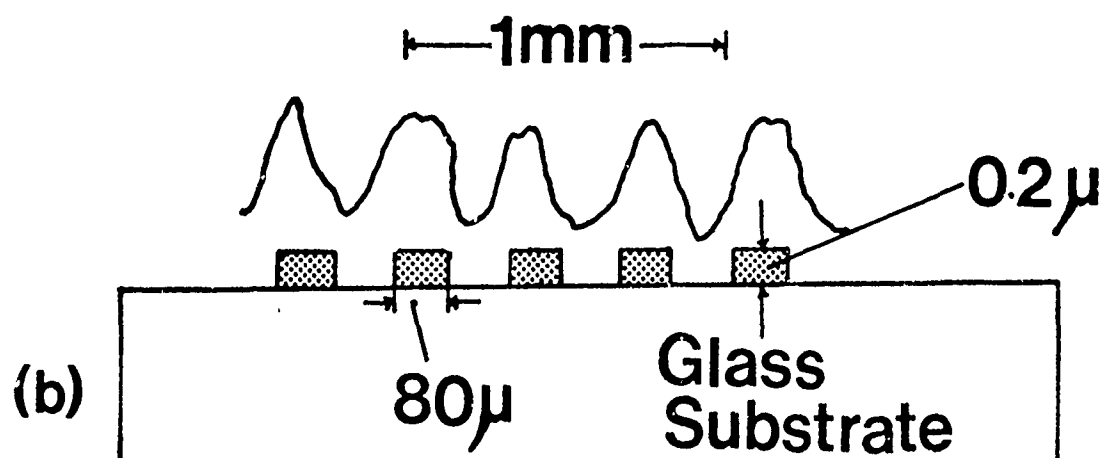
Aperture Dia.=200μ

Resolution = λ/375

Figure 6.3   Resolution Tests on Thin Metallic Gratings,
for Two Periodicities

two slots of different cross-sections against the depth of the
slot, together with the theoretically predicted results.
The theory and experiment suggest that we are not able to
provide information of the depth of the slot if the WIDTH/
DEPTH$\ll$1. However, for certain n.d.t. applications it is
only necessary to indicate the presence of the defect and
for these cases the instrument could be used to advantage.

Experiments were also carried out on slots of
variable width and constant depth. The results are shown
in Fig. 6.4(b) and are compared with the curve computed from
the theory developed in Section 3.4. While the theory
predicts that the signal should be proportional to the square
of the width, the experimental results indicate that the
dependence on width is in fact more nearly linear. The gap
between the theory and experiment has been previously explained;
any improvement in the theory would entail performing a detailed
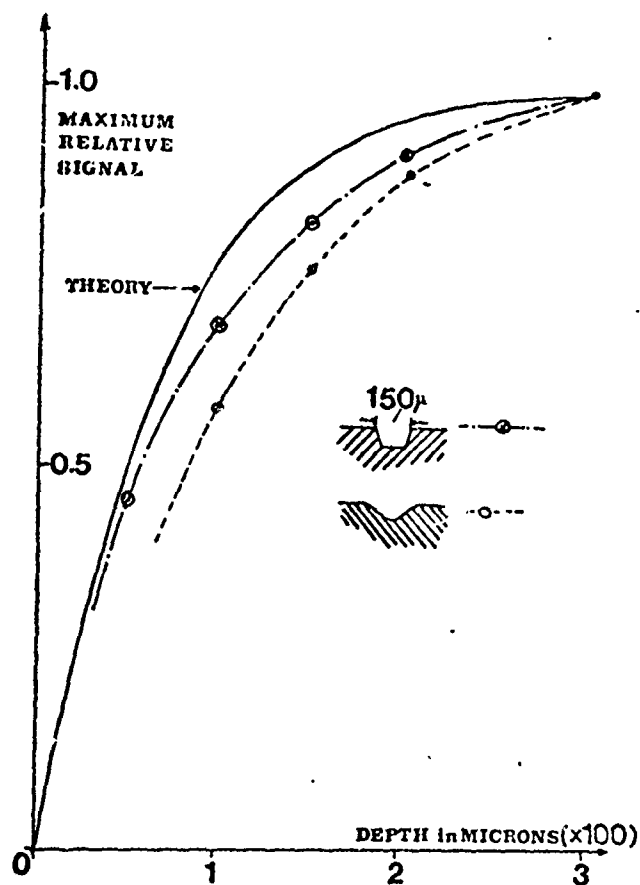quasi-static field calculation.

Figure 6.4(a)   Signal Strength vs. Depth of Slot for
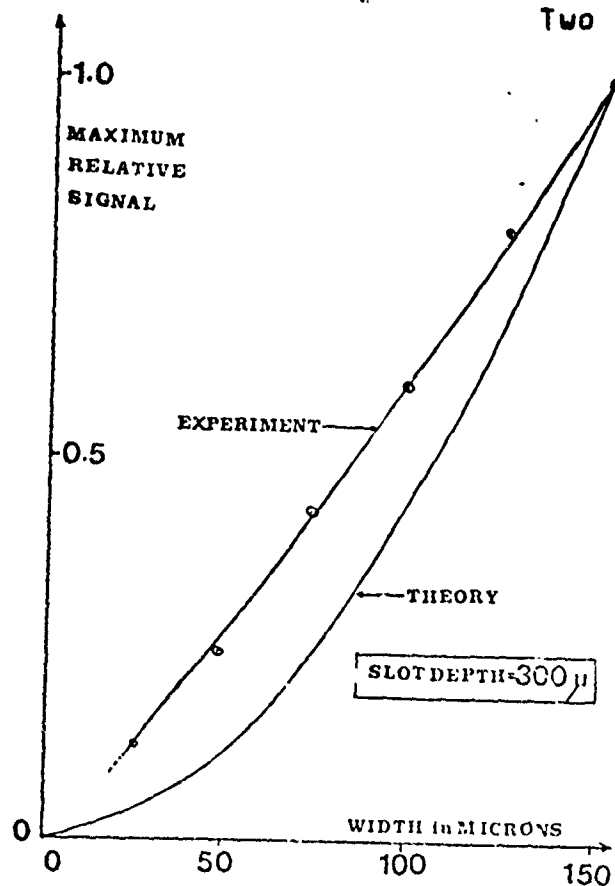Two Cross-Sections

Figure 6.4(b)   Signal Strength vs. Width of Slot

7.   APPLICATION TO NON-DESTRUCTIVE TESTING

In this chapter we assess the potential application of our microscope to the non-destructive evaluation of surface topography and surface properties of materials.

Microwave methods are naturally the most direct for testing materials such as dielectric[6,7] and ferrite materials[8] used in microwave components. Their use is also increasing in other n.d.t. problems such as the evaluation of bonded films[9], of surface texture[10], and detection of fatigue cracks in metals.

Most of these methods rely on the mode conversion or scattering due to the defect on the illuminated surface. Such methods can be made remarkably sensitive in detecting single defects. One could also imagine that they might come into use for the statistical evaluation of surface finish. However, compared to other non-destructive testing techniques such as X-rays, acoustics and luminescent paints, they suffer from the poor ability to locate the precise position of one of a series of defects. This lack of locateability and

resolution derives from the wavelength of the microwaves. There is thus a potential need for a technique, which gives a resolution capability which is very much greater than with

other methods at the same frequency. In order to ascertain
the potential areas in which our microscope would be particularly
advantageous, we have carried out tests on a variety of samples
which may be classified into five basic categories:

1.   The detection of micro-cracks in solid
     metal objects.

2.   The detection of hairline breaks in thin
     metallic films on dielectric substrates.

3.   Recording changes in the relative per-
     meability of ferrite samples.

4.   Imaging small variations in the electric
     permittivity of dielectric objects.

5.   Characterising the properties of thin
     films.

In this chapter, we shall present the results obtained on
each of the five classes of defects outlined above and discuss
the possible applications of the microscope to realistic n.d.t.
situations.

7.1   Detection of Micro-Cracks in Metals

Initial experiments were directed towards examining
the potential use of the instrument in the evaluation of
surface topography. Fig. 7.1 shows a typical result of a
defect in a sample of steel, where a scan of the flaw is
compared with a cross-section of the object as viewed through
a metallurgical microscope. It is interesting to see that
some of the irregularities in the observed record do in fact
correspond to the actual shape of the object; though naturally
extended and distorted due to the fact that the record is
essentially a convolution of the defect with the aperture
and electronic system functions. This implies that, provided
the defects we wish to image are larger than the resolution
limit of the instrument, the microscope could be used in the
statistical examination of surface topography if suitable
calibration techniques were used to relate the signal to
actual height variations.

The experiments on fabricated slots in metals presented
in Section 6.5 suggested that the instrument was capable of
detecting defects which were significantly smaller than the

aperture dimension. We have carried out experiments to enable us to estimate the minimum detectable defect. Fig. 7.2 shows a trace from a 2 μ wide, 3 mm deep steel slot, together with a scanning electron micrograph of the slot; which was fabricated by joining two highly polished steel pieces. In this case, the sample was translated at a constant speed of 0.1 mm/10 mt.

Despite the precautions taken, we could not be sure that we might not be detecting some characteristic which would not be present in a true crack. For this reason, samples were obtained by the use of a fatigue machine on steel specimens. The smallest defect we have been able to detect was a fatigue crack believed to be less than 1 μ wide in a tool steel sample. The result is shown in Fig. 7.3, which also shows a scanning electron micrograph of the crack. Compared to other microwave crack detectors[11,12,13], these results are more than two orders of magnitude better in terms of both sensitivity of detection as well as in resolution capability. It should be pointed out that though we can detect cracks which are significantly smaller than the aperture diameter, we would not be able to resolve two 1 μ cracks separated by a distance less than the current resolution limit, 80 μ in our case (using a 200 μ aperture).

In some n.d.t. applications, the metal surface to be inspected is coated with a protective layer, which is often essentially a dielectric coating e.g. a randome. It was therefore of interest to see whether the microscope could

detect a crack beneath such a protective layer. Fig. 7.4 shows that though the crack produced signal is diminished due to the 50 μ dielectric coating, the flaw is still readily detected. This result was obtained with an aperture of diameter, 700 μ.

7.2 Detection of Breaks in Thin Metallic Films

We have demonstrated the ability of the microscope to resolve thin metallic gratings having line widths less than 80 μ. . A closely related situation, and one which comes very much closer to a class of material testing problems, is to locate a single hairline crack in an otherwise continuous metal film. Fig. 7.5 shows a result for a deliberate micro-crack of width 2 μ, which, it is seen, is still within the detection limit of the instrument. Similar results were obtained for cracks in thin metallic films on silicon sub-strates.

In order to be useful as a n.d.t. instrument, the microscope should be capable of discriminating between two surface defects: first, a break in a thin metallic film on a dielectric substrate and secondly, a surface scratch of similar dimensions. Fig. 7.6 shows that though the scratch (or surface depression) is not detected by our microscope, the break is clearly resolved. In this experiment we chose the aperture fields to correspond to a purely magnetic dipole for which the near-field stored electric energy is very small, so that the signal in the case of the break in the metallic

Figure 7.4   Detection of Steel Slots
(a) With Protective Dielectric Layer
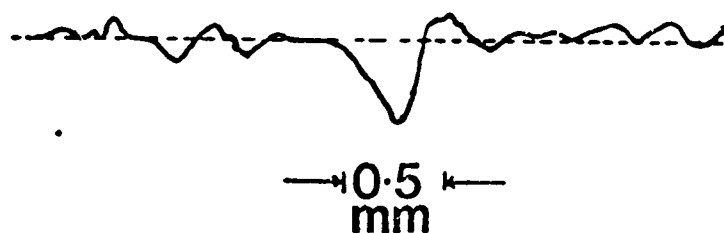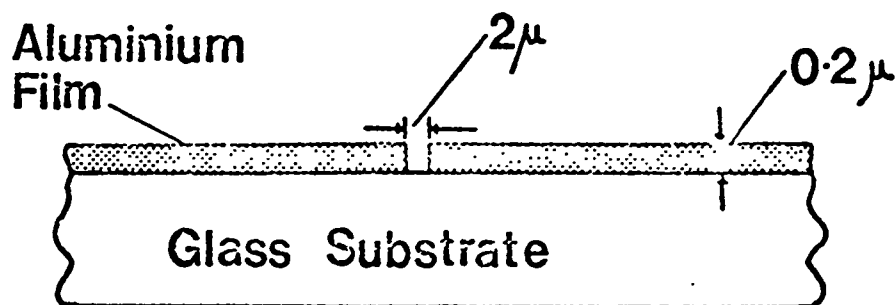(b) Without Protective Layer

Figure 7.5   Detection of Hairline Breaks in
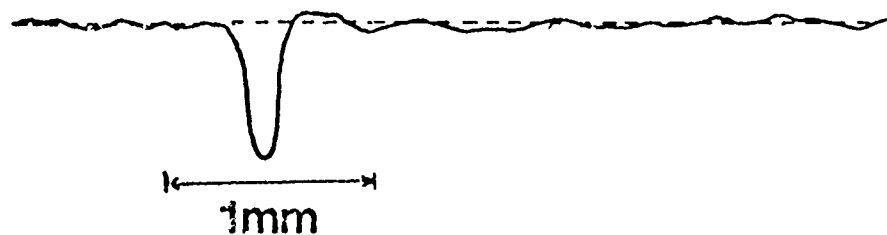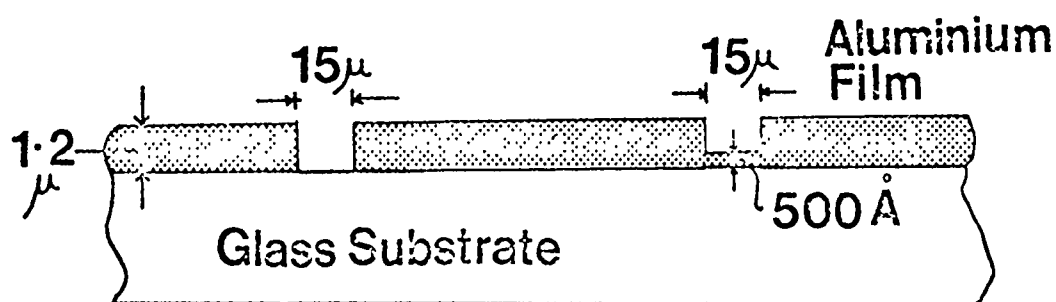Thin Metallic Films

Figure 7.6   Discriminating Between Breaks and
Scratches in Thin Metallic Films

film arises predominantly from gradients in the distribution. In the case of the surface scratch, currents are set up in the depression and consequently, the resulting field is not altered significantly to effect a detectable change in the signal. The ability to detect hairline cracks in thin metallic layers is already on the edge of direct usefulness in applications such as thin film circuitry.

We have performed quantitive experiments to be able to determine how the signal varies as a function of the width of the slit in a thin metallic film on a dielectric substrate. Variable width slits were fabricated in a 0.2 μ aluminium film on a glass substrate. Fig. 7.7 shows that the signal is very nearly a linear function of the slit width. We have made no attempt to predict this relationship rigorously as this would require a very complex field calculation.

More theoretical work is required to predict the smallest break in a thin metallic film on a dielectric substrate.

7.3   Imaging Variations in Dielectric Constant and Magnetic Permeability

Besides its use in high resolution inspection of surface topography, the microscope is capable of providing information about the electric and magnetic properties of the test specimen. It
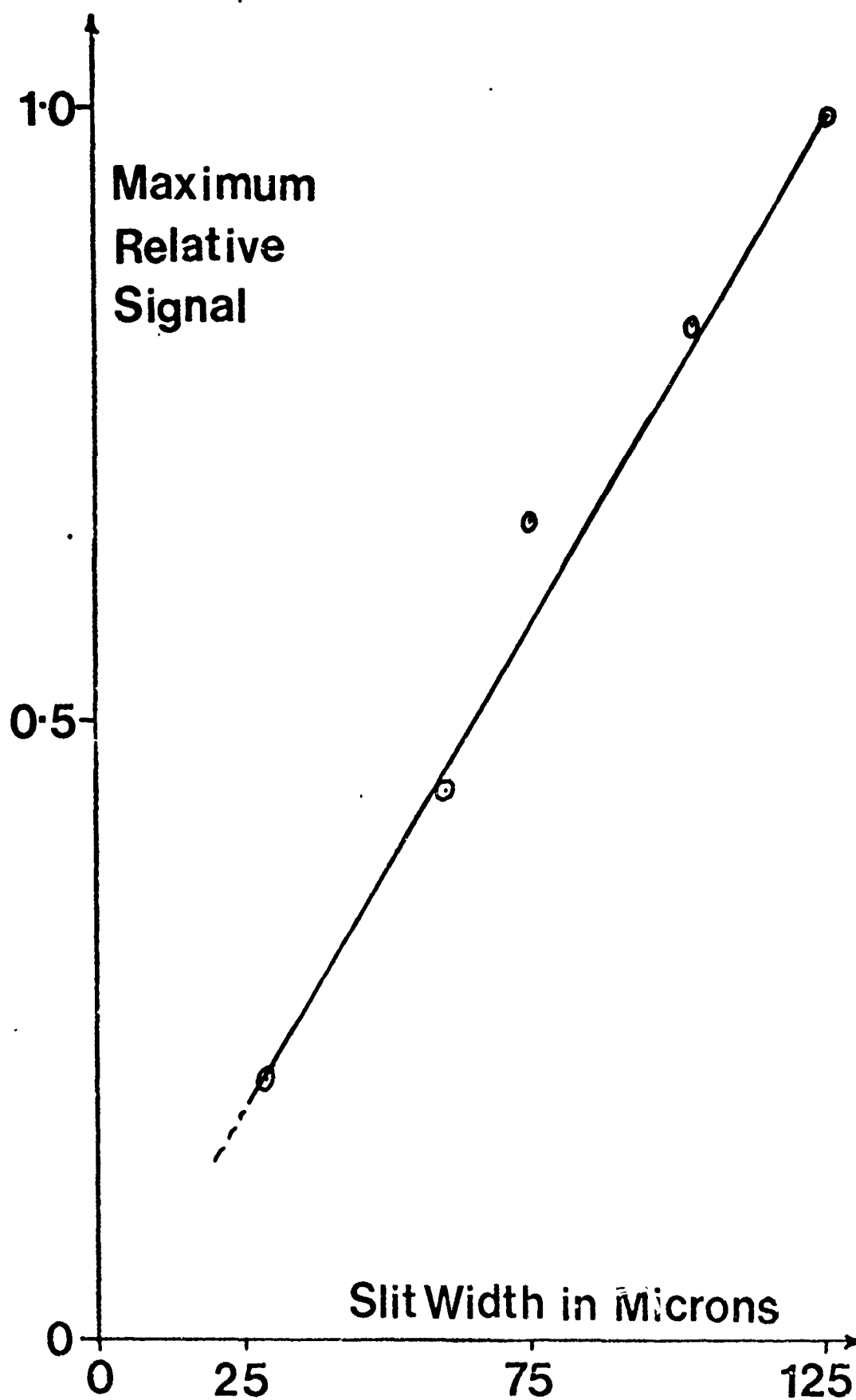
Figure 7.7   Signal Strength vs. Width of Slit in
Thin Metallic Film

was shown that if an electric dipole was used, the microscope would be very much more sensitive to changes in the relative dielectric constant than to changes in the magnetic permeability of the object.   Similarly, for a magnetic dipole, the instrument would be more sensitive to variations in the permeability of the sample.   This provides the basis of a novel technique to selectively image variations in either the dielectric constant or the magnetic permeability of an object with a very high resolution.   In order to corroborate this theory, we have carried out a series of experiments on dielectrics, ferrites and finally cast iron alloys.

The microscope was used to record spatial variations of the relative dielectric constant with an electric dipole. Fig. 7.9 shows a scan from the edge of a polystyrene sample to a perspex sample, where it can be seen that a variation of only 2.5% in relative dielectric constant was easily detected. The figure suggests that with the present instrument, variations of only 0.3% in dielectric constant could be resolved.   This makes the microscope potentially useful in the high resolution testing of dielectric substrates such as microstrip substrates.

It is important to appreciate that since the depth of field is itself very much smaller than the aperture diameter, that we can "see" surface changes which would be extraordinarily difficult to detect in any other way at the same frequency (simply because for handlable specimens, the "filling factor"
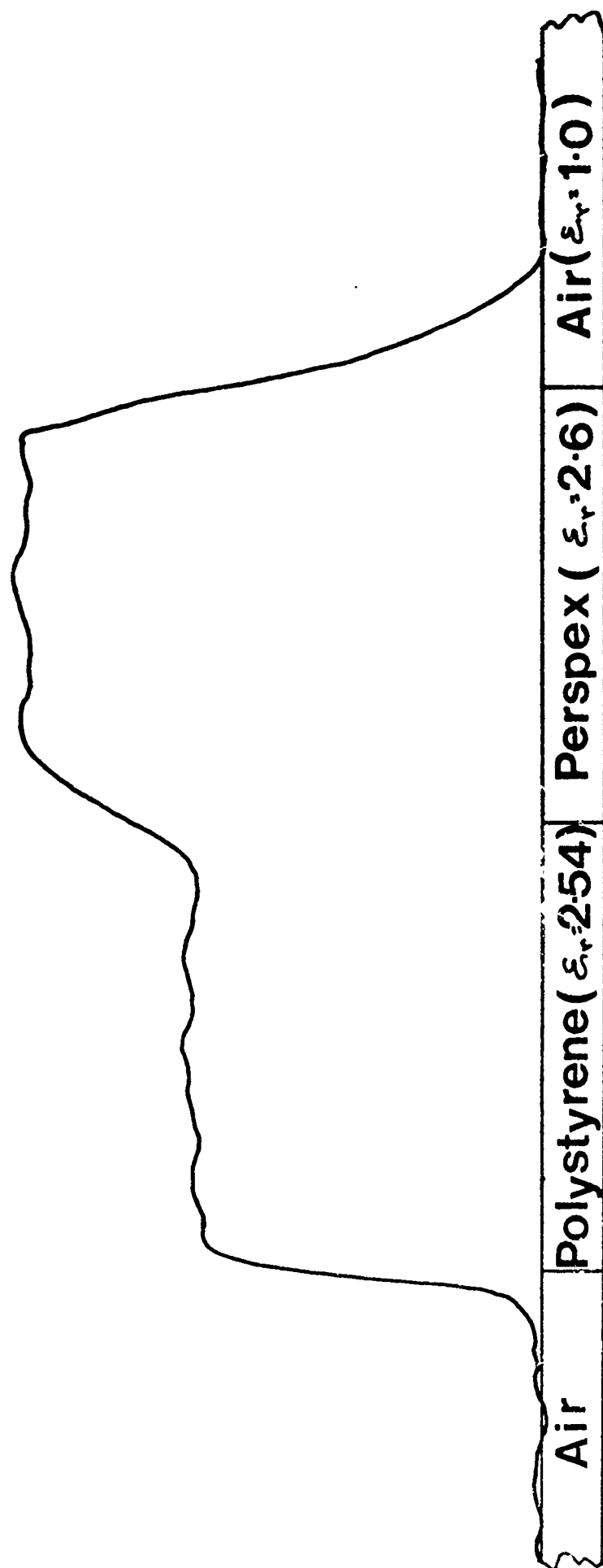
Figure 7.9   Imaging of Dielectric Variations Using an Electric Dipole

71.

would be very poor).   This opens up quite a new form of microwave measurements - to reveal the behaviour of dielectric and ferrite thin films.   We have carried out tests on thin dielectric films to verify this important property.   As Dielectric films serve many essential functions in modern solid state device technology

it is   important to measure their quality and to determine the presence and nature of any imperfections that may give rise to device failure so that appropriate corrections can be made in their processing.

Recently, Giallorenzi et al[13] and, Pitt and Manku[14], have demonstrated the possibility of using ion-exchange in glasses to fabricate low loss optical waveguides. The depth of the guide and the diffused ion concentration profile are important parameters in determining the performance of the guide; however, they are difficult measurements to make in practice accurately.   We have carried out preliminary tests on a sample of soda-glass substrate with an ion-exchanged (silver in our case) film grating which was only about 5 μ deep.   The results are shown in Fig. 7.10; where it is seen that the thin dielectric film is readily detected.   The change in dielectric constant of the film to the substrate was estimated to be of the order of 10%.

Recently, the suitability of electrostrictive materials, such as potassium tantalate niobate (KTN) have
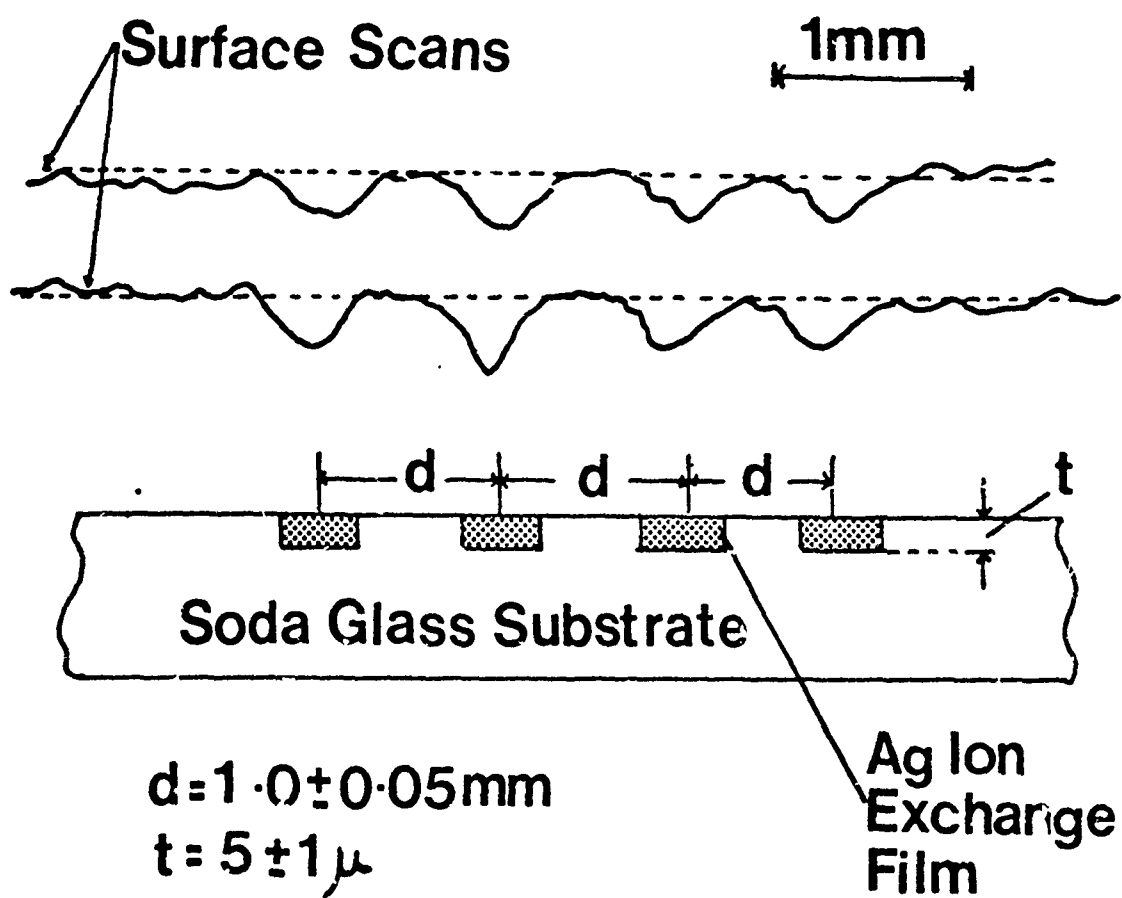
Figure 7.10   Imaging of Variations in Dielectric
Thin Films

been investigated[15] as substrate materials for the genera-
tion of surface acoustic waves.   An important parameter in
determining the efficiency of generation is the dependence
of dielectric permittivity on the applied bias voltage.   We
are not aware of any published information on the dielectric
behaviour of KTN as a function of electric field;   it was
therefore of interest to see whether the microscope could
record changes in the dielectric constant on application of
a bias field.   Using the configuration shown in Fig. 7.11(a),
we recorded the signal as a function of the distance from the
two electrodes.   The asymmetric behaviour of the signal with
position on the top surface (Fig. 7.11(a)) indicates that
dielectric permittivity is dependent on the polarization of
the electric field with respect to the crystal orientation.
Fig. 7.11(b) shows how the dielectric constant varies with
applied bias when the aperture was positioned midway between
the two electrodes.

These results are potentially useful in assessing the perform-
ance of the material for possible applications in SAW genera-
tion.   The results must be interpreted carefully if
they are to provide useful data: as for large
perturbations in the dielectric constant, the signal is no
longer a linear function of the dielectric permittivity.

The possibility of seeing magnetic contrast was
also explored.   By using an aperture distribution correspond-
ing to a magnetic dipole, we have shown the "visibility" of
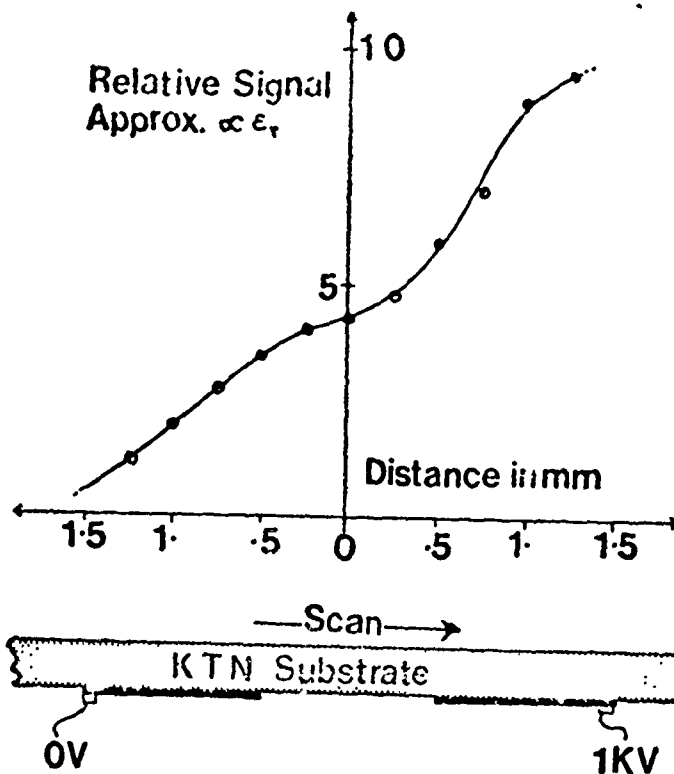a ferrite sample.   Fig. 7.12 shows a scan across a metal/

Figure 7.11(a)   Mapping of Relative Dielectric
Constant of KTN Sample

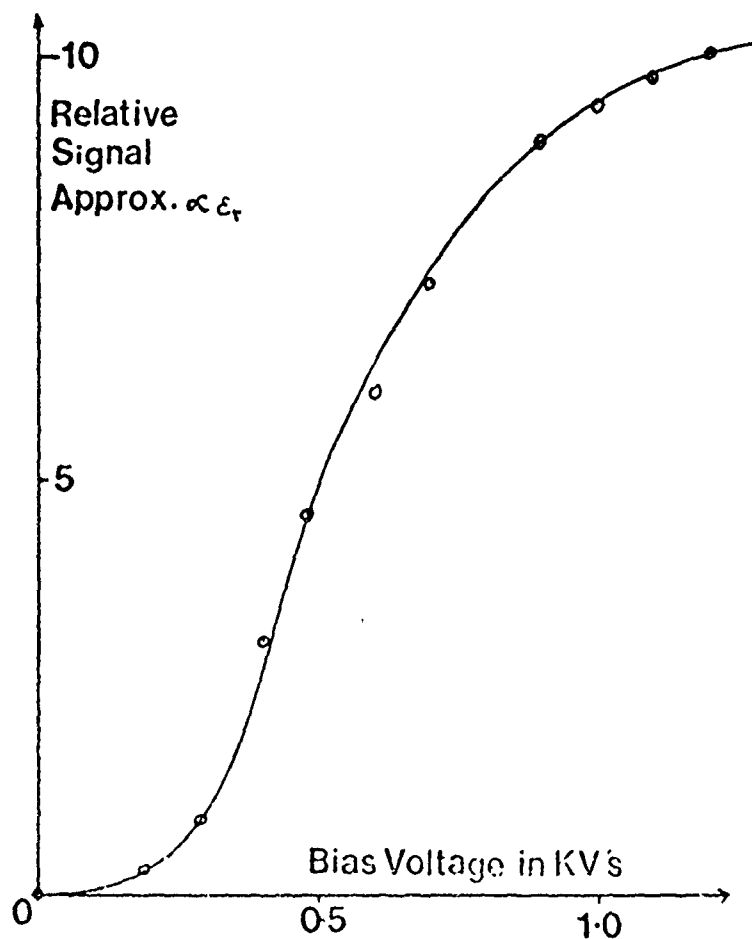Figure 7.11(b)   Measuring Changes in Relative Dielectric
Constant with Applied Bias of KTN Specimen

Metal
Alumina ε_r=9.0
Spinel Ferrite ε_r=13.2; M_S=187
Air
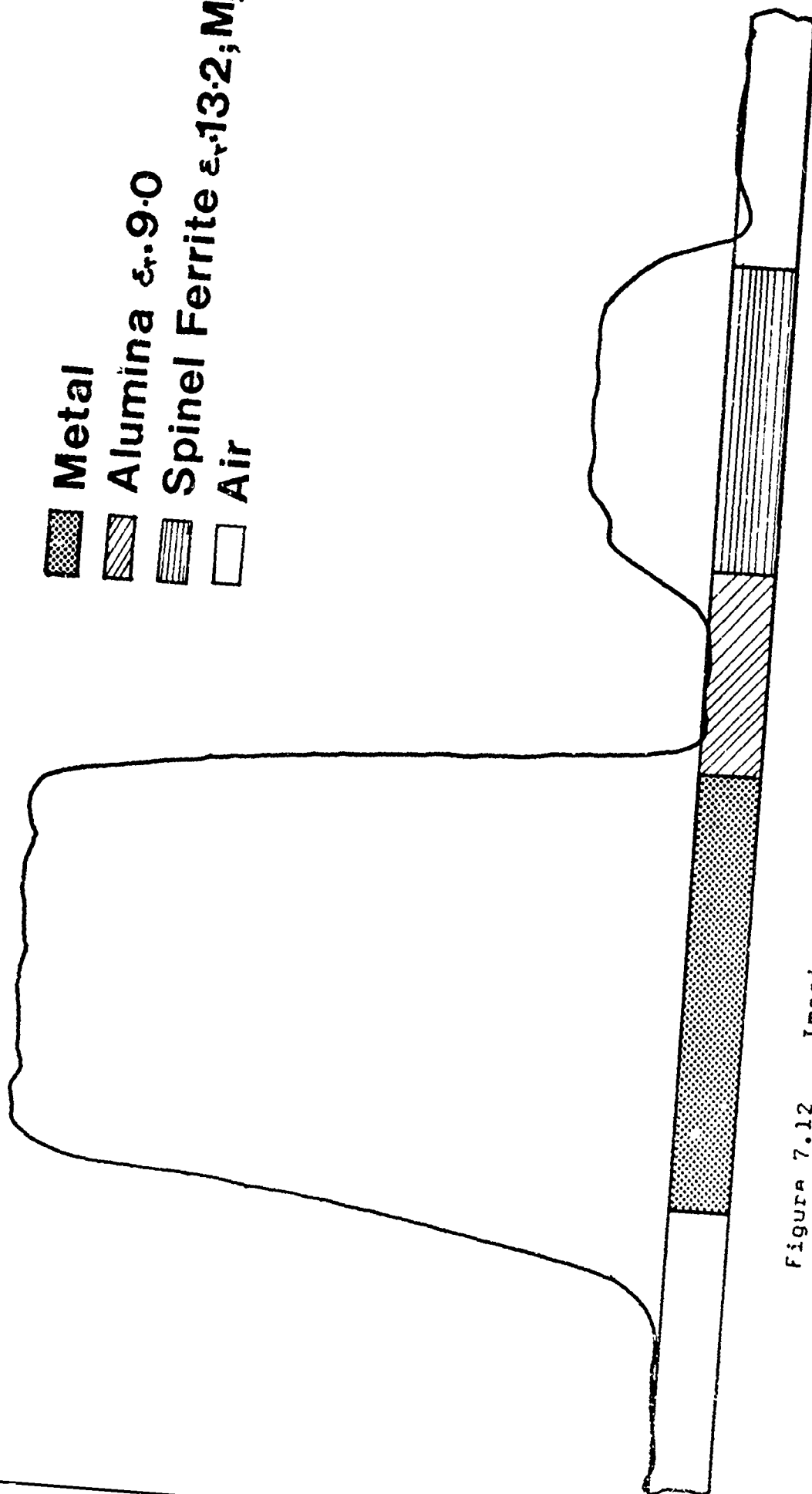
Figure 7.12   Imaging of Ferrite Sample Using a Magnetic Dipole

alumina/spinel ferrite substrate. The dielectric/ferrite boundary is clearly resolved. Having demonstrated the ability of "seeing" magnetic contrast, it was of interest to assess the sensitivity of the instrument to changes in the magnetic permeability of a ferrite sample. Preliminary experiments were performed on a low-frequency tuning coil ferrite to measure the change in magnetic permeability with applied magnetic field. The ferrite was poled in one direction by applying a large d.c. field and the change in permeability with an increasing field in the opposite sense was recorded. The result is shown in Fig. 7.13(a); on integration of this curve, we obtain the B vs. H for the ferrite at microwave frequencies. Though we would expect some variation of the microwave permeability (μ_r) as a function of the magnetic field, it is not clear what the effective μ_r vs. H curve should look like. However, the real value of the experiment is in that it clearly demonstrates that by using a magnetic dipole aperture, the microscope can image small variations in the magnetic permeability. We believe that the microscope has direct application in imaging small variations in magnetic thin film materials such as used in bubble memories[16,17] to assess for example the material uniformity which is an important parameter in determining the performance of the ferrite.

One further application of the microscope may be in the field of metallurgy. Conventional optical metallographic techniques involve three basic steps: first, preparation of a section surface; secondly, the development of a
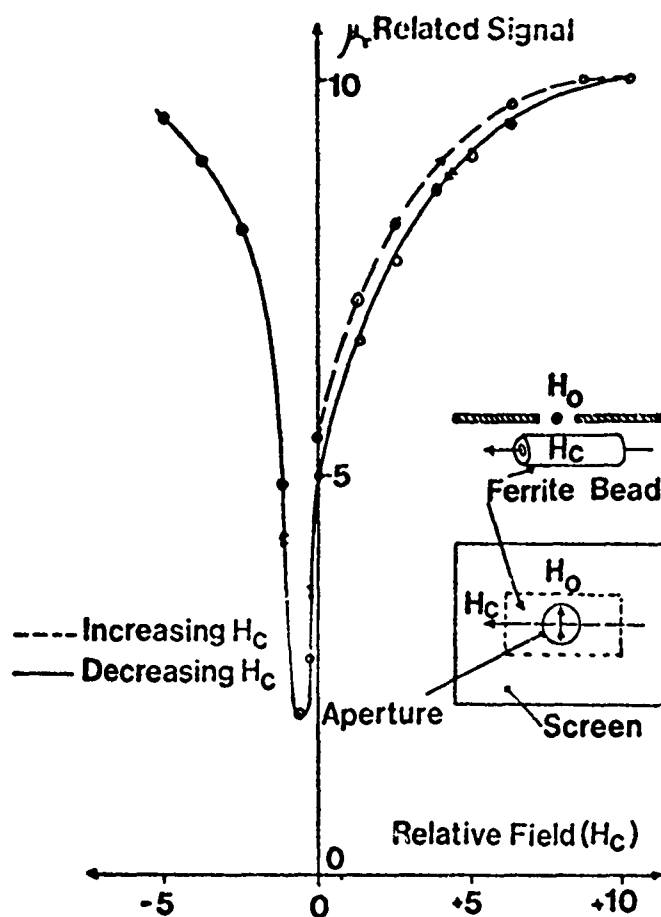
Figure 7.13(a)   Detecting Changes in Magnetic Permeability of Ferrite Bead with Applied Magnetic Field
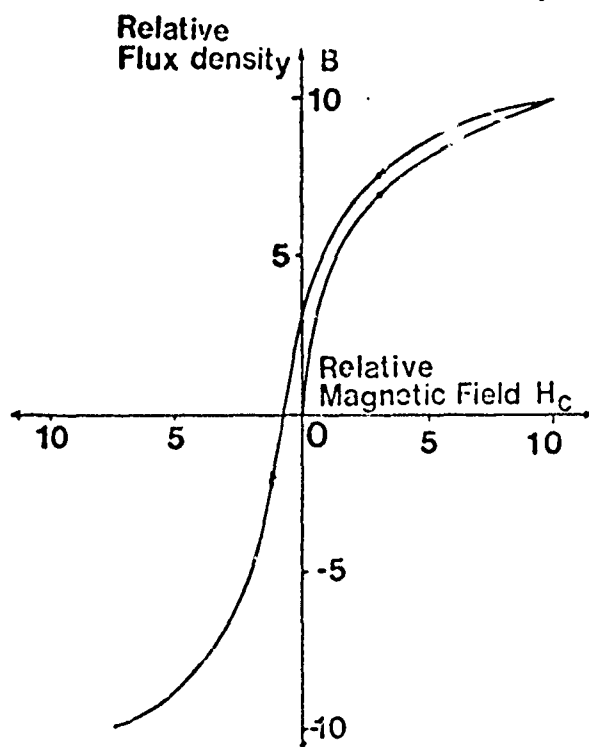
Figure 7.13(b)   Plot of Relative Flux Density (B) vs. Variation of Relative Magnetic Field (H_s)

structure usually by a chemical etching process; and finally, the actual observation and recording of the structure. This is both destructive and time consuming. Provided the resolution of our microscope is adequate for resolving the details we wish to investigate, it may be used to advantage to characterise certain alloys. We have investigated three commercially used cast iron alloys. These alloys were of interest as they contained secondary phase particles[18], the electric and magnetic properties of which varied over the specimen. Fig. 14(a) and (b) show the results of scans across a sample of hyper-eutectic white cast iron and a specimen of phosphoric white cast iron respectively, together with a scanning electron micrograph of the area under inspection. In Fig. 14(a), the most prominent dark cementite needles (Fe_3C) are resolved as is the small nest of flake graphite. In Fig. 14(b), the large 30 μ surface crack is easily detected and recorded as a dip in the signal, whereas the two dark pearlite (ferrite and cementite) regions show up as an increase in the relative signal.

We have demonstrated that besides its possible use in the non-destructive testing of metal surfaces to detect sub-micron cracks, the microscope has potential application in providing information about the surface properties of both ferrite and dielectric thin films which would be very difficult to detect in any other way. However, before the instrument can be used in practical n.d.t. situations, more work in calibrating the sensitivity of the microscope to specific perturbations would be necessary.

REFERENCES

1. Watkins, J., "Circular Resonant Structures in Microstrip",
   Elect. Letts., 5, p.524, (1969).

2. Troughton, P., "High Q Factor Resonators in Microstrip", Elect. Letts.
   4, p.520, (1968).

3. Wheeler, H.A., "Transmissionline Properties of Parallel Strips
   Separated by a Dielectric Sheet", I.E.E.E. Trans. M.T.T. 13, p.172, (1965).

4. Yamashita, E., Mittra, R., "Variational Method for the Analysis of
   Microstrip Lines", I.E.E.E. Trans. M.T.T. 16, p.251, (1968).

5. Troughton, P., Ph.D. Thesis, University of London (1970).

6. Hochschild, R., Materials Evaluation, 21, p.2, (1963).

7. Kovalev, V.P., Aleksandrov, Yu. B, Radiotechnical Methods, UDC, 621,
   370:620.199, p.126, (1966).

8. Lax and Button, "Microwave Ferrites and Ferrimagnetics", McGraw Hill,
   N.Y., (1962) Chapter 10.

9. Lavelle, T.M., Materials Evaluation, 25, p.252, (1967).

10. Collins, J.T., U.S. Pat., May 4, 1971, No: 3577071.

11. Feinstein, L., Hruby, R.J., The Rev. of Sci. Instr., 41, 5, (1970).

12. Feinstein, L., Hruby, R.J., AIAA/ASME 9th Structures, Dynamics and
    Material Conf. Calif. U.S.A. p1. (1968).

13. Giallorenzi, T., West, E.J., Kirk, R., Ginther, R., and Andrews, R.A.,
    "Optical Waveguides Formed by Thermal Migration of Ions in Glass",
    Appl. Optics, 12, 6, p.1240, (1973).

14. Pitt, C.W., Manku, University College London, Dept. Electronic and
    Electrical Engineering, Internal Report EEE75/8th April, 1975.

15. Iamsakun, K., Elder, W., Wilkinson, C.D.W., De La Rue, R.M.,
    Journ. Appl. Phys. 8, p.267, (1975).

16. Almasi, G., Proc. I.E.E.E., 61, p.438, (1973).

17. Dotsch, H., Schmitt, H.J., Muller, J., Philips Forschungs Laboratorium,
    Hamburg GmhB 2, 54 Germany.

18. Annotated Metalographic Specimens, Foundary Metallography, Metallurgical
    Services, U.K. (1971).

B. SURFACE DEFECT DETECTION USING ONE-DIMENSIONAL ACOUSTIC HOLOGRAPHY

1. INTRODUCTION

The basis of the method is to illuminate the surface to be tested with acoustic surface waves, launched at one end of the sample and then to record the amplitude and phase distribution along a scanning line at the other end of the sample. This record can be regarded as a hologram which can subsequently be reconstructed so as to reveal features at any point on the surface. At the time of the original proposal which led to the current work, we had succeeded in making such a hologram with a phase sensitive laser probe, and reconstructing the record using conventional laser-optic techniques. We had already recognized though that there would be very substantial advantages in using a computer reconstruction of the data. Since the record is one-dimensional the reconstruction computation is not arduous - it takes only a few seconds on an IBM 360 65. We have also succeeded in effecting the reconstruction on quite a small laboratory computer.

The work which has been accomplished on this project has to a large extent been published - at least in preliminary form. Since the published statement is suitably concise, we are reprinting the three relevant papers in the following. The first paper describes the work immediately preceding the award of the contract and the initial work on computer reconstruction carried out during the first quarter of the work. The most significant results relevant to n.d.t. appear in figure 7, which shows the successful computer reconstruction of a number of small gold dot "defects", and the first successful determination of a slowness characteristic in figure 11. In addition it gives a concise description of the laser probe system, and also of the effects of noise on the reconstruction of images.

Subsequently a considerable amount of further effort was devoted to improving the laser probe both with regard to its electrical as its mechanical performance. This led eventually to the much superior results on slowness determination, described in the second publication, section 3.

In section 4 we present a letter publication which reports a major improvement

in the holographic defect detection technique. It rests on the linearity of the process which permits one to <u>subtract</u> the record of a known good sample from that obtained with a sample which may have a defect. It led to the identification of a gold dot "defect" only 30 µin diameter and 0.4 µ thick a defect which was totally buried in the "noise" without the use of this subtraction technique. We believe that this technique will prove of major importance in the development of these methods.

In section 5 we briefly summarize the results obtained, and attempt an assessment of their potential importance to n.d.t. applications.

2. OPTICAL PROBING OF ACOUSTIC SURFACE WAVES—APPLICATION TO DEVICE DIAGNOSTICS AND TO NONDESTRUCTIVE TESTING

H. K. Wickramasinghe and E. A. Ash

Department of Electronics, University College, London, ENGLAND

Optical laser probes have for long been used for measurements on acoustic surface wave devices. At frequencies below a few hundred megahertz one can use a probing system in which the focused spot is small as compared with the acoustic wavelength. This enables one to derive fine-grained amplitude and phase information on the surface wave field. Some examples of the diagnostic use of a particular instrument of this design will be presented.

Since the probe gives complete amplitude and phase information, a scan transverse to an acoustic surface wave beam contains in principle a complete diffraction limited record of the two-dimensional field, right up to the transmitting transducer. We can regard the line scan as a one-dimensional hologram of the two-dimensional object space. The hologram can be reconstructed either optically or on a computer. Experiments relating to both methods will be presented. The technique is seen as having potential for the nondestructive testing of surfaces. It is not necessarily confined to plane surfaces.

Effective reconstruction on the computer implies a detailed knowledge of the slowness surface of the substrate. Conversely one can derive the slowness surface from a comparison of the complex distribution along two line scans. The technique therefore represents a method for measuring the slowness surface, and is capable of attaining very high accuracies. Preliminary results of some measurements will be presented.

I. INTRODUCTION

Acoustic surface waves are readily launched and received; it is less easy to observe their propagation from transmitter to receiver. The displacement amplitudes involved are small–typically several orders of magnitude less than one angstrom. Nevertheless, a number of successful probe detection systems have been devised. In one class of device, one uses a stylus directly attached to a piezoelectric transducer [1]; when probing nonmetallized substrates which are themselves piezoelectric, a simple metal stylus picks up a voltage which can be directly amplified [2]. Such probes have the inherent advantage of simplicity.

A second class is based on the use of lasers, in which the phase modulation occasioned by the surface displacement is in some way detected. Laser probes can themselves be divided into a number of categories depending on whether the interaction can be regarded as a diffraction process, extended over many acoustic wavelengths [3], or as a phase modulation, confined to at most one half acoustic wavelength. The present work

is based on the use of the latter type, in a form first described by Whitman and Korpel [4]. Laser probes have the immediate advantage of causing a negligible perturbation of the acoustic surface wave, and of avoiding any possible scratching of the surface. Moreover they work as well on insulating as on conducting surfaces. The price is a greater degree of complexity.

The laser probe as originally described was designed for amplitude measurements only [5]. For many of our purposes we were particularly interested in the phase distribution. For example, in the far field of a transducer the relevant information is almost entirely phase information. We therefore decided to make our probe capable of measuring phase as well as amplitude. The basic design adopted has been previously described [6], and analyzed. We will in Section II give a very brief description of the apparatus in its present improved form.

In this paper we want to address ourselves to the use of laser probes for two different classes of application. The first is concerned very directly with the development of acoustic surface wave devices, and measurements to diagnose sources of malfunction. In Section III we will give one example of the use of the laser probe for such purposes. The probe is seen to be of particular importance in connection with devices which are truly two dimensional in character (i.e., where the propagation effects in the transverse direction are of essential significance to the basic working of the device).

The laser probe can, however, also be used in a somewhat different manner for the characterization of a complete two-dimensional field in a single scan. Just as a two-dimensional holographic record can store information about a three-dimensional object space, a one-dimensional record—a single laser scan—can contain complete information (within the usual resolution limits) on a two-dimensional field. The process by which one can reconstruct the scene from the scan information has been discussed by a number of workers in the context of ordinary (i.e., three-dimensional) optics, and acoustics. In the case of surface waves, it leads to the reconstruction of the two-dimensional fields, and in particular to the detection of scattering sources within that field by observation at a distance. The concept is therefore one which lends itself, in principle, to the non-destructive testing of components. Some preliminary experiments to this end are described in Section IV.

In the case of anisotropic materials the reconstruction of the field from a scan requires an accurate knowledge of the slowness curve of the substrate. Where this is not known with sufficient accuracy, the method suggests a new measurement technique: it involves the recording of two scans separated by a distance. The relationship between the spectra of the two scans then leads directly to the delineation of the slowness curve. A discussion of the method, and some preliminary results are also presented in Section IV.

II. LASER PROBE

The basic design of the probe [6] is shown in Figure 1. It can be regarded as a modified Michelson interferometer in which the beam splitter is replaced by a Bragg cell thereby providing a carrier frequency for the signal. The introduction of such a carrier frequency brings some advantages in the subsequent signal processing; above all it ensures that spurious optical path length variations are not detrimental provided that their spectrum does not fall into the signal processing bandwidth, centered on tens of megahertz.
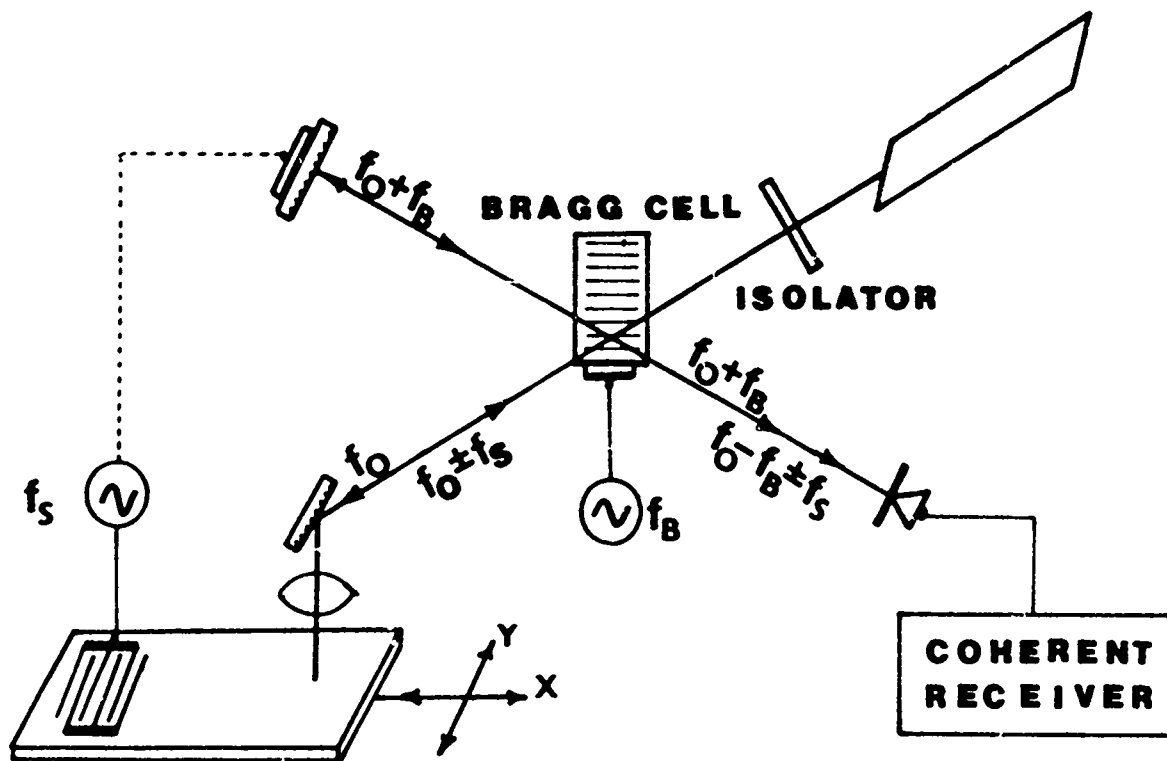
Fig. 1. Laser heterodyne probe.

The system is therefore remarkably free from disturbances which would otherwise be occasioned by microphonics, small temperature gradients, etc.

In our first experiments to obtain phase discrimination [7], we vibrated the reference mirror at the acoustic signal frequency f_s, while retaining simple square law detection of the signal. This technique allows one to use a bridge method, where the phase of the measured signal is derived from the phase change setting in the reference arm to obtain a null in the detection system [8]. It is a method which works effectively but which is difficult to extend so as to give a continuous phase record as the sample is scanned. The natural alternative is to use a fixed reference mirror, but with a phase-coherent detection system. The frequency component of interest after photodetection is $(2f_B - f_s)$, where f_B is the Bragg cell frequency. This suggests that one could derive a local oscillator signal by doubling the Bragg cell drive frequency. However, it turns out that by so doing, one looses the insensitivity to path length fluctuations at low frequencies which is such a vital factor in the realization of a stable instrument. Fortunately there is another source of $2f_B$ in one component of the photodetected laser current. This component contains the same optical phase information as the $(2f_B - f_s)$ component. After mixing one has therefore once again restored the immunity to optical phase jitter. These considerations then led to the detection scheme shown in Figure 2.

We have found that even in this situation one can experience signal fluctuations arising from hydrodynamic streaming instabilities in the Bragg cell. With careful design, and control of temperature of operation this effect can be largely avoided.

The present instrument is designed to work at a series of bands up to 100 MHz. No major obstacles to its extension to frequencies two or three times greater are envisaged.

In operation the sample is mechanically scanned under the laser beam; the vector voltmeter output can be displayed directly on an XY recorder. Alternatively, and this is the technique used exclusively in connection with the holographic work (Section IV),
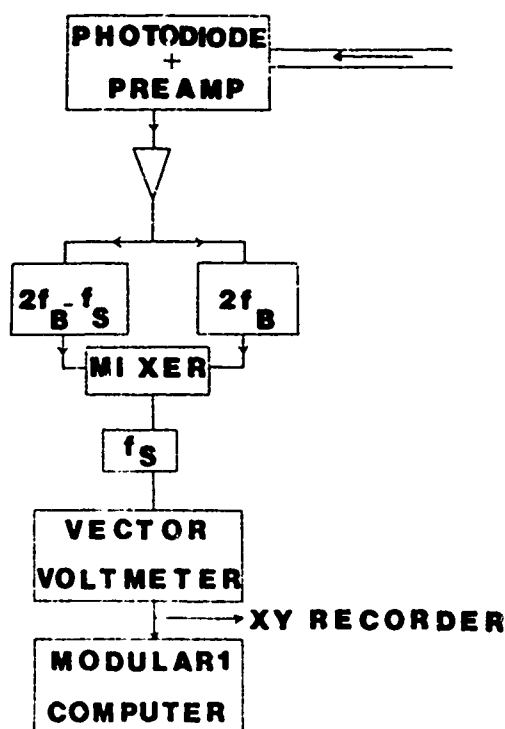
OPTICAL AND ACOUSTICAL MICRO-ELECTRONICS

Fig. 2. Coherent laser probe detection system.

the signal can be fed directly to a minicomputer which digitizes and in some cases processes the signal.

It is of particular relevance briefly to examine the phase resolution of the instrument. At a frequency of 60 MHz, the acoustic wavelength in quartz and in $LiNbO_3$ is of the order of 50 μ. The laser probe can be focused to less than 5 μ. The phase detection system has a resolution limit which is better than 10°. Since one can expect to obtain a resolution which is less than the phase width of the spot, it is this latter figure which is probably the limiting factor. We can therefore achieve a resolution at this frequency of around $\lambda/20$. With a sample length of 5 cm, we have a total path length of 10^3 wavelengths. The instrument should therefore be capable of measuring velocity with an accuracy of around 5×10^{-5}. The performance could be improved if longer samples are available. In practice, the attainment of such accuracies also implies considerable effort on removing or discriminating against bulk wave and other spurious signals.

III. DEVICE DIAGNOSTICS

Measurements of amplitude distribution along acoustic surface wave devices have been published by many authors. In some cases these have served to reveal aspects of performance which it would have been hard to explore in any other way [9]. The basis and many examples of such measurements are presented in a recent review article [3]. In this section we will give a single recent [10] example of the use of the laser probe in a situation where both the amplitude and phase distribution was of importance.

The problem is concerned with transduction onto a topographic waveguide. The difficulty of direct transduction [11, 12] stems from the fact that the "aperture" of the guide is less than one wavelength, so that the transducer has to be fabricated at the very edge of the guide, a process which it is difficult to accomplish using normal photolithographic techniques. We have sought to effect this coupling using a conventional interdigital transducer feeding a thin film waveguide, which is in turn synchronously coupled
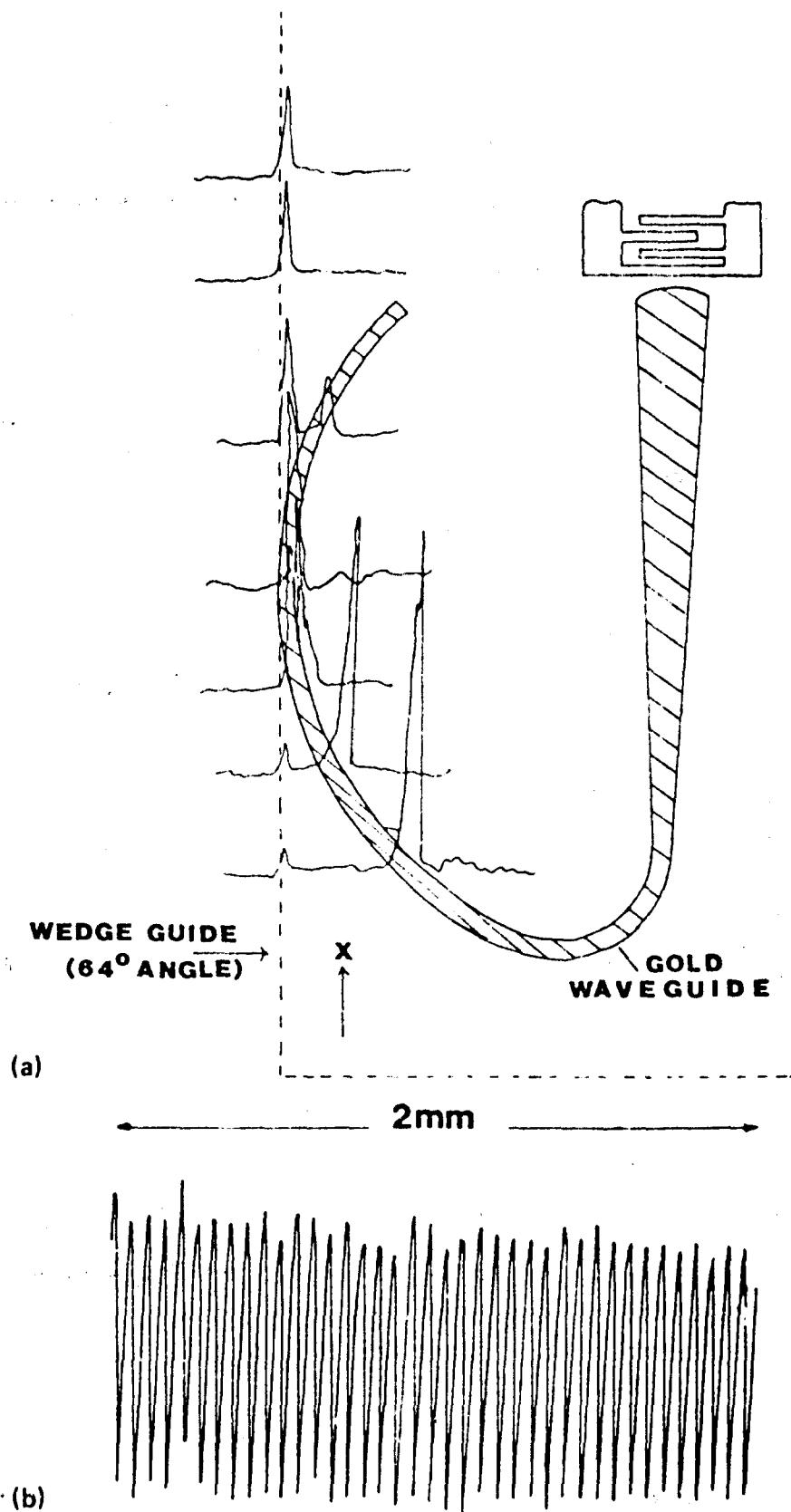
Fig. 3. (a) Thin film to wedge guide directional coupler. The amplitude distribution, recorded at 60 MHz shows the progressive transfer of energy to the wedge guided wave. (b) Phase plot along the edge of the wedge guide. There are 39 wavelengths in the 2 mm scan corresponding to a velocity of 3088 m/sec.

to the topographic waveguide. Figure 3 shows the system used in a particular experiment to couple 60 MHz waves onto a 64° angle wedge waveguide. The gold waveguide has a thickness so that its velocity is depressed 10% below the Rayleigh velocity for the Y-cut sample (in the x propagation direction). Computations subsequently showed [13] that the wedge wave for this angle is only 2% below the Rayleigh velocity; however since in this case the thin film guide actually touches the edge of the wedge guide, the coupling is very strong; a substantial transfer of energy therefore takes place, in spite of the lack of synchronism. The probe amplitude distributions, Fig. 3(a), clearly show the manner in which the guide wave is launched, and the decrease in the amplitude of the thin film guide mode.

Since the synchronous condition is central to the operation of this device, it is clearly important to have an accurate knowledge of the wedge guide velocity. This is obtained using the laser probe, simply by recording the phase as the probe is scanned along the edge of the wedge guide. The phase record is shown in Figure 3(b). Although in this case only a relatively short scan was used, the measured velocity is determined within an accuracy of a few parts in 10^3, in good agreement with the value computed by LaGasse [13].

IV. ONE-DIMENSIONAL HOLOGRAPHY

We will now turn to the use of the laser probe for the recording of one-dimensional holograms. It is possible to record such a hologram as a one-dimensional record on a photographic plate, and then subsequently to effect the reconstruction optically. An example of this technique [14] is shown in Figure 4(a). The "object" consisting of two gold dots on a quartz substrate was illuminated with surface waves at 60 MHz, and laser probed at a distance of 400 wavelengths. The scan was recorded in the form of a binary phase hologram which is shown in Fig. 4(b); the optical reconstruction which clearly resolves the two dots is shown in Figure 4(c).

The optical reconstruction however represents a troublesome additional step. Moreover it leads to the distortion arising from the difference of lateral and longitudinal magnifications in the ratio of the acoustic to the optical wavelength [15]. It is therefore natural to seek to effect the reconstruction numerically. The main difficulty encountered in doing this in the case of two-dimensional holograms—the sheer magnitude of the numerical task—is not a significant factor in the case of a one-dimensional record. Moreover one can use a reconstruction wavelength identical to that used in the recording, so that object distortion is totally avoided. There is in addition the opportunity to use a number of techniques which can be adopted to make the fullest possible use of any a priori knowledge of the "object" which is sought. Finally it is possible to use the technique for anisotropic media, even in the case where the slowness curve cannot be adequately represented by a parabola.

The process with which we are concerned is equivalent to "inverse diffraction" [16-20], and there are a number of publications which have specifically applied the technique to the reconstruction of normal (three-dimensional) acoustic holograms [21-24]. Our case is somewhat simpler in that we are concerned with only two dimen-
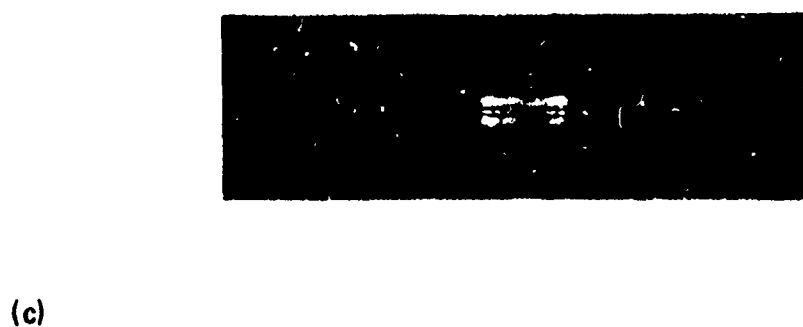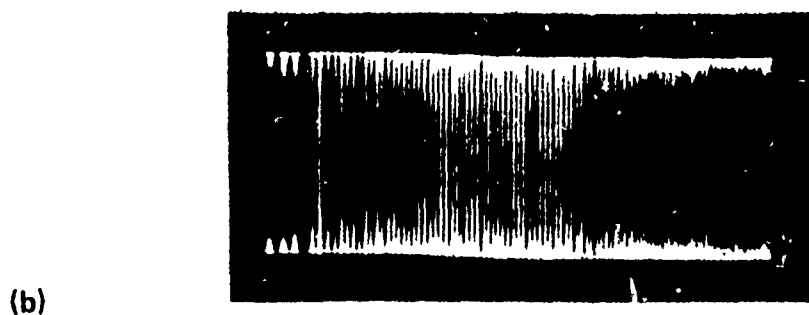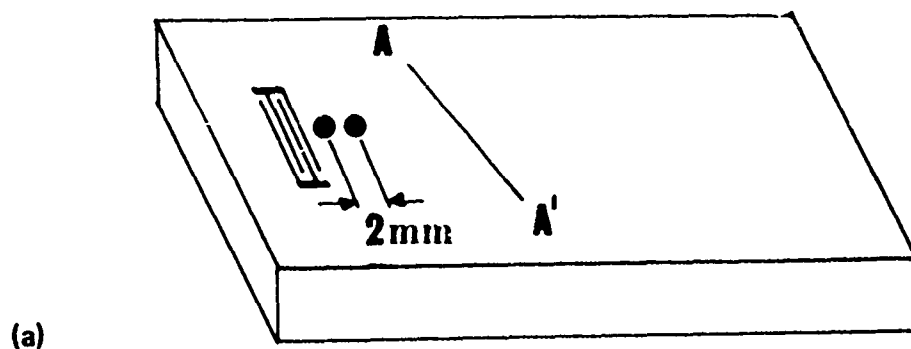
(a)

(b)

(c)

Fig. 4. (a) Sample used in two-dimensional holography. (b) Binary phase hologram recorded at 60 MHz, 400 wavelengths from object. (c) Optical reconstruction of object.

OBJECT   IMAGE

$U_O(x)$ $U_I(x)$

A. Reconstruction Theory

Figure 5 shows an "object" distribution $U_0(x)$ at $z = 0$ and an "image" distribution $U_I(x)$ at $z = L$. A plane surface wave, propagating in the θ direction will have a spatial dependence of $\exp(-j(\alpha x + \beta z))$, where

$$\alpha = k(\theta)\sin(\theta),$$

$$\beta = k(\theta)\cos(\theta), \tag{1}$$

and $k(\theta)$ is the wavenumber. We can obtain an expansion of the object distribution in terms of the plane wave spectrum,

$$U_0(x) = \int_{-\alpha_m^-}^{\alpha_m^+} f_0(\alpha) e^{-j\alpha x} \, d\alpha. \tag{2}$$

The waves corresponding to values of α greater than the maximum value attained by $k(\theta)\sin(\theta)$ are evanescent, and can certainly be excluded from our calculations, since we will be concerned with object-image distances of many wavelengths. We have therefore used the limits α_m^+ and α_m^- corresponding to the maximum values of α for θ positive and negative, respectively. Provided that the magnitude of $f_0(\alpha)$ drops to low values by the time we approach these limits, we may regard Eq. (2) as a simple Fourier transform, with the inverse

$$f_0(\alpha) = \int_{-\infty}^{\infty} U_0(x) e^{j\alpha x} \, dx. \tag{3}$$

Since $f_0(\alpha)$ can be interpreted as the amplitude of the plane wave corresponding to θ, we can [25] immediately write down the corresponding spectral density at the image plane

$$f_I(\alpha) = f_0(\alpha) e^{j\beta L}. \tag{4}$$

This is a standard procedure in isotropic diffraction theory. It applies equally in the anisotropic case, provided that $\theta(\alpha)$ is a single valued function of α. We will make
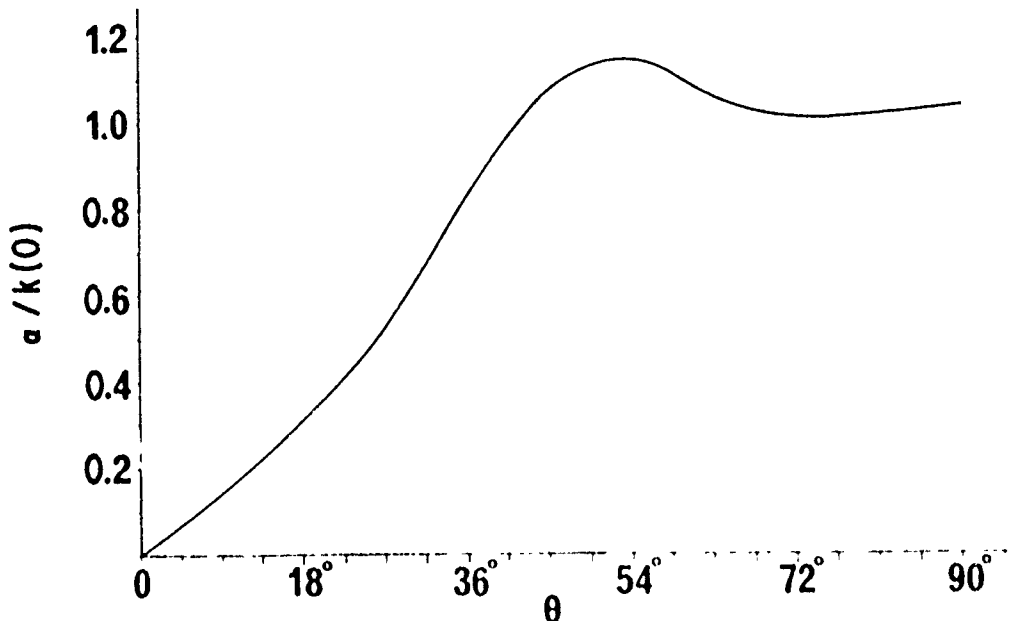

Fig. 6. Slowness characteristic for Z-cut rutile; propagation at $0°$ to the Y direction.

this assumption for the moment, but revert to the problem raised by double valued functions. We can then at once take the transform of $f_I(\alpha)$ and hence obtain the image distribution

$$U_I(x) = \int_{-\alpha_{\dot{m}}}^{\alpha_{\dot{m}}} f_0(\alpha) e^{-j(\beta L + \alpha x)} \, d\alpha. \tag{5}$$

The procedure can be reversed so as to yield the "object" distribution, from a known "image" distribution. Using precisely the same method one obtains

$$U_0(x) = \int_{-\alpha_{\dot{m}}}^{\alpha_{\dot{m}}} e^{j(\beta L - \alpha x)} \left\{ \int_{-\infty}^{\infty} U_I(x) e^{j\alpha x} \, dx \right\} d\alpha. \tag{6}$$

In the case of some materials, the function $\theta(\alpha)$ is not single valued for the whole range of $|\theta| < \pi/2$. An example is presented in Fig. 6 which shows $\alpha(\theta)$ as a function of θ for Z-cut rutile, $\theta = 0$ corresponding to the Y axis. We see that for θ greater than $43°$, there are two and for some ranges of α, three possible values of θ, and hence through Eq. (1), two possible values for β; there is no longer a unique result for the integral of Equation (6). The physical significance of this conclusion is that the distribution $U_0(x)$ is simply not uniquely defined by $U_I(x)$.

It is interesting to relate this conclusion to a simple case, where the object distribution is due to two plane waves, having the same value of α, but two different values of θ, θ_1, and θ_2. If A_1 and A_2 are the corresponding complex amplitudes

$$U_0(x) = (A_1 + A_2) e^{-j\alpha x}, \tag{7}$$

and

$$U_I(x) = (A_1 e^{-j\beta_1 L} + A_2 e^{-j\beta_2 L}) e^{-j\alpha x}. \tag{8}$$

Clearly the relationship between A_1 and A_2 cannot be derived from a measurement of only U_0 or only U_I. However if we measure both U_0 and U_I we have two complex equations for the two complex amplitudes, and we can proceed to solve for both A_1 and A_2. In fact we see that if we measure any two distributions displaced by a known length in the z direction, we can obtain the complete plane wave spectrum, and hence derive the distribution at any other plane; We see therefore that in order to reconstruct an object in this situation, we need to measure two image distributions displaced by an arbitrary distance in the z direction. Finally it is interesting to note that the spectral intensity of the two distributions of Eqs. (7) and (8), are no longer identical, as they inevitably are when $\theta(\alpha)$ is single valued.

The experimental work so far completed relates to the single valued case, to which we will now return. The formulation of Eq. (6) is still a step or two removed from the reality of an experiment, where $U_I(x)$ is obtained as a sampled rather than as a continuous function. The function is sampled at N equally spaced points, displaced by Δx. It is convenient, particularly when using Fast Fourier Transform techniques, to compute the spectrum also at N points, displaced by $\Delta \alpha$. Finally the object distribution is again reconstructed in terms of N samples with the same spatial increment Δx. The discrete Fourier transform version of Eq. (6) then reads

$$U_0(q \Delta x) = \sum_{p=-(N/2)}^{(N/2)-1} e^{j(\beta_p L - pq \Delta \alpha \Delta x)} \sum_{q'-(N/2)}^{(N/2)-1} U_I(q' \Delta x) e^{jpq' \Delta \alpha \Delta x}. \tag{9}$$

OPTICAL AND ACOUSTICAL MICRO-ELECTRONICS

where

$$\beta_p \equiv (k\,(\theta)^2 - (p\Delta\alpha)^2)^{1/2} \, .$$

If we use the Fast Fourier Transform, we must restrict N to a binary number. Also we must adopt a specific relationship between $\Delta\alpha$ and Δx

$$\Delta\alpha\Delta x = \frac{2\pi}{n} \, . \tag{10}$$

With Eq. (10), Eq. (9) can be written in the final form

$$U_0\,(q\Delta x) = \sum_{P=-(N/2)}^{(N/2)-1} e^{j(\beta_p L - 2\pi pq/N)} \sum_{q'=-(N/2)}^{(N/2)-1} U_I\,(q'\Delta x)e^{j(2\pi pq'/N)} \, . \tag{11}$$

This is the form in which the computations were carried out.

In the case of such a one-dimensional record the use of Fast Fourier Transform methods is not mandatory, and indeed it would be entirely possible to use diffraction formulations other than plane wave expansions. It is however, for our purpose, the particular merit of the plane wave expansion that the anisotropy of the medium is so readily included, at least as long as $\theta\,(\alpha)$ remains single valued. One can see at once that in order to achieve an accurate reconstruction of the object distribution the form of the anisotropy, $k\,(\theta)$ must be known with considerable precision, as the transform contains a
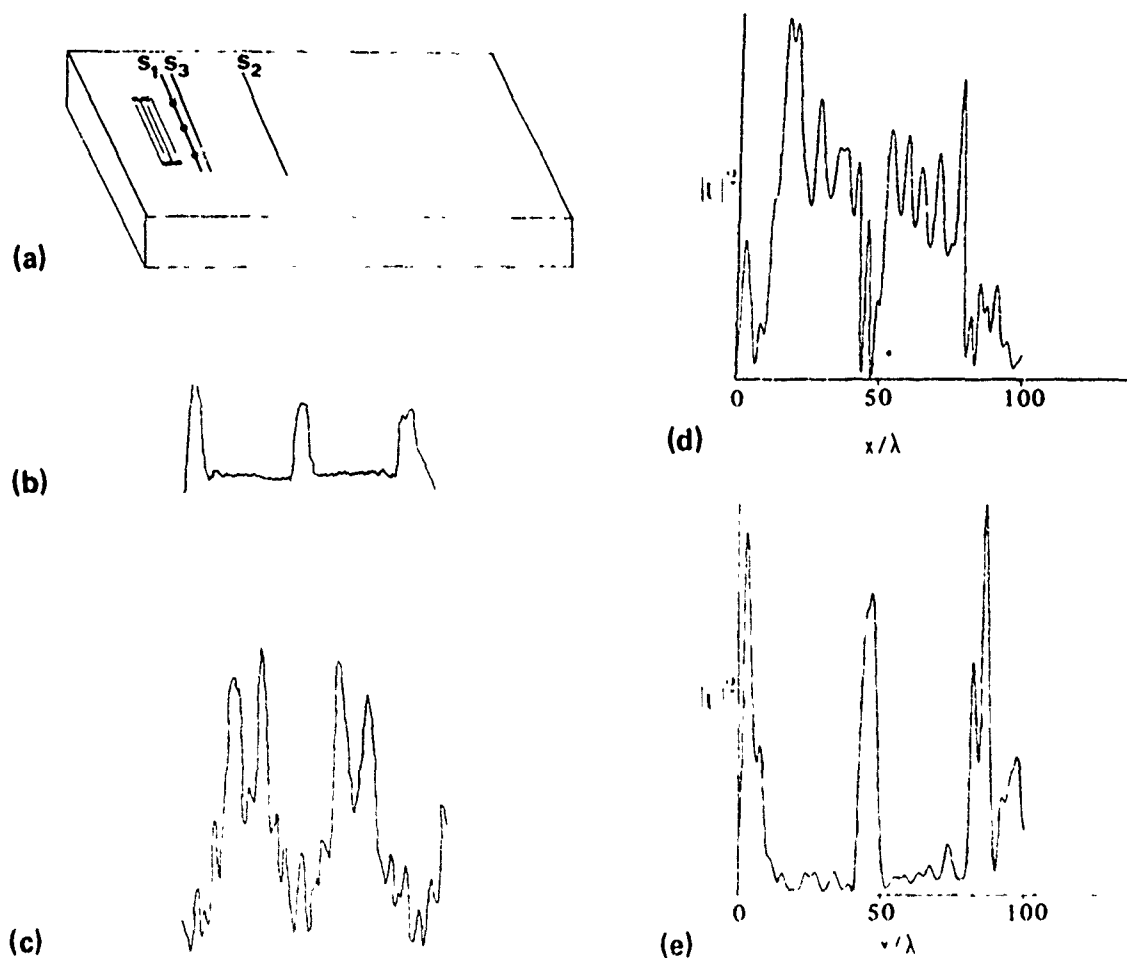

(a)

(b)

(c)

(d)

(e)

Fig. 7. Computer reconstruction of object from single scan information. (a) Arrangement of gold
(b) Experimental scan S_1. (c) Experimental scan S_2. (d) Computer reconstruction at

phase factor of the order of $k(0)L$, and L may in practice be a large number of wavelengths.

B. Reconstruction of Experimental Data

Preliminary experiments have been carried out using a quartz substrate and using a distribution of gold dots to represent the "object." Figure 7(a) shows the arrangement and the position of the various scan records. The gold dots had diameters of $\frac{1}{2}$ mm, and a thickness of 8000 Å. The "object" distribution S_1, taken immediately adjacent to the line of dots is shown in Fig. 7(b), and the "image" distribution S_2 in Figure 7(c). The computer reconstruction in accordance with Eq. (11) is shown first for a line S_3 displaced by $\frac{1}{2}$ mm from the object (Fig. 7(d)) and finally focussed onto the object line itself Figure 7(e). It is seen that the three dots are well resolved.

In nondestructive testing applications (Section IV.D) it may prove valuable to be able to reconstruct unknown defects, in the presence of known "defects" (e.g., the edge of the sample). Since all the manipulations involved in the reconstruction process are linear, it is clearly possible to add and subtract records. Experiments to demonstrate this possibility are in progress.

The experiments are in an early phase, and the limits of the detection sensitivity of the laser probe has yet to be explored. However in the next section we will discuss some preliminary considerations which bear on this issue.

C. Detection and Resolution Sensitivity

The resolution and detection sensitivity are limited both by the normal limits of resolution of any optical instrument, as by the finite accuracy and signal-to-noise ratio achieved in the laser probe. However it is of interest to note that in principle the detection limit may be far below the Rayleigh criterion, provided that one has some a priori knowledge of the nature of the object. It is a common place that one can see stars which one cannot resolve. Very simple considerations indicate that this situation is one which one might well encounter in practice. Suppose that the sample is illuminated by a total power P, applied over a width W. The power density is then P/W, and, if we are probing in the near field, will be of the same order in the image scan position. Suppose that we have a totally absorbing object, width δW, spaced D from the image line. This object can then be represented as giving rise to a cylindrical wave having a (negative) power of $P\delta W/W$. The amplitude ratio between this scattered wave and the largely unperturbed illumination is then R, where

$$R^2 = (\delta W/2\pi D).$$

The scattered wave will at different points have a phase of $\pm \pi/2$ relative to the main wave, leading to total phase variations of the resultant $\delta\phi$, where

$$\delta\phi = (2\delta W/\pi D)^{1/2}. \tag{12}$$

Suppose that we are able to measure ϕ with an accuracy of $1°$, and that $D = 100\lambda$. We then find that $\delta W \sim \lambda/20$. The resolution must of course always be of the order of a wavelength. However, if one is looking for a sparse set of defects, or even for the possible presence of a single one, we see that it may prove possible to detect very small disturbances.

In order to obtain a more detailed picture of the probe performance required to achieve a particular resolution, we have simulated the random errors in a theoretical

OPTICAL AND ACOUSTICAL MICRO-ELECTRONICS
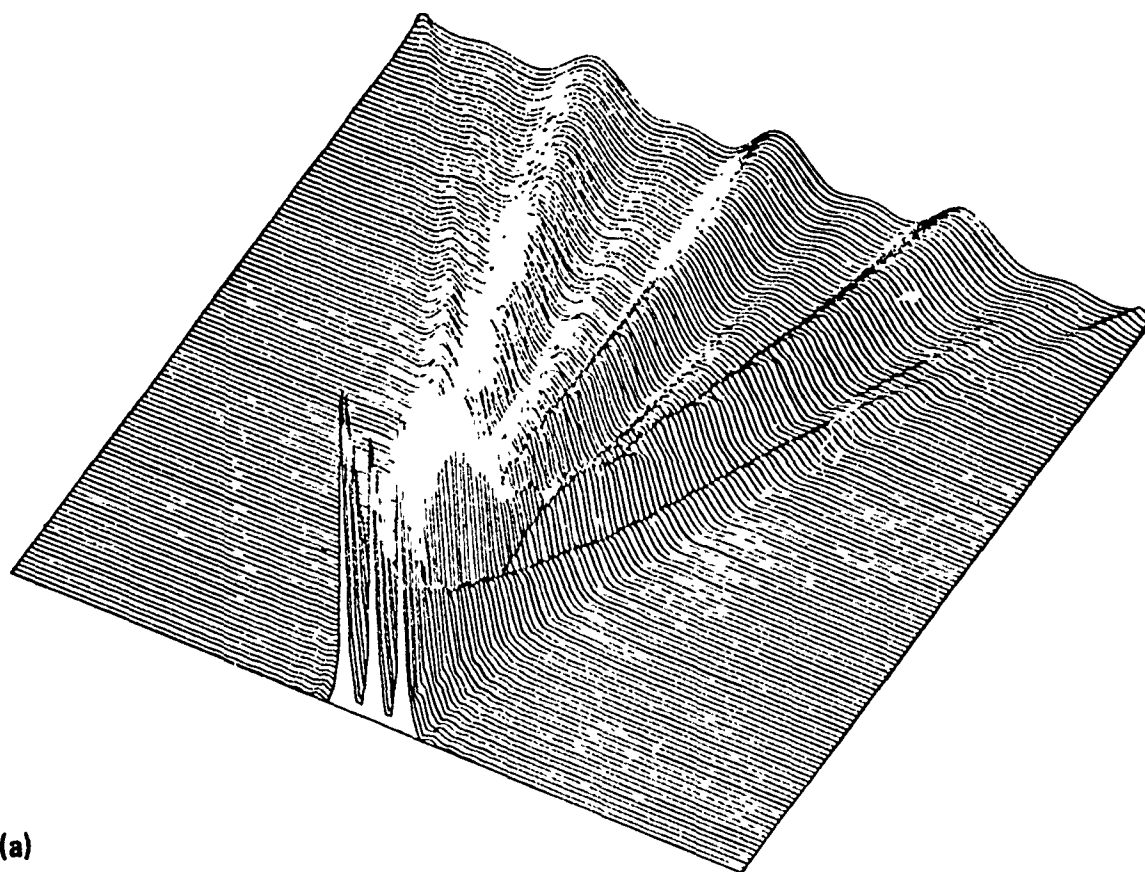
(a)
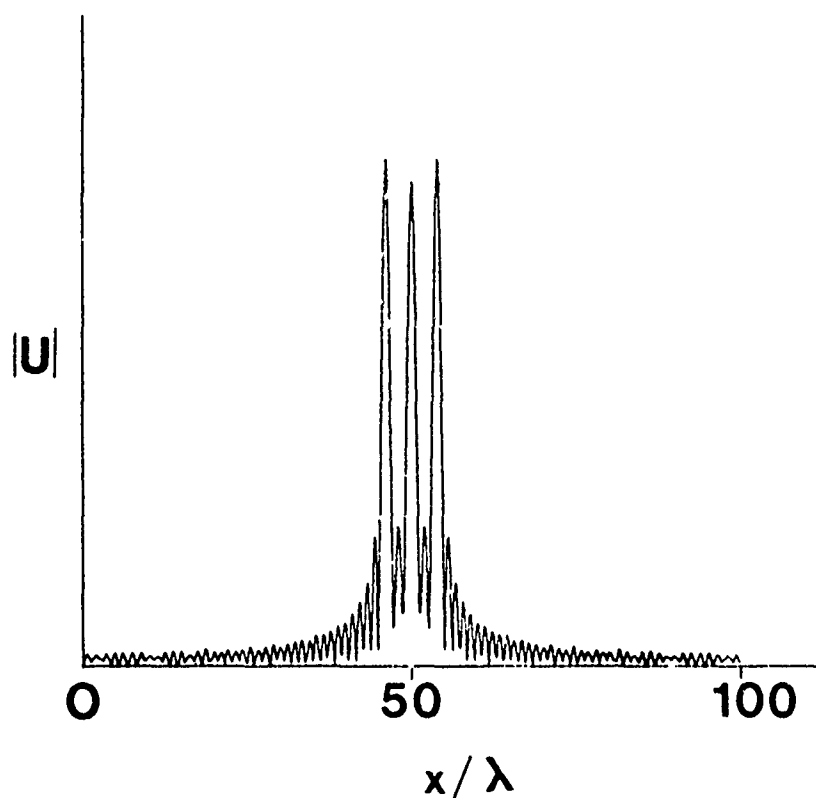
(b)

Fig. 8(a). Reconstruction of three point sources from computed data, at various planes. (b) Computed reconstruction at object plane.

Fig. 9. Noise degradation of reconstruction. (a) $\Delta A/A = 0.6$; $\Delta\phi = 0$; $n = 1$. (b) $\Delta A/A = 1.2$; $\Delta\phi = 0$; $n = 1$. (c) $\Delta A = 0$; $\Delta\phi = 20°$; $n = 1$. (d) $\Delta A = 0$; $\Delta\phi = 80°$; $n = 1$. (e) $\Delta A = 0$; $\Delta\phi = 60°$; n variable.
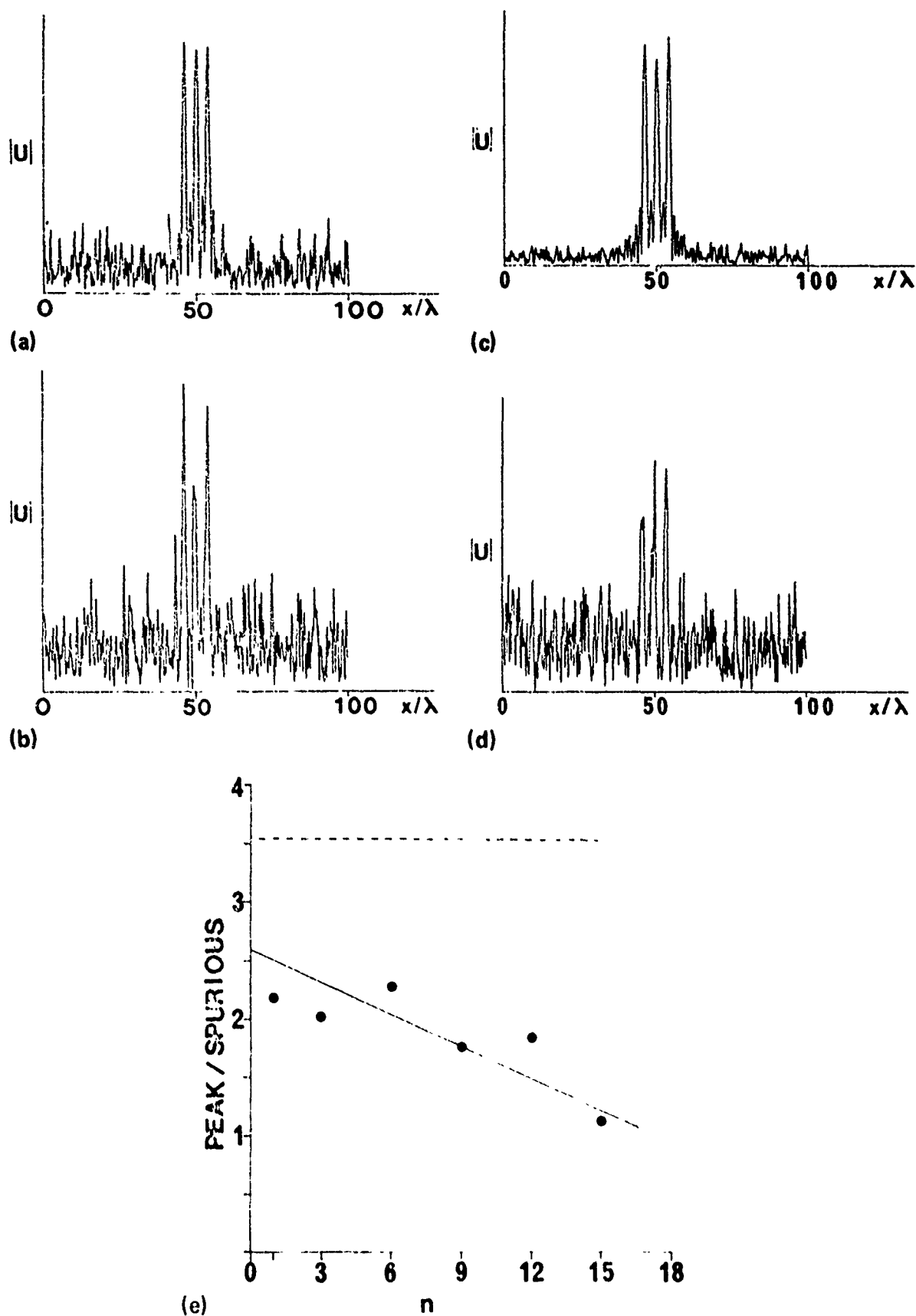
reconstruction of three point sources, spaced by four wavelengths. We have computed (for an isotropic substrate) the image distribution at a plane 100 wavelengths from the object. Using Eq. (11) with $N = 512$, we have then reconstructed the distribution at various positions back to the original object plane (Fig. 8(a), with the actual distribution at the object plane shown separately in Figure 8(b)). The point source distribution has been broadened, as expected from the finite spatial bandwidth of the assumed system.

We can now simulate the inadequacies of the laser probe by adding random signals to the theoretical sampled probe output. In conducting such a simulation we must choose the standard deviation for amplitude and phase, which we wish to impose. At the same time, we must simulate the approximate spatial frequency of the assumed noise. The highest frequency noise is obtained if we add random uncorrelated signals to each adjacent cell. We can simulate lower spatial frequency disturbances by choosing a random signal for every nth sampling interval, and making a linear interpolation for the intermediate sampling points.

Figures 9(a) and (b) show the effect of adding pure amplitude noise, with no correlation between adjacent sampling points (i.e., with $n = 1$). It is seen that even for $\Delta A/A$, the standard deviation referred to the peak value, as large as 1.2 the three sources are still just resolved. Figures 9(c) and (d) show similar results, again for $n = 1$, for pure phase noise. Here we find that the reconstruction still allows for identification of the sources for $\Delta\phi$ as large as $80°$.

The addition of uncorrelated noise at adjacent sampling steps provides a good model of the deleterious effects arising from errors in the analog-to-digital converter, and also for the effects of relatively high frequency noise in the detection circuitry. However just because there is no correlation between adjacent steps, which, in this case are separated by about $\lambda/5$, the noise spectrum lies mainly in the evanescent part of the spectrum, and in the propagating spectrum corresponding to waves which travel at large angles to the normal so that their effect on the reconstruction is minimized. Noise with the same standard deviation, but correlated over several sample points (i.e., for $n > 1$), has a larger deleterious effect on the quality of reconstruction. This is apparent from Fig. 9(e), where we have used the ratio of the peak in the reconstruction of the point sources to the amplitude of the largest competing spurious maximum as a somewhat arbitrary measure of the damage done by the presence of the phase noise. The figure shows how this ratio varies with the value of n. The dashed line indicates the ratio for the reconstruction in the absence of noise.

D. Nondestructive Testing

Experiments on a polished quartz surface are admittedly at least one step away from a realistic n.d.t. situation. However there are at least some problems which do involve the detection of microcracks in smooth surfaces, though more generally the techniques with which we are concerned are usable on components which are *not* optically flat; we have carried out a wide range of measurements on metal samples using an earlier version of the present laser probe [7].

The reconstruction of the gold dots (Fig. 7(e)) is a primitive example of the "defect" detection possibilities. It is clear however that one could improve the detection sensitivity by resorting to more complex detection of small defects. In many cases therefore the task will be concerned with the identification of point sources. This a priori knowledge of the nature of the "object" should greatly facilitate in both its detection and

location. At present we are digitizing the data on a minicomputer, but carrying out the reconstruction on a larger machine. In fact it is entirely feasible to carry out the whole process, in (almost) real time. Now the assumed point defect will give rise to a phase distribution having the character of a Fresnel zone plate. If then we correlate the scan data with such a phase distribution, we will for each choice of range obtain a correlation peak, the largest occurring for the range corresponding to the actual object location. The processing gain associated with this technique can be quite large, and could lead to a detection sensitivity which is substantially better than that indicated by the simple calculation leading to Equation (12).

Having suspected the presence of a defect at a particular location, one could then seek confirmation by the use of a second scan, somewhat nearer to the defect. Indeed it might prove convenient always to work with more than one scan, and directly to process the results obtained from each.

In practice few of the objects that one would wish to test would be planar. Provided that the shape of the object is such that it can be illuminated by surface waves, and provided that at one end there is a suitable location for a scanning line, the laser scan technique is in principle applicable. In such a case one could not usually be able to effect direct computer reconstructions. However, it might be possible to map the surface by measuring the "image" scan distribution when particular points on the sample surface are excited. In effect one would be obtaining an experimental Green's function for the particular sample. This could then be compared with potentially defective samples, to identify and locate faults.

E. Slowness Curve Determination

The reconstructions for the quartz samples discussed in Section IV. B, involved an accurate knowledge of the slowness. In fact earlier attempts where the slowness data was inaccurate to the extent of a few parts in 10^3 led to reconstructions marred by violent ripples. This suggests that the technique offers a means for the accurate determination of slowness curves. In principle, the procedure is quite simple. One measures $U_0(x)$ and $U_I(x)$ and hence derives $f_0(\alpha)$ and $f_I(\alpha)$. From Eq. (4) we then have

$$\beta I. = \cos^{-1}\left(\frac{1}{2}\left[\frac{f_I(\alpha)}{f_0(\alpha)} + \frac{f_I^*(\alpha)}{f_0^*(\alpha)}\right]\right) + 2\pi N$$

$$= F(\alpha) + 2\pi N, \tag{13}$$

where $F(\alpha)$ is defined by Eq. (13), and N is an integer. Now

$$\alpha = k(\theta)\sin(\theta),$$

and

$$\beta = \frac{1}{L}(F(\alpha) + 2\pi N) = k(\theta)\cos(\theta),$$

so that

$$[K(\theta)]^2 = \alpha^2 + \frac{1}{L^2}(F(\alpha) + 2\pi N)^2, \tag{14}$$

$$\theta = \tan^{-1}\left(\frac{\alpha L}{F(\alpha) + 2\pi N}\right). \tag{15}$$
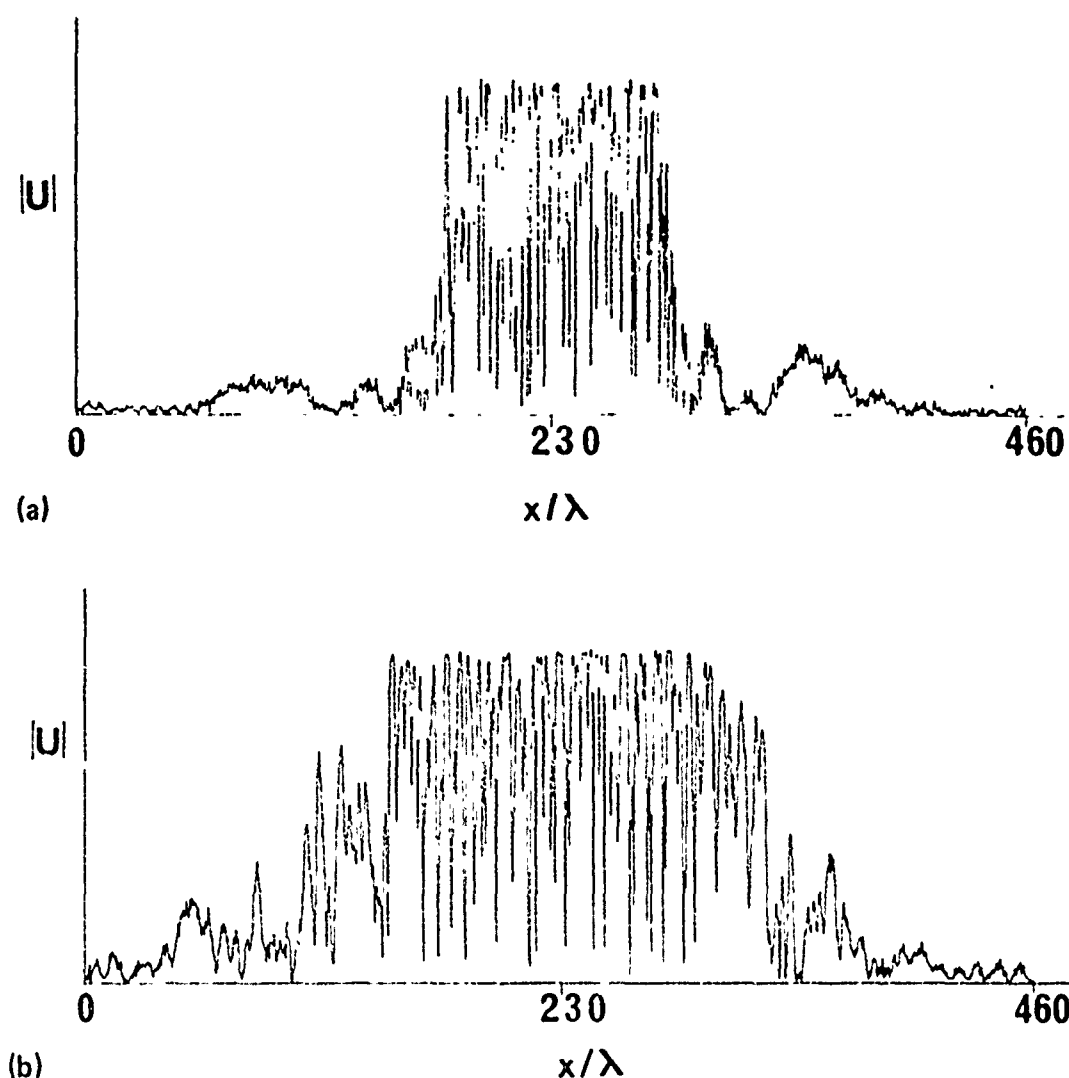
Fig. 10. Amplitude scans for slowness determination. (a) Immediately beyond random array of dots.
(b) 100 λ beyond random array.

Equations (14) and (15) are applicable to the case when θ (α) is single valued. In order
to obtain usable results it is naturally essential that the object spectrum contains com-
ponents over the whole range of θ for which the slowness surface is required. A simple
solution to this requirement is to use a very narrow aperture transducer; however this is
at the expense of the total available signal. One can also use a large suitably curved trans-
ducer. An alternative which we have adopted in our preliminary experiments is to use
a *random* array of small gold dots illuminated by a normal, wide interdigital transducer.

Figure 10(a) shows the amplitude scan as measured just beyond the second (of two)
rows of dots, and Fig. 10(b), the amplitude at the image plane. We then computed k (θ)
as a function of θ from Equations (14) and (15). The results are shown in Fig. 11, and
are compared with the curves computed from elastic constant data by Slobodnik [26].
The form of the slowness characteristic is reproduced, though the accuracy is modest.
It is believed that the gap between the achieved accuracy and that which we believe to
be possible with the apparatus is primarily due to the fact that we had taken only minimal
precautions against bulk and other spurious waves. Future experiments are being
designed with this problem very much in mind.

In principle the accuracy which one could achieve ought to approach the basic
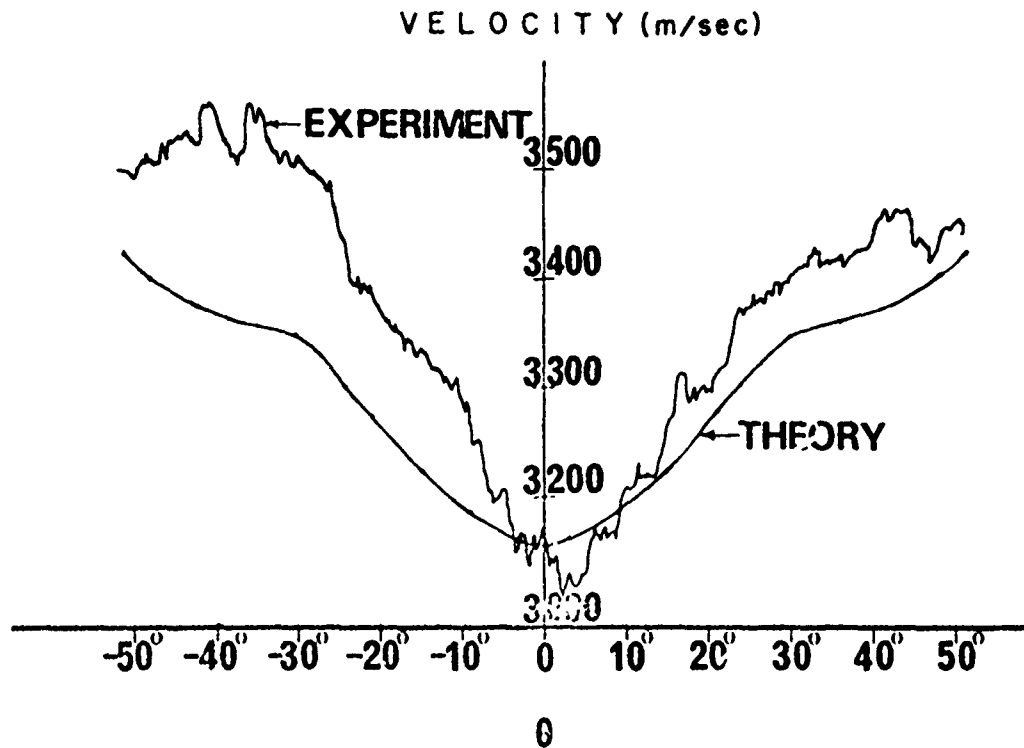instrumental precision discussed in Section II. One can also hope to improve the basic

Fig. 11. Velocity results for Y-cut quartz at $\theta°$ to the x direction compared with Slobodnik et al. [26].

accuracy by making post-recording corrections. These can be based on one known relationship between the object and image records - the fact that for single valued θ (α), the amplitude of the spectral density functions, $f(\alpha)$ must be identical. As a simple example, consider the case of a scan recorded subject to a slow phase drift in the recording system. This means that instead of recording the true distribution $U(x)$ one will be recording $U'(x)$, where

$$U'(x) = U(x)\,e^{ik_r x},$$

where k_r indicates the magnitude of the phase drift. This will lead to a transform $f'(\alpha)$, related to the true transform $f(\alpha)$ by

$$f'(\alpha) = f(\alpha + k_r). \tag{16}$$

Thus we see that uniform drift leads to a simple shift in the spectrum. We can readily shift the two spectra, $f_0(\alpha)$ and $f_1(\alpha)$, to bring them into optimum coincidence, before computing $f(\alpha)$ through Eq. (4) and then $k(\theta)$ through Equation (14). Removal of a linear drift does not exhaust the possibilities of correction for more complex distortions; one can anticipate that further improvements in the recorded data can be obtained in this way.

The question remains as to how one can extend this technique for the case of an anisotropic substrate, for which $\theta(\alpha)$ is no longer single valued. The procedure is in this case somewhat more involved but not in any basic way more complicated. Essentially one needs to record additional scans, the number depending on the multiplicity of the $\theta(\alpha)$ function. For a double valued function we record one additional scan (i.e., three in all) and additional scans for each unit increase in the multiplicity. This then provides enough information to allow a unique determination of $k(\theta)$.

OPTICAL AND ACOUSTICAL MICRO-ELECTRONICS

REFERENCES

[1] F. Rischbieter, "Messungen ad Oberflachenwellen in Festen Korpern," *Acustica*, 16, 75–83 (1965/56).

[2] B. A. Richardson and G. S. Kino, "Probing of Elastic Surface Waves in Piezoelectric Media," *Appl. Phys. Lett.*, 16, 82–84 (1970).

[3] E. G. Lean, "Interaction of Light and Acoustic Surface Waves," *Progr. Opt.*, XI, 123–166 (1973).

[4] R. L. Whitman and A. Korpel, "Propagation of Acoustic Surface Perturbations by Coherent Light," *Appl. Opt.*, 8, 1567–1576 (1969).

[5] R. L. Whitman, L. J. Laub, and W. J. Bates, "Acoustic Surface Displacement Measurements on a Wedge-shaped Transducer Using an Optical Probe Technique," *IEEE Trans.*, SU-15, 186-9 (1968).

[6] R. De LaRue, R. F. Humphryes, I. M. Mason, and E. A. Ash, "Acoustic Surface Wave Amplitude and Phase Measurements Using Laser Probes," *Proc. IEE*, 119, No. 2, 117–26 (February 1972).

[7] E. A. Ash, R. De LaRue, and R. F. Humphryes, "Microsound Surface Waveguides," *IEEE Trans.*, MTT-17, 882–92 (1969).

[8] W. Puschert, "Optical Detection of Amplitude and Phase of Mechanical Displacements in the Angstrom Range," *Opt. Comm.*, 10, No. 4, 357–61 (April 1974).

[9] I. M. Mason, J. Chambers, and P. E. Lagasse, "Spatial Harmonic Analysis of the Multistrip Coupler," *IEEE Ultrasonics Symposium Proceedings*, 159–62, Monterey, CA (November 1973).

[10] P. Nannayakara and E. A. Ash (to be published).

[11] P. Lagasse, "Acoustic Surface Waveguides," *IEEE Ultrasonics Symposium Proceedings*, 115–20, Monterey, CA (November 1973).

[12] ——, "Finite Element Analysis of Piezoelectric Waveguides," *IEEE Trans.*, SU-20, No. 4, 354–59 (October 1973).

[13] ——, Private Communication.

[14] H. K. Wickramasinghe and E. A. Ash, "Surface Wave Nondestructive Testing Using One-Dimensional Acoustic Holography," *Electron. Lett.*, 9, No. 15, 327–28 (July 26, 1973).

[15] R. K. Mueller, E. Marom, and D. Fritzler, "Some Problems Associated with Optical Image Formation from Acoustic Holograms," *Appl. Opt.*, 8, No. 8, 1537–42 (August 1969).

[16] J. R. Shewell and E. Wolf, "Inverse Diffraction and a New Repciprocity Theorem," *J. Opt. Soc. Am.*, 58, No. 12, 1596–1603 (December 1968).

[17] E. Wolf and J. R. Shewell, "The Inverse Wave Propagator," *Phys. Lett.*, 25A, 417–18 (September 1967).

[18] G. C. Sherman, "Application of the Convolution Theorem to Rayleigh's Integral Formula," *J. Opt. Soc. Am.*, 57, 546–7 (April 1967).

[19] A. Banos, Jr., "Dipole Radiation in the Presence of a Conducting Half Space" (Oxford Pergamon Press, 1966).

[21] M. M. Sondhi, "Reconstruction of Objects from their Sound Diffraction Patterns," *J. Acoust. Soc. Am.*, 46, No. 5, 1158–64.

[22] A. L. Boyer, P. M. Hirsh, J. A. Jordan, Jr., L. B. Lesem, and D. L. Van Rooy, "Reconstruction of Ultrasonic Images by Backward Propagation," *Acoustical Holography*, 3, 333–48 (New York: Plenum Press).

[23] J. P. Powers and D. E. Mueller, "A Computerized Acoustic Imaging Technique Incorporating Automatic Object Recognition," *Acoustical Holography*, 5 (New York: Plenum Press) (to be published).

[24] D. L. Van Rooy, "Digital Ultrasonic Wavefront Reconstruction in the Near Field," IBM Publication No. 320.2402 (May 19, 1971).

[25] J. W. Goodman, *Introduction to Fourier Optics* (New York: McGraw-Hill, 1968).

[26] A. J. Slobodnik, Jr. and E. D. Conway, "Surface Wave Velocities," *Microwave Acoustics Handbook*, 1, Physical Sciences Research Papers, No. 414 AFCRL-70-0164, Air Force Cambridge Research Laboratories (March 1970).

3. SURFACE ACOUSTIC WAVE SLOWNESS SURFACE MEASUREMENT

H.K. Wickramasinghe and E.A. Ash

ABSTRACT. Surface wave velocity curves can be measured with high precision using a phase sensitive laser probe. The method does not imply any assumptions about the wave field distribution used. Accuracies of a few parts in 10^4 have been attained, and suggest that the technique may also prove valuable in the determination of fundamental elastic constants.

Introduction

Critical design problems involving surface acoustic waves require an accurate knowledge of the slowness curve of the substrate. For some commonly used materials such as Lithium Niobate and Bizmuth Germanium Oxide, these surfaces are not known with great accuracy. In this paper, we report a technique whereby the slowness surface can be measured with high accuracy over a wide angular range.

The technique involves the measurement of two transverse complex field distributions spaced by a known distance using a phase sensitive laser probe[1]. Relating the spectra of these two scans leads directly to the slowness curve of the substrate. The evaluation makes no assumptions about the distribution of the incident surface acoustic wave field.

A detailed analysis of the theory involved was presented in a previous publication[2]. Following a brief outline of this theory, we will present experimental results demonstrating accuracies of a few parts in 10^4 for some commonly used materials. Finally we will discuss the capabilities of the technique in the light of our results.

Theory

Figure 1 shows as "object" distribution $U_0(x)$ at $Z = 0$ and an "image" distribution $U_I(x)$ at $Z=L$. A plane surface wave propagating in the θ direction will have a spatial dependance of $\exp{-j(\alpha x + \beta z)}$ where

$$\alpha = K(\theta) \sin\theta$$
$$\beta = K(\theta) \cos\theta \qquad (1)$$

and $K(\theta)$ is the wave number. We can expand $U_0(x)$ in terms of the plane wave spectrum

$$U_0(x) = \int_{-\alpha_m^-}^{\alpha_m^+} f_0(\alpha) e^{-j\alpha x} \, d\alpha \qquad (2)$$

The waves corresponding to values of α greater than the maximum value attained by $K(\theta) \sin\theta$ are evanescent, and can certainly be excluded from our calculations since we are concerned with propagation distances of many wavelengths. We have therefore used the limits α_m^+ and α_m^- corresponding to the maximum values of α for θ positive and negative respectively. Provided that the magnitude of $f_0(\alpha)$ drops to low values by the time we approach these limits, we may regard equation (2) as a simple Fourier transform with the inverse

$$f_0(\alpha) = \int_{-\infty}^{\infty} U_0(x) e^{j\alpha x} \, dx \qquad (3)$$

since $f_0(\alpha)$ can be interpreted as the amplitude of the plane wave corresponding to θ, we can[3] immediately write down the corresponding spectral density at the "image" plane,

$$f_I(\alpha) = f_0(\alpha) e^{-j\beta L} \qquad (4)$$

This is a standard procedure in isotropic diffraction theory. It applies equally to the anisotropic case provided $\theta(\alpha)$ is a single valued function of α[1]. We can then at once take the transform of $f_I(\alpha)$ and hence obtain the image distribution,

$$U_I(x) = \int_{-\alpha_m^-}^{\alpha_m^+} f_0(\alpha) e^{-j(\beta L + \alpha x)} \, d\alpha \qquad (5)$$

To calculate an accurate image distribution $U_I(x)$ from a measured object distribution $U_0(x)$, the form of the slowness curve $K(\theta)$ must be known with considerable precision since the integrand in equation (5) contains a phase factor βL and L may in practice be several hundred wavelengths. Clearly, one can reverse this process to obtain an accurate representation of the slowness curve by measuring $U_I(x)$; the accuracy achieved being directly proportional to L.

To do this, one measures $U_0(x)$ and $U_I(x)$ and hence derives $f_0(\alpha)$ and $f_I(\alpha)$. From equation (4) we then have

$$\beta L = \cos^{-1} \frac{1}{2} \left[\frac{f_I(\alpha)}{f_0(\alpha)} + \frac{f_I^*(\alpha)}{f_0^*(\alpha)} \right] + 2\pi N \qquad (6)$$

$$= F(\alpha) + 2\pi N$$

where $F(\alpha)$ is defined by equation (6) and N is an integer. One then finds that

$$K(\theta)^2 = \alpha^2 + \frac{1}{L^2}\left[F(\alpha) + 2\pi N \right]^2 \qquad (7)$$

and

$$\theta = \tan^{-1}\left[\frac{\alpha L}{F(\alpha) + 2\pi N} \right] \qquad (8)$$

The theory as it stands does not enable us to make an absolute measurement of the slowness surface, since the value of N is not known. The value of N can be determined however if we know $K(\theta)$ for any arbitrary value of θ. This information could be obtained experimentally by making a separate measurement in the particular direction of interest. For the sake of convenience we measure $K(0)$. The value of N follows immediately from equation (7).

$$2\pi N = K(0) L - F(0) \qquad (9)$$

The velocity determination effected by a measurement of the number of wavelengths in a known distance implies far field conditions. Using the wider transducers this condition is not met, and can lead to phase errors which are significant in the context of the high accuracies attainable by the method. One can avoid the need for such a separate measurement by resorting to a third scan $U_I'(x)$ at $Z = L'$. From equation (5) we have

$$U_I^+(x) = \int_{-\alpha_m}^{+\alpha_m} f_0(\alpha)e^{-j\beta L'}\,e^{-j\alpha x}\,d\alpha \qquad (10)$$

substituting for β from (3) gives

$$U_I^+(x) = \int_{-\alpha_m}^{+\alpha_m} f_0(\alpha)e^{-J(F(\alpha)+2\pi N)\frac{L'}{L}}\,e^{-j\alpha x}\,d\alpha \qquad (11)$$

- In order to determine the integer, N, we then simply vary N until we obtain the best correlation between the measured distribution $U_I^+(x)$ and that calculated from equation (11).

Experimental Results

It is essential that the object spectrum contains components over the whole range of α for which the slowness surface is required. A simple solution to this requirement is to use a very narrow aperture transducer. However, this is at the expense of the total available signal. An alternative is to use a random array of small gold dots illuminated by a wide interdigital transducer. The latter alternative has an advantage in that one can subtract the effect of bulk and other spurious waves by recording $U_0(x)$ and $U_I(x)$ with and without the random gold dots [5].

Figure 2 shows the measured slowness curve for YX Quartz with a 600 Å overlay of chrome, compared with the theoretical curve for non-metallized Quartz computed by Slobodnik[4]. Agreement is to within a few parts in 10^3 over a + 25^0 angular range. The curve appears to be slightly shifted about the $\theta = 0$ line. This is attributed to a small misorientation in the crystal. Departure from theory over the remainder of the angular range could be accounted for by a slight misorientation in the plane of propagation. The object distribution chosen for this experiment was a random array of small gold dots and L was approximately 100 wavelengths. Although we reached the expected accuracy estimated from simple theoretical considerations, the gold dots produced a very non-uniform object spectrum. We believe that the rather "noisy" slowness curve is accounted for by this fact.

Figure 3 shows the measured slowness curve for YZ Lithium Niobate again compared with the theoretical curve computed by Slobodnik[4]. The object distribution in this case was a 2λ transducer which enabled us to measure the slowness curve over + 18^0. As in the previous example, a slight shift in the slowness curve about the $\theta = 0$ line is observed. L was 400 wavelengths and the estimated accuracy is in this case within a few parts in 10^4. Although the noise in the slowness curve has been considerably reduced, a discrepancy, up to 0.3 at 18^0 is observed. Subsequent sensitivity calculations on the theoretically computed curve indicated that this discrepancy is well within the limits of uncertainties arising from the limited known accuracy of the elastic tensor elements and the orientation of the crystal.

In the experiments described so far, the transducers were fired along a symmetry axis of the crystal. Consequently, the measured slowness curves were all symmetrical about the $\theta = 0$ line. Clearly one could make better use of the available object spectrum by firing the transducers at an angle to the symmetry axis, thereby deriving slowness data over a wider angular range. Figure 4 shows the measured slowness curve for YZ Lithium Niobate obtained by firing the 2λ transducer at an angle of 20^0 to the Z axis. All other parameters

were chosen to be the same as those for the previous experiment. The experiment enabled us to obtain the slowness curve over a wider (34^0) angular range.

Discussion and Conclusion

We have demonstrated a technique for measuring the slowness curves of acoustic surface with an accuracy of a few parts in 10^4 - substantially better than can be attained by other means. The results are indeed more precise than the known values of the velocities as derived from separate measurements on elastic and piezoelectric tensor elements. This suggests the possibility of using a measured slowness curve and "working backwards" to improve the accuracy of the measured elastic constants. The basic approach is firstly to obtain the differential effect of the variation of each independent element on the velocity curve, followed by an optimization procedure to obtain the closest possible fit to the experimental data. For any particular cut, the effect of certain elements will predominate. One can increase both accuracy and the number of elements measured by undertaking measurements on several cuts. In a very similar way we can also derive the crystal orientation. It seems probable that this technique will permit an accuracy substantially better than the $\pm\frac{1}{2}^0$ normally obtained from X-ray measurements.

Acknowledgement

References

(1) R. De La Rue, R.F. Humphryes, I.M. Mason and E.A. Ash, "Acoustic Surface Wave Amplitude - Phase Measurements, using Laser Probes", Proc. IEE, v.119, no.2, Febr. 1972, pp.117 - 26.

(2) H.K. Wickramasinghe and E.A. Ash, "Optical Probing of Acoustic Surface Waves - Application to Device Diagnostics and to Non-Destructive Testing" to be published in the MRI symposium on optical and acoustical micro-electronics, Polytechnic Institute of Brooklyn, New York, Apr. 1974.

(3) J.W. Goodman "Introduction to Fourier Optics", McGraw Hill, 1968.

(4) A.J. Slobodnik, Jr., and E.D. Conway, "Surface Wave Velocities", Microwave Acoustics Handbook Volume 1, Physical Sciences Research Papers, No. 414AFCRL-70-0164, Airforce Cambridge Research Laboratories, U.S.A., March 1970.

(5) H.K. Wickramasinghe and E.A. Ash "Subtraction techniques in two dimensional holography for non-destructive testing". To be published.
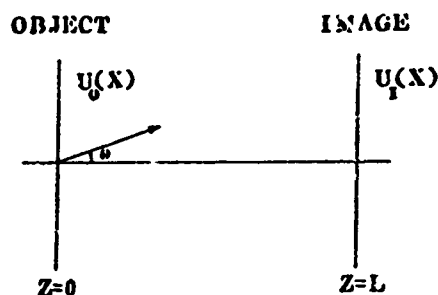
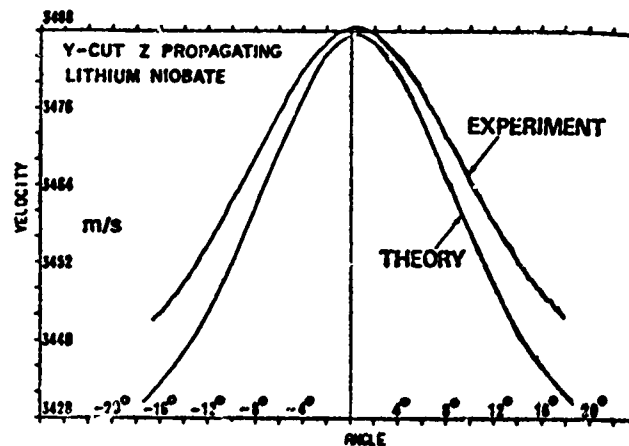Figure 1: Configuration for slowness surface measurement

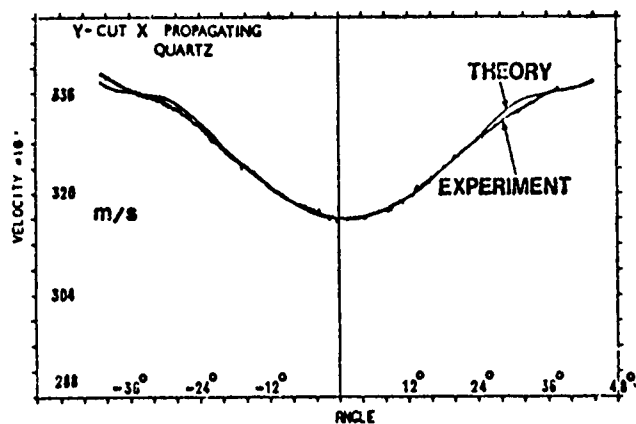Figure 3: Velocity results for YZ Lithium Niobate compared with Slobodnik et al.

Figure 2: Velocity results for YX Quartz compared with Slobodnik et al.
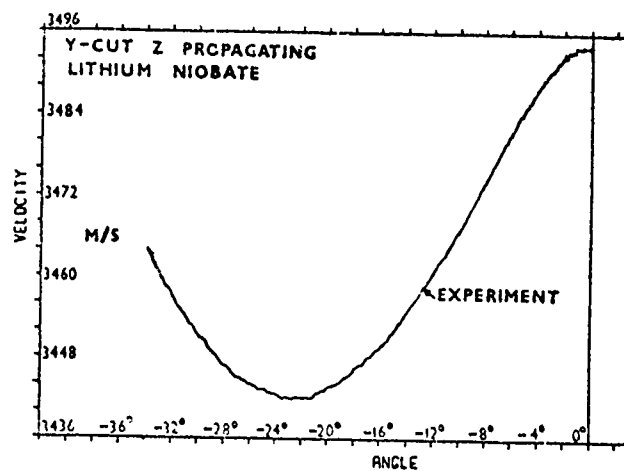

Figure 4: Velocity results for Lithium Niobate obtained using a narrow aperture transducer firing at 20° to the z axis.

4. BACKGROUND SUBTRACTION IN SURFACE-WAVE HOLOGRAPHY

Surface-wave holographic techniques can be used to detect the presence of small defects. The detection limit is usually determined not by signal to noise considerations, but rather by the presence of spurious background signals, such as bulk waves. The letter describes a technique for eliminating this background, and demonstrates the improvement in the detection limit.

Defects on a surface can be identified by observing their influence on the propagation of acoustic surface waves. A particular technique for implementing this procedure is the use of 2-dimensional acoustic holography.[1,2] With reference to Fig. 1, the surface is illuminated by acoustic surface waves, using an interdigital transducer for a piezoelectric material, or, in other cases, by a wedge transducer. The complex field
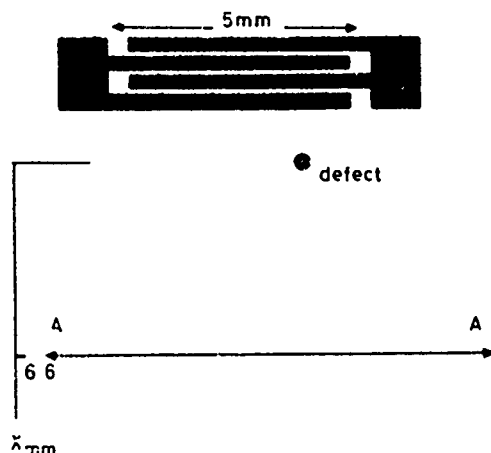

Fig. 1 *Complex field distribution is measured along line AA'*

distribution is measured along the line AA', this record contains, in principle, complete information on the field distribution over the whole surface up to the transmitting transducer, provided only that the defects are small and sparse. One can regard the record as a 1-dimensional hologram from which we can reconstruct any line on the 2-dimensional surface.

The distribution can be recorded on film and subsequently reconstructed optically.[1] More conveniently, one can digitise the record and reconstruct using purely numerical techniques.[2] It is important to appreciate that the large-scale computations needed for the reconstruction of typical 2-dimensional holograms become quite insignificant for a 1-dimensional record. Using 256 samples and 8 bit accuracy, the reconstruction can be effected in seconds on a large computer and in times of the order of a minute on a typical laboratory minicomputer.

The area of search for defects will normally lie in the near field of the transmitting transducer. The field distribution, even in the absence of defects, is therefore complex. Moreover, in practice, the record will be degraded by reflections from the edge of the sample, and by the presence of bulk waves. In consequence, there is a distinct limit to the smallest defect which can be discerned, which is independent of the signal/noise ratio attained in the recording. This limitation can be overcome if one has available a defect-free sample for comparison. The process of reconstruction is, of course, linear; one is therefore at liberty to subtract the 'perfect' record from that obtained on the test sample and reconstruct the difference. It is important to appreciate that the reference sample need not in fact be totally free of defects. All that is needed is that there shall be so few that one can discount the possibility of a defect on the reference sample in the same position as one on the test sample.

To demonstrate this technique, we adopted the configuration of Fig. 1, using a y-cut quartz sample. The complex field distribution was measured by a laser probe system,[3] the separate amplitude and phase records being digitised and stored. The reconstruction process consists essentially of expanding the field into a plane-wave spectrum, multiplying each elementary wave by the appropriate phase delay, allowing for the anisotropy of the material, and subsequently recombining at the desired reconstruction plane.

The experiment was conducted at 60 MHz with a 'defect' consisting of a gold dot approximately 30 μm in diameter and 4000 Å thick, i.e. approximately $\lambda/2$ in diameter and $\lambda/100$ in thickness. The 'perfect' comparison sample was obtained very simply by wiping off the gold dot. Fig. 2a shows the hologram with the defect present and Fig. 2b shows its reconstruction in the plane of the dot. It would clearly be impossible to deduce the presence of a defect from this
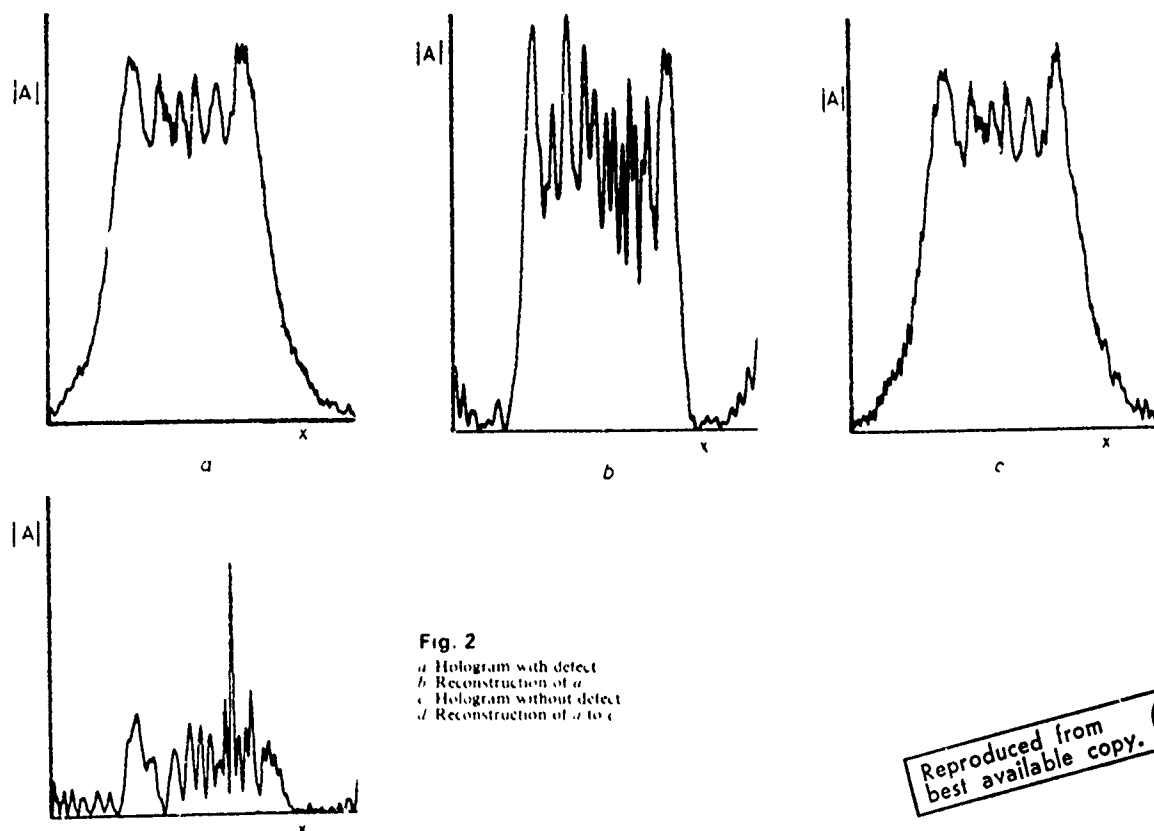

Fig. 2
a Hologram with defect
b Reconstruction of a
c Hologram without defect
d Reconstruction of a to c

evidence. The hologram with the gold dot removed, Fig. 2c, is not easily distinguished, by eye, from that of Fig. 2a. However, the reconstruction of the difference between them, Fig. 2d, shows the presence of the defect clearly. The background level in Fig. 2d is due to long-term instabilities in the laser probe system rather than to the basic noise level. Further improvements in the detection limit can therefore be expected.

The use of the same sample for both the reference and the test object simplified the demonstration. In practice, one would have to take additional steps to ensure that the location of the recording line corresponds as closely as possible in the two experiments. A lateral displacement, i.e. along the recording line, can be readily eliminated by progressively shifting one record with respect to the other, to obtain maximum correlation. Similarly, small displacements of the recording line in the y-direction can be allowed for by recording three records to span the uncertainty in the x-position, and again correlating to obtain the best fit. The amount of computation needed for these adjustments is again insignificant.

The preliminary experiments encourage the view that the method may be capable of development into an instrument capable of detecting extremely small defects on a surface by recording one, or possibly three, linear surface-wave field distributions.

A. F. ASH   *25th September 1975*
H. K. WICKRAMASINGHE*

Department of Electronic & Electrical Engineering
University College London
Torrington Place, London WC1E 7JE, England

References

1 WICKRAMASINGHE, H. K., and ASH, E. A.: 'Surface wave nondestructive testing using 1-dimensional acoustic holography', *Electron. Lett.*, 1973, 9, pp. 327-328
2 WICKRAMASINGHE, H. K., and ASH, E. A.: 'Optical probing of acoustic surface waves--Application to device diagnostics and to nondestructive testing'. Proceedings of the symposium on optical and acoustic microelectronics, Polytechnic Institute of New York, 1974
3 DI LA RUE, R., HUMPHRYES, F., MASON, I. M., and ASH, F. A.: 'Acoustic-surface-wave amplitude and phase measurements using laser probes', *Proc. IEE*, 1972, 119, (2), pp. 117-126

* Now with the Hansen Laboratories, Stanford University, Calif., USA

5. Conclusions

We believe that the results we have obtained amount to prima facie case for the use of these technique as for n.d.t. We have been able to find extemely small - though artificial - defects. There is still a good deal of room for further refinement of the method. However the work has been confined so far to piezo-electric materials. It is clear that the next stage must be to extend the work to non-piezo electric materials. Amongst those that are most likely to be of direct interest are glasses and semiconductor materials. The main problem is to devise an effective surface wave transducter. It was hoped that results on this - though obtained after the termination of the contract - would still become available in time to include in the final report. This unfortunately was not possible - as a result of a number of purely technological problems. We are however continuing to work towards this end.

The work on slowness determination is, in our view, also of possible relevance to n.d.t. Of course slowness is a measurement averaged over a surface. It is not therefore able to identify individual defects. However it is possible to identify quite small changes in the average characteristics of a surface - for example as a result of surface stress. There are also possibilities of measuring occlusion of gases in semiconductor slices after processing. The current precision in velocity which we have achieved is about one or two parts in 10^4. We are however confident that with further effort we should be able to achieve at least one additional order of magnitude in precision. We believe that in this technique we are on the verge of developing an extremely sensitive surface measurement device.

C OVERALL ASSESSMENT - PLANS FOR FURTHER WORK

The major portion of the effort* on this contract has been deployed on the microwave scanning technique.   The results which we have obtained are, we believe, sufficient to encourage the further pursuit of this method.   We have been able to identify <u>and locate</u> cracks in metals with dimensions of one micron or less. We believe therefore that there may be direct applications for surface defect detection in metals.   Beyond that we have demonstrated the use of the method for inspection of <u>electrical</u> parameters of materials - notably dielectric constants, permeability ferrimagnetic resonance effects etc.   In this area we believe that the instrument we have developed is capable of performing not only a competitive but a unique task.   We know of no other way in which the <u>surface value</u> of these parameters can be established with comparable accuracy.

There are a number of ways in which the instrument could be developed so as to lead to a more fully engineered version, - and giving superior performance. Briefly the improvements one would seek include the following:

   (i). Use of higher frequency.   Using available solid state sources one
        might work at 8mm wavelengths.

  (ii) Use of a pair of integrated resonators, one for measurement the
        other for carrier cancellation.   This would improve stability.

 (iii) Simplification of electronic system; use of lower noise components
        which have recently become available.

  (iv) Improved mechanical scanning stage.

The work we have done, has been exploratory.   We have tried to assess the attainable performance for a wide range of quite different materials testing problems.   In our view, further development should probably be concentrated on a more limited set of objectives, and aimed at attaining the highest performance within that set.

---

*The doctoral student whose salary was paid on the contract worked on this exclusively.

The acoustic holography and velocity determination work has also reached a stage where we believe serious consideration should be given to developing the technique for n.d.t. purposes.   The main bottleneck has been the lack of effective transducers for non-piezo electric materials - which of course represent the largest class of samples one would consider testing.   Here again, we feel that further work should probably be concentrated on a limited class of materials to be tested.   We believe that glasses and semiconductor materials are likely to prove particularly suitable.   In the case of glasses one would be able to detect microcracks and also stress.   In the case of semiconductors the sensitivity of the technique has now reached a point where quite small defects will show up. Again the overall velocity measurement is believed now to be sufficiently sensitive to allow the assessment of a number of surface characteristics - including stress, and distribution of impurities.   There is a possibility that one might be able to assess the effect of occluded gases as well.

We are intending to submit a new proposal for the extension of the acoustic surface wave work.